# Trabajo Fin de Máster

## *STUDY AND IMPROVEMENT OF THE PERFORMANCE OF AN INDUSTRIAL SETTLING TANK USING CFD MODELS IN OPENFOAM*

**Intensificación: ANÁLISIS DE SISTEMAS DE RECURSOS HÍDRICOS**


**Autor:**
**DECLAN AHERN**

**Director:**
**ENRIQUE JAVIER ASENSI DASÍ**

**Codirector/es:**
**ELENA ALEMANY MARTÍNEZ**


***JULIO, 2017***


UNIVERSITAT POLITÈCNICA DE VALÈNCIA

máster en ingeniería hidráulica y medio ambiente
mihma

# Resumen del Trabajo de Fin de Máster

| Datos del proyecto |
|---|
| **Título del TFM en español:** Estudio y mejora del funcionamiento de un decantador industrial mediante el uso de modelos CFD con OpenFOAM |
| **Título del TFM en inglés:** Study and improvement of the performance of an industrial settling tank using CFD models in OpenFOAM |
| **Título del TFM en Valenciano:** Estudi i millora del funcionament d'un decantador industrial mitjançant l'ús de models CFD amb OpenFOAM |
| **Alumno:** DECLAN AHERN |
| **Tutor:** ENRIQUE JAVIER ASENSI DASÍ |
| **Cotutor/es:** ELENA ALEMANY MARTÍNEZ |
| **Fecha de Lectura:** JULIO, 2017 |

| Resumen |
|---|
| **En español (máximo 5000 caracteres)** |
| En el tratamiento de aguas residuales se utilizan decantadores para mejorar la calidad del agua eliminando los sólidos suspendidos por gravedad. Los procesos de separación por gravedad y la hidrodinámica interna de los decantadores suelen ser poco conocidos y su diseño a menudo está basado en relaciones empíricas y en la experiencia. Los CFD (Dinámica de Fluidos Computacional) permiten un conocimiento profundo del funcionamiento interno de los decantadores. En este proyecto se aplican los CFD para estudiar el funcionamiento de un decantador industrial en el tratamiento de las aguas subterráneas y superficiales generadas en las obras de construcción, y de este modo asegurar que su posterior vertido cumpla con los estándares medio ambientales.<br><br>Se desarrolla un modelo numérico CFD para estudiar los procesos hidrodinámicos y de sedimentación que tienen lugar en el tanque. El objetivo es entender mejor estos procesos, identificar zonas muertas, corto-circuitos, y observar el efecto de la colocación de deflectores internos para mejorar la eficiencia del decantador. También se estudiará la sedimentabilidad de los sólidos. Primero se simulará el campo de flujo con una fase y posteriormente se realizará la simulación multifase euleriana para modelar la fase sólida con la aproximación 'drift flux' y con un modelo de turbulencia k-ε. El modelo será parcialmente calibrado con ensayos de sedimentación. Se ha elegido el software CFD de código abierto OpenFOAM® por ser libre y ampliamente utilizado en el ámbito profesional y científico. Se propondrán cambios para mejorar el rendimiento y la eficiencia del decantador en la eliminación de sólidos suspendidos. Se pretende que el modelo sea flexible y pueda ser utilizado por la empresa en distintas situaciones. |

**En valenciano (máximo 5000 caracteres)**

En el tractament d'aigües residuals s'utilitzen decantadors per millorar la qualitat de l'aigua eliminant els sòlids suspesos per gravetat. Els processos de separació per gravetat i la hidrodinàmica interna dels decantadors solen ser poc coneguts i el seu disseny sovint està basat en relacions empíriques i en l'experiència. Els CFD (Dinàmica de Fluids Computacional) permeten un coneixement profund del funcionament intern dels decantadors. En aquest projecte s'apliquen els CFD per estudiar el funcionament d'un decantador industrial en el tractament de les aigües subterrànies generades en les obres de construcció, i d'aquesta manera assegurar que el seu posterior abocament complisca amb els estàndards mediambientals.

Es desenvolupa un model numèric CFD per estudiar els processos hidrodinàmics i de sedimentació que tenen lloc en el tanc. L'objectiu és entendre millor aquests processos, identificar zones mortes, curt-circuits, i observar l'efecte de la col·locació de deflectors interns per millorar l'eficiència del decantador. També s'estudiarà la sedimentabilitat dels sòlids. Primer es simularà el camp de flux amb una fase i posteriorment es realitzarà la simulació multifase euleriana per modelar la fase sòlida amb l'aproximació 'drift flux' i amb un model de turbulència k-ε. El model serà parcialment calibrat amb assajos de sedimentació. S'ha triat el programari CFD de codi obert OpenFOAM® per ser lliure i àmpliament utilitzat en l'àmbit professional i científic. Es proposaran canvis per millorar el rendiment i l'eficiència del decantador a l'eliminació de sòlids suspesos. Es pretén que el model siga flexible i puga ser utilitzat per l'empresa en diferents situacions.

**En inglés (máximo 5000 caracteres)**

Settling Tanks (STs) are used in wastewater treatment to improve water quality by elimination of suspended solids via gravitational settling. Gravitational separation processes and the internal hydrodynamics of the STs are often poorly understood and their design is often based on empirical relationships and past experience. CFD (Computational Fluid Dynamics) allows for a thorough understanding of the inner workings of STs. In this project, CFD is used to study the operation of an industrial ST in the treatment of groundwater and surface water generated at construction sites to ensure that any subsequent discharge meets environmental standards.

A CFD model is developed to study the hydrodynamics and sedimentation processes taking place in the tank. The aim is to gain a better understanding of these processes, identifying dead zones and short-circuiting, and observe the effect of internal baffle positioning to see how efficiency of the ST could be improved. Sedimentability of solids will also be studied. First, the single-phase flow field will be simulated and then, the multiphase Eulerian approach will be taken to model the dispersed phase using the 'drift flux' approximation with a k-ε turbulence model. The model will be partially calibrated with experimental settling tests. The open source CFD software OpenFOAM® has been chosen because it is free and state of art. Proposals to improve tank performance and efficiency of the ST in the removal of suspended solids of the ST will be outlined. It is intended that the model be flexible and of use to the company in a variety of settings.

**Palabras clave español (máximo 5):** Sedimentación, aguas residuales, decantador, CFD, OpenFOAM

| |
|---|
| **Palabras clave valenciano (máximo 5):** Sedimentació, aigües residuals, decantador, CFD, OpenFOAM |
| **Palabras clave inglés (máximo 5):** Sedimentation, wastewater, settling tank, CFD, OpenFOAM |

# Acknowledgements

I would like to express deep gratitude to my two supervisors, Enrique and Elena. Their input, guidance and support throughout the process was invaluable and their time invested working with me is highly appreciated. Their care and expertise helped to endow the project with quality, direction and clarity. Moltes gràcies Enrique y Elena.

I would like to thank the company for presenting me with an opportunity to study their tank and provide me with the necessary data and resources to be able to so. Thank you Cecil and also to Aidan whose time and input at various times during the project were a big help.

Thanks to Pablo Lavalle, who started me off on the path that has led me here over many years.

Thanks to my parents who's support is always behind me and without whom I could never have completed this course and project.

Thanks to Kayla and Storm, who were with me every minute along the way.

‘Ní dhéanfaidh smaoineamh an treabhadh duit.’

*Irish proverb*

# Contents

# List of Tables

# List of Figures

# Chapter 1

# Introduction

## 1.1 Motivation and Objectives

Settlement tanks (STs) are used widely in municipal and industrial settings to remove solids and other undesirable elements from wastewater. Their design is traditionally based on empirical formulae that neglect their complex inner mechanisms, but the advent of CFD (computational fluid dynamics) offers a powerful tool for understanding and improving STs.

This study focuses on an industrial rectangular ST used primarily on construction sites in the dewatering process. When a site is being excavated to a level below the water table then groundwater ingress can be expected and it will need to be expelled to maintain a workable excavation. Rainwater may also pool and accumulate in areas that need to be emptied for work to continue.

Water is pumped from the excavation through a ST and then discharged. Depending on the medium into which it is discharged there are certain criteria the effluent quality must fulfil. The function of the ST is to ensure the effluent meets these criteria which generally pertain to concentration of TSS (total suspended solids) and other parameters of importance such as pH, BOD (biological oxygen demand), COD (chemical oxygen

demand), concentration of heavy metals etc.

The inner workings of the tank and its performance under varying conditions is not well understood. The aim of this study was to use CFD models to investigate the current performance of the tank and ways in which it may be improved.

The hydrodynamics of the tank with a single, continuous phase under different flow regimes was first studied using CFD. The theoretical background to CFD models was explored and a suitable model for the inclusion of a second, dispersed phase, was then developed with the assistance of experimental results.

Unlike most treatment tanks which are designed based on a known range of inflows and water quality, the tank in this study is required to function in a range of scenarios which can involve significantly different operating conditions. Its design and performance therefore does not follow a rigid definition of one tank classification though it is treated as a primary clarifier where discrete sedimentation processes dominate.

The goals were to determine the influence of the tank's inner configuration in terms of flow field distribution (existence of dead zones or large recirculation zones), the effects of each individual internal component on the tank's functionality, the effects of sludge bed scouring, the settling processes that take place inside the tank and the characteristics of the sediment it treats, the conditions under which short circuiting occurs, and the limitations of the tank in general.

A literature review is conducted in the following section, and then in Chapter 2 we introduce the background concepts of dewatering, sedimentation, clarifiers along with other background knowledge. Chapter 3 goes into the mathematical details behind the model formulation and justifies the choice of model. Chapter 4 introduces the setup of CFD cases and model calibration, then the results of the simulations and their analyses are contained in Chapter 5. A conclusion is presented in Chapter 6.

## 1.2 Literature Review

A modern theoretical description of settling solids in ST's was first outlined by Hazen, 1904 [24] and later elaborated upon by Camp, 1946 [11]. These theories of 'ideal' settling made vast simplifications about the flow and settlement processes that occur in ST's but nonetheless became widely used in the design of wastewater treatment plants.

Larsen, 1977 [31] was the first to apply CFD models to a ST. He obtained comprehensive velocity and concentration distributions in rectangular secondary ST's (SST's) for comparison with a numerical model and was able to characterise the flow field and sludge properties. He examined the energy balance in SST's and highlighted the importance of phenomena such as density currents, turbulence and recirculating flow not considered by the traditional Camp models.

Primary treatment was one of the first areas in wastewater treatment where CFD was applied. Early numerical modelling of primary ST's (PST's) was conducted by Imam et al, 1983 [27] who used a finite difference approach to model the flow field and distribution of suspended solids. The latter considered only discrete settling for a distribution of particle sizes and was determined with a passive scalar transport equation. They found that the numerical predictions for tank efficiency were consistently lower than those found using classical Camp theory due to non-ideal behaviour. The model was calibrated with dye testing in a laboratory tank.

Stamou et al, 1989 [58] used a similar model for flow and settlement in a rectangular PST but used a $k-\epsilon$ turbulence model in contrast to the above models which used a constant eddy viscosity. They compared their model's results with experimental data for a working primary ST under varying conditions. They reported good agreement of modelled data for solids concentration and tank efficiency. Celik & Rodi [12] produced a model that focussed on sludge bed behaviour and sediment transport.

The effects of density stratification were investigated by Zhou & McCorquodale, 1992 [69] via a buoyancy-modified momentum equation. They successfully simulated the 'density

waterfall' phenomenon and also compared two different settling velocity models with data collected from SST's in California. Lyn et al, 1992 [37] included a buoyancy term in the $k$ equation in their turbulence model and also included a simple flocculation model, whose importance was examined. The density current reproduced in these studies causes a large recirculation region in the upper parts of the tank, consistent with experimental observations.

Dahl, 1993 [14] included the mixture rheology in his SST model to account for the non-Newtonian nature of ST fluid. He outlined experimental methods used to determine rheologial and settling properties and used the model to propose improvements to a working SST resulting in a 7% improvement of effluent SS.

With increasing computer power and speeds more advanced CFD modelling of ST's was possible. Brennan, 2001 [7] created a 3D model of a SST using the drift flux model for the two-phase flow (in contrast to the scalar transport coupling used for the dispersed phase in previous models) with finite volume discretisation. His results showed good agreement with experimental observations in a SST. De Clercq, 2003 [15] produced a 2D numerical model included submodels for settling velocity, rheology and the sludge removal scraper mechanism.

Liu & García, 2011 [34] used a 3D numerical model to assist in the design of a PST being built in Chicago, USA. Griborio et al, 2014 [22] summarised the state of PST modelling with CFD and which inputs are necessary, in particular a good characterisation of particle settling velocity distributions. They evaluated two PST's with 2D and 3D models.

Authors such as Goula, 2008 [20], Hadi & Kris, 2009 [23], Tamayol et al, 2010 [60], Shahrokhi et al, 2010 [55] and Liu et al, 2011 [33], use CFD to optimise performance of various types of ST's by altering their internal configuration.

A CFD study of the effect of lamellar plates in a rectangular potable water treatment tank was conducted by Tarpagkou, 2014 [62]. They highlighted the importance of coupling the dispersed and continuous phases due to momentum transfer, a topic also discussed

by Elghobashi, 1994 [17]. Many of these studies ([62, 23, 21] used Lagrangian particle tracking models where coupling can be introduced explicitly, another feature of increased computational capacity of CFD in the 2000s.

Mazzolani et al., 1998 [40] identified weaknesses in prior modelling of settling velocities in STs. They proposed new models to predict settling velocities in heterodisperse suspensions and favourably compared them with other models. This result had previously been found by Adams & Rodi, 1990 [1]. Burt, 2010 [9] proposed an extended drift flux model for settling velocities in a SST and shows it is superior to single drift flux models. Ramin et al, 2014 [49] propose new settling velocity models to include hindered, transient and compression settling and applied it to a SST, showing its effect on sludge distribution.

Bürger et al, 2011 [8], Laurent et. al, 2014 [32] and Wicklein et al, 2016 [68] attempt to establish consistency and protocol for good modelling practice in the field of CFD for wastewater treatment. Samstag et al, 2016 [54] offer an up-to-date overview of CFD applications to different process units in wastewater treatment while identifying needs for further research. Karpinska, 2016 [28] critically reviews CFD models in activated sludge systems and provides useful comparisons of models and sub-models.

To the author's knowledge, no CFD study of a tank used for dewatering sites has been published in the literature.

# Chapter 2

# Background Theory

## 2.1 Introduction

The goal of this project was to study the flow fields and sedimentation processes inside a rectangular industrial settlement tank (ST) and investigate ways in which the performance of the tank could be improved. The tank in question is shown in Figure 2.1 and the tank will be referred to throughout the text as 'MEL5', its designation within the company itself. It is primarily used as a treatment vessel on construction sites during the dewatering process (discussed in Section 2.2). Its function is to treat outgoing site water to ensure compliance with municipal discharge requirements which include chemical parameters such as pH, TSS, BOD, COD, and heavy metals among others.

This study focuses special attention on the treatment of suspended solids inside the tank, where they settle out of suspension and form a sludge bed at the bottom of the tank. Although the tank is known to perform well in certain situations, its inner workings have never been studied and it is not known what the effect of its internal structure is on performance or what can be done to improve it.

To study the hydrodynamics of the tank the open source computational fluid dynamics (CFD) software was used and the resulting model was calibrated against existing data and

field tests. Having obtained the flow field of the fluid phase inside the tank a sedimentation model was added for the dispersed solid phase.

Improvement of tank performance was then investigated by making design adjustments and studying their effect on the flow field and settlement behaviour.

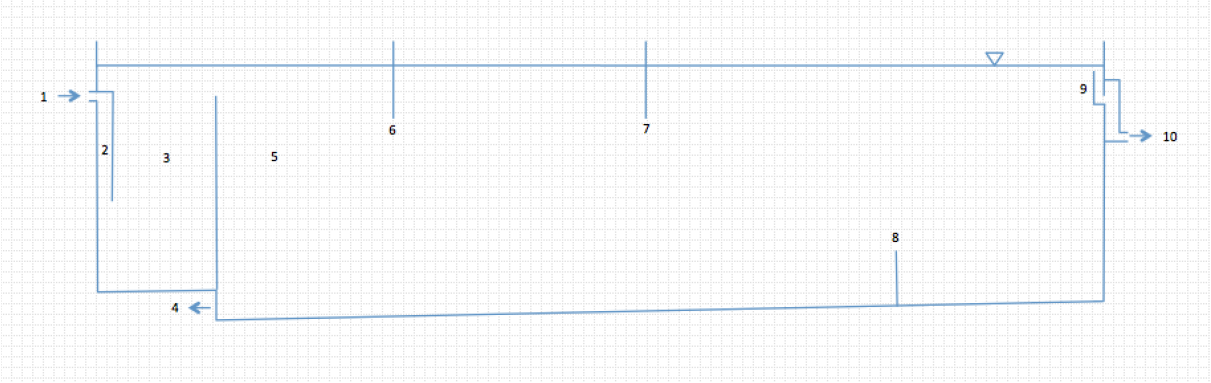


Figure 2.1: Cross section of MEL5 clarifier

| Component | | Description |
|---|---|---|
| 1 | Inlet | 75mm diameter inlet controlled by a gate valve and located at the centre (W/2) of the tank. |
| 2 | Velocity reduction chamber | Chamber designed to dissipate kinetic energy of incoming flow and distribute the flow evenly into the tank. |
| 3 | Stage 1 | This section is known as stage 1 and is designed to distribute the flow evenly into the tank. It is divided from section 2 by an internal wall. |
| 4 | Sludge withdrawal | Pipe that can be opened to withdraw settled sludge. |
| 5 | Stage 2 | This section is known as stage 2 and comprises the majority of the tank. |
| 6 | Baffle 1 | First baffle spanning the entire width of the tank designed to hold back oil. |
| 7 | Baffle 2 | Second baffle spanning the entire width of the tank designed to hold back oil passing Baffle 1 |
| 8 | Baffle 3 | Third baffle spanning the entire width of the tank and submerged to keep the sludge bed from approaching the outlet weir |
| 9 | Stage 3 weir | Sharp-crested weir spanning the entire width of the tank |
| 10 | Outlet | Several valved outlets of varying diameter |

Table 2.1: Components of the MEL5 clarifier

Its different sections and components are annotated in the Figure and detailed in Table

2.1.

To study the underlying treatment mechanisms inside the tank some background knowledge is necessary. This chapter introduces the dewatering process on construction sites such as those MEL5 is employed on, explores the basics of sedimentation theory, clarifier design, and sediment characteristics and behaviour. We introduce the concept of CFD and delve further into the mathematical formulation of the model in Chapter 3.

## 2.2 Dewatering

Dewatering is an essential part of large construction projects in areas with a high water table and also has applications in mining and tunnelling. During a construction process where the bulk dig level is below the water table the site will experience groundwater ingress [48]. The purpose of dewatering is to lower the water level to permit concrete foundations to be poured in a dry environment and maintain a safe, workable open excavation. The dewatering phase usually ends when the building is deemed to carry sufficient weight to overcome buoyancy against groundwater pressure in no-pumping conditions.

Dewatering can be achieved in a number of ways and usually involves the use of pumps. Dewatering wells are drilled or dug at strategic locations on site based on information obtained from preliminary geotechnical site investigations such as depth to rock, thickness and geology of overburden, faulted areas etc. Ideally pumping begins before digging and the water level is gradually lowered and tracked in monitoring wells.

A hydraulic barrier will exist around the site preventing re-entry of groundwater to areas that have been pumped dry and a hydraulic gradient exists. The barrier is usually a secant wall or sheet-piled wall. Thus the excavation can be thought of as a sealed box whose water level must be reduced to a certain level below that of the bulk dig.

The extracted groundwater can vary in quality between sites depending on underlying geology, previous land usage and proximity to other sources of contamination. There are

several options for effluent discharge:

- *Discharge to sewer* - A storm, foul, or combined sewer. This is the most common receptor
- *Recharge to ground* - The discharged water can be reintroduced into the ground outside the site with the secant wall providing the barrier to re-entry
- *Discharge to water Body* - A lake, river, or stream.

Associated with of these media are regulations regarding the quality and quantity of water they can receive. MEL5 is used to treat the water before discharge allowing for control over outgoing water quality parameters and continuous monitoring.

A licence is applied for through the relevant local authority that oversees management of the proposed receptor medium. They are provided with a characteristic sample of the site groundwater to assess its quality and likely impact on the receiving medium. Limits of chemical parameters and flow volume are set out in a discharge licence which must be complied with and reported on throughout the dewatering phase of the project. A typical discharge licence for a project in Dublin city centre for a construction project discharging to a storm drain over a 6 month period is shown in Table 2.2 for reference.

| Parameter | Minimum Value | Mean value limit | Maximum value | Daily Maximum |
|---|---|---|---|---|
| Temperature | - | 25°C | 25°C | - |
| pH | 6 | - | 10 | - |
| Total suspended solids | - | 400 mg/l | 500 mg/l | 240 Kg |
| Biological oxygen demand | - | 100 mg/l O2 | 200 mg/l O2 | 60 Kg |
| Chemical oxygen demand | - | 200 mg/l O2 | 400 mg/l O2 | 120 Kg |
| Chlorides (as Cl) | - | - | 12000 mg/l | 7200 Kg |
| Sulphates (as SO4) | - | - | 1500 mg/l | 900 Kg |
| Ammonium (as N) | - | - | 50 mg/l as N | 30 Kg as N |
| Mineral Oils | - | - | 10 mg/l | 6 Kg |
| Total Petroleum Hydrocarbons | - | - | 5 mg/l | 3 Kg |
| Arsenic | - | - | 0.5 mg/l as As | 0.3 Kg as As |
| Cadmium | - | - | 0.1 mg/l as Cd | 0.06 Kg as Cd |
| Chromium | - | - | 1mg/l as Cr | 0.6 Kg as Cr |
| Copper | - | - | 2mg/l as Cu | 1.2 Kg s Cu |
| Lead | - | - | 0.5 mg/l as Pb | 0.3 Kg as Pb |
| Zinc | - | - | 2mg/l as Zn | 1.2 Kg as Zn |
| Flow quantity | - | - | - | 600 $m^3$ |

Table 2.2: Typical discharge licence parameters

In the above table the mean value limit is the mean value of the parameter over a 24-hour period which can be exceeded at certain peak times to a value indicated by the maximum. The Daily Maximum column is the maximum allowed quantity discharged during a 24-hour period. The discharge licence will furthermore state the frequency of effluent sampling required (e.g. weekly) which is to be analysed by a laboratory to ensure compliance with the licence.

Ensuring the effluent complies with the discharge licence requirements is what gives rise to the need for water treatment and monitoring during the dewatering process. The tank in question has been shown to improve concentrations of all parameters most commonly found in licences on a variety of projects. Investigating its workings and potential improvements is the ultimate goal of this study.

A typical site cross Section and dewatering setup (not to scale) is shown in Figure 2.2 The cross section is bordered on either side by the secant wall which is constructed with interlocking male and female concrete piles drilled into the bedrock or aquiclude to prevent groundwater ingress from outside the excavation, essentially sealing it off. A more detailed overview of this and other cutoff methods can be found in Powers, 2007 [48]. Secant walls are not guaranteed to provide full cutoff and leaks sometimes occur.

The geological strata are described on the right hand side. The target dig level is shown in the lower clay stratum. The water table and potentiometric surfaces are shown as blue dashed lines crossing the site before dewatering has begun. In the example shown there is an upper sand and lower sand and gravel aquifer separated by a clay aquitard.

There are dewatering and monitoring wells for the upper and lower aquifers. Each of these has a water level monitor which feeds live data into a remote telemetric unit (RTU) which allows remote monitoring. The RTU also sends data from water chemistry sensors inside the tank and flow meter readings. Remote monitoring of site conditions allows for immediate alerts of problems such as pump failure or exceedance in permissible pH values and long term data is useful for project management and progress tracking.

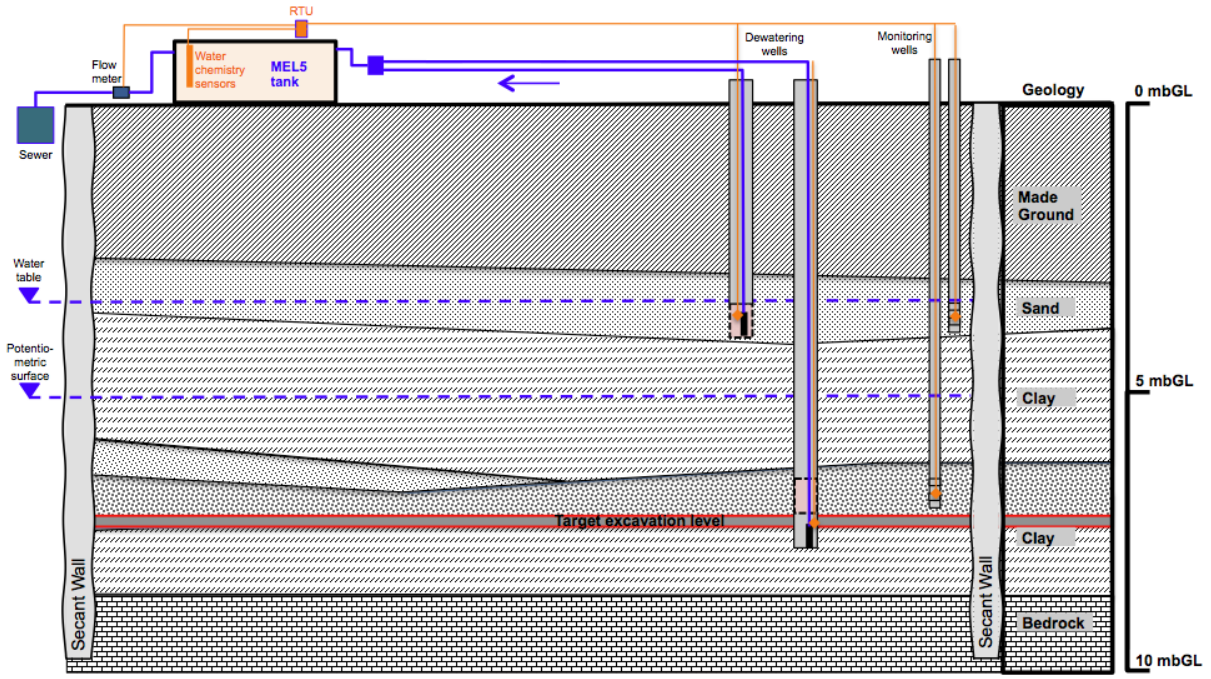


Figure 2.2: Typical site cross section and dewatering setup

A pump is installed in each dewatering well and pumps water into the MEL5 tank. The pumps are usually 110V submerisble pumps with 10m head but larger, three-phase pumps with up to 50m head are employed in sites with larger flow requirements. Water leaves the tank via the stage 3 weir and flows through an impellar flow meter before being discharged into the sewer.

The dewatering process continues until the area within the secant wall has been entirely dewatered to the target excavation level. Often dewatering continues beyond this point if groundwater ingress persists and if the building has insufficient weight to counter the upward pressure from the surrounding groundwater.

The water that enters the tank from site comes from one or a combination of sources i.e. groundwater ingress, water from construction processes such as power-hosing or concrete truck washout, or rain water. Flows can vary between trickle (<1l/s) to 10-12l/s in this area of Dublin depending on the size of the site, the productivity the aquifer, and the time of year.

The quality is typically highly turbid, especially before the foundation is poured and

(a)

(b)

Figure 2.3: Typical view of (a) an open excavation and (b) an open sump on site

the excavation is open. Two typical photos from a construction site where MEL5 was employed is shown in Figure 2.3. It is easy to see how any water that pools on the surface easily becomes laden with sediments and how necessary it is to expel this water from site in order not to delay works.

The pH of the water entering the tank is often high, i.e. frequently between 12 and 14, due to the water running under or over freshly-poured concrete or lean mix as it travels to the tank. This is usually treated with HCl dosing in the tank though this process is not addressed in this study. Some areas of the city are highly contaminated with hydrocarbons in the upper geological layers while others exhibit naturally high COD. Each site requires

individual assessment of treatment needs.

## 2.3 Clarifier design

The two primary factors to consider in the design of sedimentation tanks are [41, 58].

- suspension characteristics - types of settling dominant in the suspension (discrete, flocculated, zonal, compression)
- hydrodynamics - the flow patterns inside the tank

This section gives an overview of the theoretical concepts and approaches to clarifier design and how it relates to their operation.

### 2.3.1 Classical design

In the traditional design of primary treatment tanks the surface overflow rate (SOR), $v_0$, [4, 42] is considered to be the most influential parameter. This is due to the seminal works of Hazen, 1904 [24] and Camp, 1946 [11] who extolled its importance over other parameters such as hydraulic residence time, $\theta_r$, and tank depth, $H$, when dimensioning primary treatment tanks. The SOR is thought of as the velocity at which a particle settles a distance $H$ equal to the depth of the tank in a time $\theta_r$ equal to the tank's hydraulic residence time:

$$v_0 = \frac{H}{\theta_r} \tag{2.1}$$

Since $\theta_r = \frac{V}{Q}$ where $V$ is the volume of the tank of length $L$ and width $W$ we can rearrange to give:

$$v_0 = \frac{H}{\theta_r} = \frac{H}{V/Q} = \frac{HQ}{V} = \frac{HQ}{LHW} = \frac{Q}{LW} \tag{2.2}$$

and $v_0$ is now expressed independently of depth and retention time.
The theoretical basis for the SOR assumed that treatment tanks behaved as 'ideal basins' (see Figure 2.4) which ignored some important effects, outlined in Table 2.3. An excellent discussion on early sedimentation theory is given in chapter 6 in Hendricks, 2006 [26].

An ideal basin consists of four distinct zones, seen in Figure 2.4 [11]:

1. The inlet zone where the suspension is uniformly distributed over the vertical cross section

2. The settling zone where all settling takes place. In this zone the horizontal flow through velocity is identical at all points and given by $v_H = Q/WH$.

3. The sludge zone containing the settled particles.

4. The outlet zone where the clarified water is uniformly collected and directed out of the basin.

In an ideal basin the we can visualise the SOR, $v_0$, as the settling velocity a particle would have that allows it to settle exactly at the end of the sludge zone after starting at the top of the inlet zone for a given $v_H$ in the tank. This is illustrated in 2.5 where we can see that any particle whose settling velocity $v_s$ is less than $v_0$ will not reach the sludge zone and so will not settle out of suspension. Conversely all particles with $v_s \geq v_0$ will settle out completely. We can also think of $v_0$ as representing the smallest size particle that will settle out of suspension (assuming all particles have the same density) since $v_s$ is a function of particle diameter, discussed later in Section 2.4. Therefore if we know the diameter of the suspended solids we wish to remove from suspension we can design $v_0$ to achieve this or use it to tell us if an existing tank will be theoretically capable of removing such a particle [52].

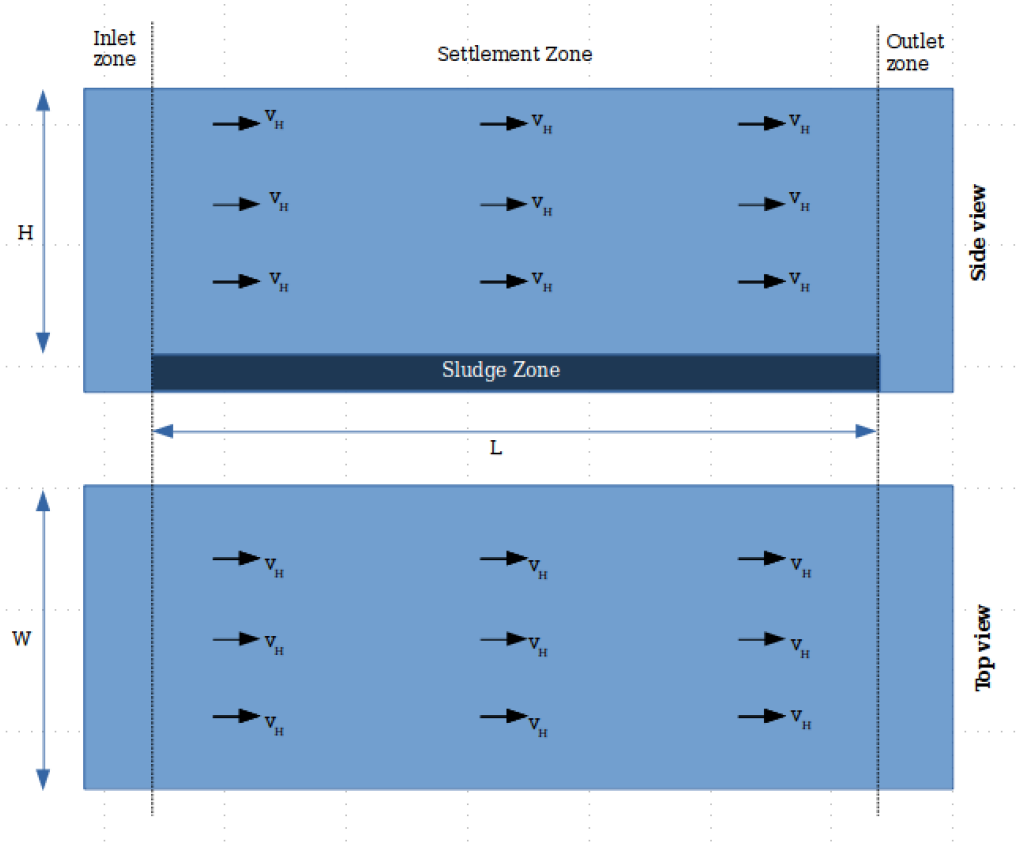


Figure 2.4: An ideal basin

Other important relationships can be derived by examining Figure 2.5 further. Using similar triangles we can deduce:

$$\frac{v_0}{v_H} = \frac{H}{L} \tag{2.3}$$

This ratio demonstrates the independence of $v_0$ on depth. For example if we were to half the depth of the tank then the horizontal flow through area would also be reduced by half ($v_H = \frac{Q}{wH/2}$) and so $v_H$ would double. At the same time the distance a particle has to settle is halved and the resulting ratio is $\frac{v_0}{2v_H} = \frac{H/2}{L} = \frac{v_0}{v_H}$, the same as before. Thus depth is not a controlling factor so long as shearing near the sludge zone does not produce scour and re-suspension of settled particles (discussed in Section 2.5.3). Equation 2.3 could also be derived by using the relationship $v_H = Q/WH$ (which is true everywhere in the settling zone of an ideal basin) with Equation 2.2.

In reality there will be a distribution of particles sizes, densities and shapes in the suspension, each member having its own settling velocity. Figure 2.5 shows us that particles with

| Assumption | Reality |
|---|---|
| The flow field is horizontal and equal in magnitude at all points in the settling zone with a velocity $v_H$ defined by $v_H = Q/wH$ where $Q$ is the flow through the tank and $w$ and $H$ are the width and height of the settling zone respectively. This implies that every particle spends an average time of $V/Q$ equal to the residence time $\theta_r$ in the settling zone whose volume is $V$. | The flow field exhibits complex interior hydrodynamics such as non-uniform flow effects which can lead to short circuiting, the existence of dead zones, vortices, velocity gradients, and back flow due to stratification. These in turn reduce the effective volume of the settling zone and thus $\theta_r$. These phenomena can have a marked effect on settling. |
| All particles are spherical and subject to ideal 'Stokes' discrete settling. | Various types of settling can occur and interact. Particles can have different shapes. |
| Particles experience a constant downward settling velocity at all points | Particles undergo a brief acceleration before reaching their 'terminal' settling velocity |
| The inlet zone has an equal concentration of solids at all points in its vertical cross section. | The concentration is not perfectly distributed. |
| A particle is deemed to be 'settled' once it reaches the sludge zone and cannot be re-suspended. | A particle can be re-suspended via scouring of the sludge zone. |
| Flow is perfectly laminar | Important turbulent effects are present |

Table 2.3: Ideal Basin Assumptions

settling velocities $v_s \geq v_0$ will settle out of suspension while particles with $v_s < v_0$ will not all reach the sludge zone and will therefore settle only partially. Assuming ideal settling where $v_s$ is directly proportional to the particle diameter $d$ let us define the fraction of particles whose diameter $d_i$ results in a settling velocity $v_i < v_0$.

Letting such a particle settle exactly at the end of the sludge zone and extrapolating back to the inlet we see that its trajectory starts at a height $h_i < H$ above the sludge zone. Thus any particle with a settling velocity $v_i < v_0$ entering the basin at a height $\leq h_i$ will settle completely. The fraction of particles with a diameter $d_i$, density $\rho_i$ and corresponding settling velocity $v_i$ that will be removed from the suspension, $\eta_i$, can then be written as:

$$\eta_i = \frac{h_i}{H} = \frac{v_i}{v_0} \tag{2.4}$$

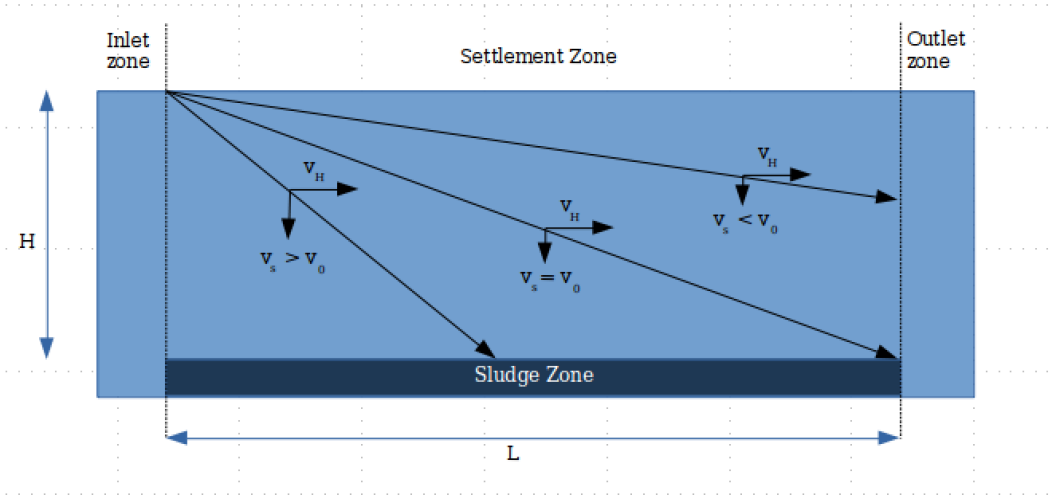


Figure 2.5: Surface Overflow Rate $v_0$

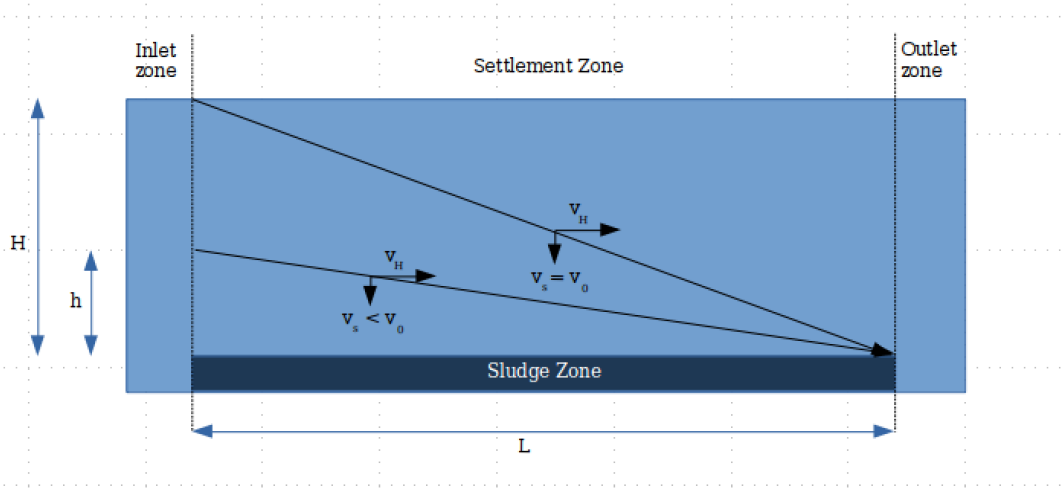


Figure 2.6: Different settling velocities in an ideal basin $v_0$

If we consider a cumulative distribution of particles with different settling velocities where the $P_0$ is the fraction of particles with settling velocity $v_0$ then we can calculate the settling efficiency of the entire size distribution, $\eta$ via:

$$\eta = (1 - P_0) + \int_0^{P_0} \frac{v_s}{v_0} dP \tag{2.5}$$

The distribution curve itself can be obtained by performing a settling column test with a sample of the suspension. The column has built-in sampling ports at different depths through which samples are taken over the course of the experiment to determine the fraction removed at each depth over time. The procedure is outlined in [11, 3, 26].

Thus in the traditional design procedure of settlement tanks $v_0$ is selected based on a given flow and the characteristics of the solids to be removed. From this $v_H$ is determined and therefore the width, $W$ of the tank keeping a fixed ratio $H : L$. Typical values from a variety of sources for different types of tank (grit, primary, secondary, tertiary, potable) are shown in Table 2.4. Although the MEL5 tank does not conform exactly to any one of these traditional categories of wastewater treatment tank types, its typical solid loading resembles that of a primary tank while the particle sizes being treated are more common to potable water clarifiers.

Table 2.4: Typical values of clarifier design parameters

| Parameter [*unit*] | MEL5 1 l/s | MEL5 2.5 l/s | MEL5 5 l/s | MEL5 10 l/s | Average flow range | Peak flow range | Tank Type | Ref. |
|---|---|---|---|---|---|---|---|---|
| SOR $[m^3/m^2day]$ | 6.6 | 13 | 33 | 66 | - | - | - | - |
| | | | | | 200-400 | - | Presedimentation | [13] |
| | | | | | 30-50 | 80-120 | Primary | [42] |
| | | | | | 32.6-40.8 | 81.5-101.9 | Primary | [66] |
| | | | | | 30-50 | - | Primary | [56] |
| | | | | | 37-60 | 110 | Primary | [58] |
| | | | | | 41 | 61-122 | Primary | [51] |
| | | | | | 16-29 | 41-65 | Secondary | [67] |
| | | | | | 150-180 | - | Potable | [52] |
| $\theta_r$ [*hours*] | 5.29 | 2.11 | 1.06 | 0.53 | - | - | - | - |
| | | | | | 2-3 | - | Presedimentation | [13] |
| | | | | | 1.5-2.5 | - | Primary | [42] |
| | | | | | 1-7 | - | Primary | [26] |
| | | | | | 1.5-2.5 | - | Primary | [34] |
| | | | | | 2-4 | - | Potable | [52] |
| Length:Width $(L:W)$ | 2.1:1 | 2.1:1 | 2.1:1 | 2.1:1 | - | - | - | - |
| | | | | | 1.5-6.5 : 1 | - | Primary | [26] |
| | | | | | 3:1 | - | Primary | [56] |
| | | | | | 2.5-5:1 | - | Secondary | [14] |
| Length:Depth $(L:H)$ | 3.6 | 3.6 | 3.6 | 3.6 | - | - | - | - |
| | | | | | 6:1 | - | Presedimentation | [13] |
| | | | | | 8.5:1 | - | Primary | [56] |
| | | | | | 4-20:1 | - | Primary | [26] |
| | | | | | 5.5-9:1 | - | Primary | [42] |

It can be seen from Table 2.4 that MEL5, which generally operates under flow rates less than $5l/s$, is within the usual design SOR range for primary clarifiers. Its hydraulic retention time is within acceptable ranges only for lower flows, and it should be borne in mind that this parameter is usually less than the theoretical value due to short-circuiting inside the tank [42]. A $\theta_r$ value could mean that particles do not have enough time to settle out of suspension, especially particles such as silt and clay which have lower settling velocities.

The dimensions of the tank generally have lower ratios than those found in the literature, in particular the tank's L:H ratio. According to AWWA, 1999[3], the L:H ratio is not as important as the L:W ratio when the depth is less than the width, which is the case with MEL5. While increasing the L:H ratio can be beneficial, its effect on cost must be taken into consideration.

WEF/ASCE, 2010[66], state that rectangular basins are generally designed to be long and narrow, with L:W ratios of between 3:1 and 5:1 as this shape is least susceptible to short-circuiting and this is also noted by WEF, 2006 [67]. The greater the L:W ratio, the better the basin conforms to plug flow conditions. A low L:W ratio could lead to end-effects dominating efficiency [3]. In this regard MEL5, with a ratio of 2.1:1, could be susceptible to short-circuiting inefficiencies though its internal design may mitigate this. Increasing the length-width ratio also has the effect of increasing the value of the Froude number which is associated with greater flow stability [30].

### 2.3.2 Lamella settlers

Following on from the idea that the available surface area for settling is more important than depth when considering tank efficiency, it was realised that inserting plates into a tank's settling zone could increase its performance by effectively reducing its SOR without increasing the physical footprint of the tank. Plates or tubes installed at an angle can also increase settling efficiency by increasing the settling area, something discovered by

Boycott, 1920 ([62]) who observed that blood settled faster in inclined test tubes compared to vertically standing ones.

Introducing parallel and inclined laminar plates (lamellas) inside a settling tank produces so-called lamella clarifiers. We define three different varieties of lamella settlers based on the direction of flow. These are:

1. 'Upflow' or 'countercurrent' where the direction of flow is opposed to that of the sliding sludge. This the most common type found in the literature.

2. 'Downflow' or 'co-current' where the direction of flow is parallel to the sliding sludge.

3. 'Crossflow' where the flow direction is accross the plates and normal to the sliding sludge.

The figure below 2.7 shows two parallel plates of length $L$ a normal distance $d$ apart inclined at a horizontal angle $\theta$ in upflow configuration. The velocity vector of a particle flowing through the plates has a velocity $v_R = v_s + v_P$ which is the sum of its settling velocity, $v_s$ and the advection velocity of the water flow between the plates, $v_P$.

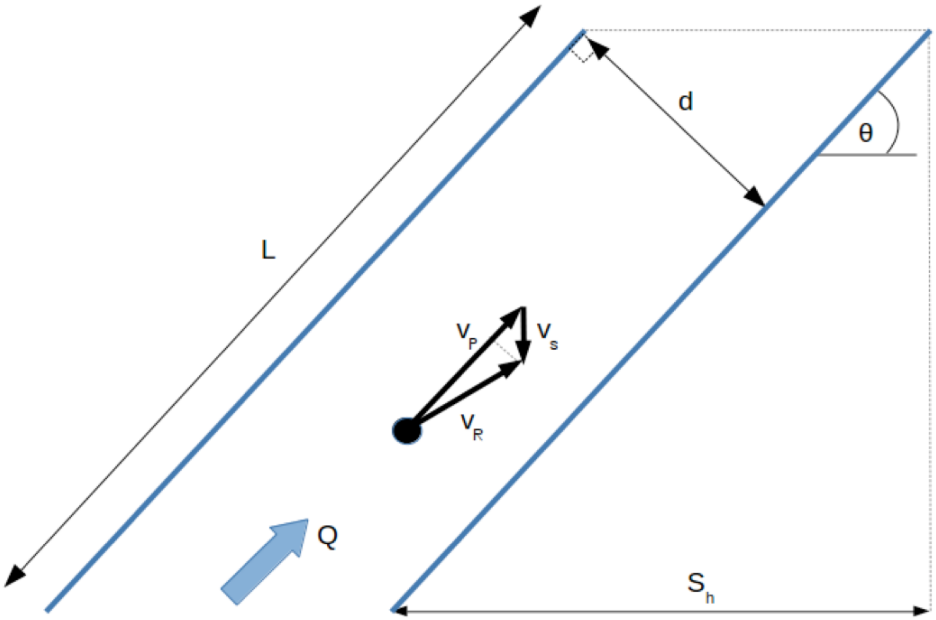


Figure 2.7: Lamellar plates

Various relationships can be derived from the above geometry. We can see that the length $L$ of one plate projected onto the horizontal plane is simply $Lcos\theta$ and so that plate's area on the horizontal plane $S_h$ is given by:

$$S_h = WLcos\theta \tag{2.6}$$

and for the whole tank with $n$ identical plates of width $W$ (that of the tank) the total projected horizontal surface area $S$ will be $S = nS_h$. This projection of the plate areas onto the horizontal plane represents the effective area for settling.

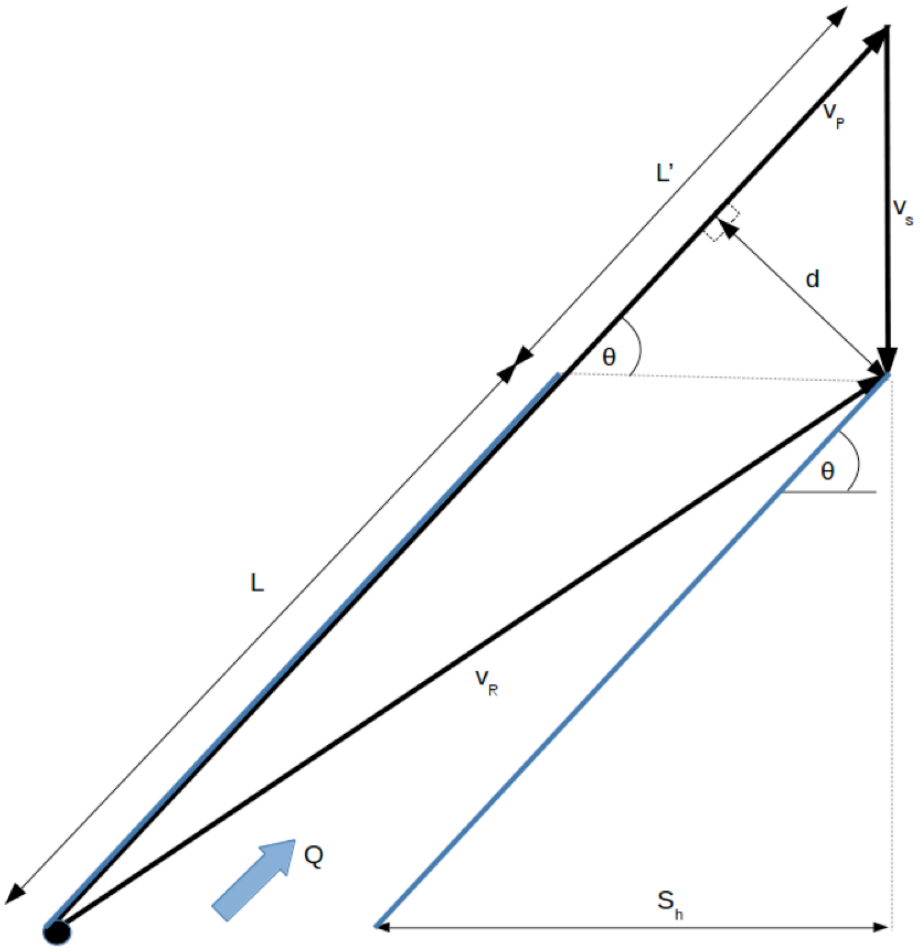


Figure 2.8: Lamellar plates vectors

If we draw velocity vectors as in Figure 2.8 using an analogous definition for the SOR whereby a particle starting at the bottom of the left plate settles exactly at the top of the right plate we can see that $v_s = \frac{d}{cos\theta}$ and $L' = \frac{v_s}{sin\theta}$ then the following relationship applies

due to similar triangles:

$$\frac{v_0}{v_P} = \left( \frac{d}{Lcos\theta + {}^{d}/_{sin\theta}} \right) \tag{2.7}$$

Rearranging and assuming $d/sin\theta \ll Lcos\theta$ allows us to write the overflow rate as:

$$v_0 \approx v_p \frac{d}{Lcos\theta} \tag{2.8}$$

Since the equivalent hydraulic loading rate is given by:

$$v_p = \frac{Q_{plate}}{W_{plate} d} \tag{2.9}$$

we can use equations 2.8 and 2.6 to write an intuitive expression for the SOR:

$$v_0 \approx \frac{Q_{plate}}{W_{plate} Lcos\theta} = \frac{Q_{plate}}{S_h} \tag{2.10}$$

An important factor to take into consideration is the critical scour velocity (see section 2.5.3, which the flow through velocity must be kept below in order not to resuspend the settled particles between the plates and WEF, 2006 [67] recommend Reynolds numbers $<$5000 between the plates.

Lamella settlers are known to be susceptible to clogging by biofouling, something that has been an issue with the company's STs on sites in the Dublin area due to iron-oxidising bacteria present in the groundwater as well as blooms of filamentous algae. The tanks used by the company are subject to frequent changes in inflow rate and concentration, which would make designing a lamellar system difficult in terms of maximising both efficiency and flexibility. The same can be said of lamellar tube settlers. Details of how to calculate the increased sedimentation efficiency after installing a lamellar system are outlined in Kowalski, 2004 [29] and general design guidelines are given in [13].

### 2.3.3 Dimensionless analysis

There are several dimensionless numbers that are useful to keep in mind for clarifier design such as the Reynolds number, Frounde number, Richardson number, Weber number, Euler number and Power number, all of which are related to the dynamics of fluid flow [26] by quantifying useful force ratios. In particular the Reynolds number $Re$ and Froude number $Fr$ are of interest in this study. They are written here as:

$$Re = \frac{\rho \mathbf{U} L}{\nu} \tag{2.11}$$

$$Fr = \sqrt{\frac{U_0^2}{g H_{in} {}^{\Delta\rho}/_{\rho}}} \tag{2.12}$$

The Reynolds number is the ratio of inertial to viscous forces, Equation 2.11, where $\mathbf{U}$ and $L$ are characteristic length and velocity scales, $\nu$ is the dynamic viscosity and $\rho$ is the density of the fluid. It is most commonly used to indicate whether or not a flow is turbulent, the ranges being $Re < 10$ for laminar flow, $10 < Re < 10000$ for transitional flow and $Re > 10000$ for turbulent flow [56]. Typically flow in ST's is fully turbulent due to the large length scales involved, even though the velocities may be low [7, 31, 69]. We note that MEL5 with a flow of 2.5l/s would have an estimated Reynolds number of 1250 in the stilling zone (stage 2) and 42441 in the inlet zone. An adequate turbulence model will thus be required to capture the turbulent behaviour of the single-phase flow. This is described in the section 3.1.1. Brennan [7] is careful to note that $Re$ alone is may not determine turbulent conditions as it does not take into account density stratification, wherein turbulence is damped out by the dispersed phase.

The Froude number is a ratio of inertial to buoyancy forces [30] and is given in Equation 2.12 where $U_0$ is the inlet velocity, $H_{in}$ the inlet height, $g$ the acceleration due to gravity and $\Delta\rho$ the difference between the mixture density $\rho_m$ and the fluid density $\rho$. In non-buoyant, single phase flows $Fr$ tends to $\infty$, and $Fr$ approaches 0 as buoyancy effects

become more important. Typical SST flows have $Fr = 10^{-4}$ [7] and should be designed to keep this number above $10^{-5}$ [13] to prevent backmixing from occurring due to the dominance of horizontal flow. As buoyancy effects become more dominant, tank depth becomes more of an important design factor according to Krebs et al, 1998[30].

Density currents (see Section 2.3.4) are an expected feature of the flow if $Fr < 1$ according to Burt, 2010 [9]. The densimetric Froude number in MEL5 is typically no lower than $10^{-2}$. Zhou & McCorquodale, 1993 [41] found that $Fr$ was a better indicator of clarifier efficiency than $Re$ and also noted that the upflow in the withdrawal zone from the sludge blanket was is inversely proportional to $Fr$ which has implications for poorly settling particles that make their way towards the end of the tank. Even small variations in $Fr$ can have a large effect on the flow field [15]. Its value can affect the optimum position of baffles [60] particularly in low $Re$ settings. Adams & Rodi, 1990 [1] suggested quantifying the importance of buoyancy based in the inlet concentration but this information alone is insufficient in high $Re$ settings [60].

### 2.3.4 Density currents

A common hydrodynamical feature of settlement tanks is the density current. This occurs due to the inflow of a heavier, more dense mixture into the fluid already occupying the tank, causing the incoming mixture to plunge to the bottom of the tank (also known as the 'density waterfall' phenomenon) and subsequently flow along its bottom (or above the sludge blanket). Its momentum is derived from the conversion of the gravitational potential energy of the inflowing mixture to kinetic energy as it falls [7, 67, 69]. The more dense inflow can be due to the presence of solids, a lower temperature difference and a higher salinity. The presence of a density current usually causes one or more large recirculation regions in the upper part of the tank directly above it. The distance along the tank floor to which the density current extends can be predicted with CFD models.

Density currents are generally considered to be undesirable [37, 53, 23]. Density currents can reflect off of the end wall of a tank and may negatively affect the effluent quality.

This in turn can affect the choice of outlet type and location. In addition a density current flowing over the sludge bed can cause resuspension of settled particles [15]. WEF, 2006 [67] note that density currents have a greater effect on activated sludge secondary clarifiers than on primary clarifiers and chemical sludges from tertiary clarifiers. The density waterfall can draw in clarified water in the upper part of the tank, reducing overall tank performance, though this can be mitigated with reactiion baffles [27, 69].

Most settling of particles takes place from the density current into the sludge bed. The rheology of the density current fluid should be considered non-Newtonian as it has important effects on its decay and turbulence properties. A vortex at the leading edge of the density current may develop, where material from the bed is picked up and deposited back into the density current, a form of scouring. Turbulence is damped in the sludge bed region and thus reduces the importance of the eddy viscosity term (see section on turbulence, Chapter 3) meaning the sludge viscosity dominates the flow and must be modelled correctly with an appropriate rheological model.

Evidence of the density current effect in the physical tank after the Stage 1 wall can be seen in Figure 2.9. Figure (a) is a photograph of two months' of sediment buildup in Stage 2 of the tank. After it has been removed the stratification marks of the bed are visible on the wall, seen in (b). Thinner, more compacted layers are on the bottom overlain by thicker, less competent layers. A distinct impression cab be seen in where the density waterfall has compressed one region more than others.

Matko et al, 1996[39] noted that density currents not only travel along the bottom of the tank but can also short circuit through the top of the tank in the winter, when the temperature of the influent is often warmer than the ambient fluid in the tank. This can occur to some degree with temperature differences as low as 0.2°. This phenomenon affects PST's more than SST's. WEF, 2006 [67] detail a range of scenarios relating to higher or lower influent temperatures and potential ramifications.


(a) (b)

Figure 2.9: Interior photo of MEL5 between Stage 1 wall and Baffle 1 (a) Before desludging (b) After desludging with visible stratification marks on wall

### 2.3.5 Modern advances

As pointed out by Dick, 1982 [16] and Imam, 1983 [27] ideal basin assumptions often fail to accurately describe tank behaviour under operating conditions and the SOR is not always a good predictor of tank performance.

Because the interior workings of settlement tanks were poorly understood by early designers the use of 'safety factors' was and often still is employed during tank design to account for non-ideal performance [67], [15]. For example a typical a safety factor of 0.65 might be applied to the overflow rate to give a design overflow rate of $v_0* = 0.65 \times v_0$.

The advent of more powerful CFD tools has precipitated significant improvements in the efficacy and cost-effectiveness of tank design though much of the industry still follows the traditional approach outlined in the above subsections [54]. Standard industry textbooks such as [4, 42, 67] still tend to teach mainly classical methods of wastewater treatment though CFD is now recognised as an invaluable tool in the process [54].

### 2.3.6 Inlet design

The reduction of a 3D to a 2D CFD model is justified by assuming uniform symmetry of the flow field in the 3rd dimension. However 3D effects are known to be present in

the inlet zone [34, 15]. The design of the inlet zone should aim to dissipate incoming turbulent kinetic energy, achieve a uniform flow distribution [7], prevent jets from travelling toward the outlet, prevent bed disturbance and short-circuiting ([4, 26]). This is usually accomplished with certain inlet baffle configurations. The baffles can be solid or perforated. In addition it is desirable to optimise flocculation conditions through mixing in the inlet zone where there is a high concentration of solids. More research is needed in this area according to Rostami et al, 2011 [53].

Lyn & Rodi, 1990 [36] studied turbulence in the inlet region of a rectangular ST and the effect of the inlet region on the downstream flow characteristics. They found that there was little difference in the flow through curves (FTC's, a measure of tank efficiency) between two different inlet baffle configurations, even though there were pronounced local differences in the flow field and inlet region lengths. The effect of variations in Reynolds number, the width-to-depth ratio, and the length-to-depth ratio were also studied. They report a marked increase in efficiency when deflectors are present in the inlet zone compared to having no deflectors present, a results previously found by [27].

In the study of Tarpagkou & Pantokratoras, 2013 [61] the Coanda effect appeared in the simulations, a phenomenon whereby fluid entering through an opening into a wider area creates an asymmetrical flow field with preferential short-circuiting to one side. This is something that may occur through the inlet of MEL5. The inlet in the single-phase simulations, Chapter 5, will be seen to distribute the flow fairly well through the tank and there is high uniformity after Baffle 1.

### 2.3.7 Outlet design

According to Stamou, 1997 [57] the outlet structures in SSTs should:

- ensure low flow velocities near the outlet, to avoid driving suspended particles towards the outlet.

- maximise the distance between the bottom layer and the outlet weir. Thus, the outlet weirs should be positioned far from the region of the rising upstream current, i.e. close to the inlet wall.

The two most common types of outlets are surface launders (overflow weirs, present in MEL5) and submerged launders (outlet tubes), the former being most often found in practice. Weirs can be oriented parallel (longitudinal weirs) or perpendicular (transverse weirs) to the flow direction and may consist of one or many units. WEF ([67]) cites options for effluent launder requirements (end wall weir trough, multiple intermediate weir troughs, submerged pipe, etc.) and emphasises its importance as a design aspect for rectangular primary clarifiers as it can reduce short circuiting and scouring, and mitigate end wall effects [4, 66].

It is logical to locate the effluent launders at the end of the tank where the most settling has occurred. However, recirculating flow patterns caused by bottom density currents may create end wall effects whereby the density current is driven upwards, possibly entraining settled solids if there is significant sludge bed buildup [41]. The surface launder can therefore be located upstream of the end wall with an inboard (facing upstream) weir, sometimes a distance of up to one third of the tank length effort to reduce velocities and carryover [4]. y increasing the surface area over which flow is collected, vertical velocity is reduced. Alternatively, deflection baffles can also be installed below the weirs to deflect the upwelling caused by the density current [67]. Scum baffles are commonly placed in front of surface launders however MEL5 uses baffles further upstream of the outlet to retain scum and oils. Alternatives to single-sided sharp-crested weirs such as the one present in MEL5 are are v-notch weirs, square opening weirs and two-sided weirs. The effect of launder moifications is greatest for cases with a very deep sludge blanket [67].

Guidelines for Weir loading rates (WLR) can be found in [67] and typical where $WLR = Q/L_{weir}$ and $L_{weir}$ is the length of the weir over which the water flows and typically values are $<200 m^3/m.day$. For low loading rates the orientation and placement is not of primary importance [67, 42]. MEL5 experiences WLR's of approximately $80 m^3/m.day$

under average flow conditions, however, it may be beneficial to introduce a second weir to reduce weir loading in high flow (>10l/s) conditions when WLR>$350m^3/m.day$.

### 2.3.8 Baffle placement

The purpose of baffles in ST's is varied and includes dissipation of turbulent kinetic energy, redirection of flow, promotion of mixing, avoiding short-circuiting and in the case of the tank in question, retention of oil and scum that floats to the surface.

Several authors have investigated optimum positioning of baffles in STs. Liu et al, 2010 [33] found that increasing baffle submergence depth in a primary rectangular ST increased the jet effect at the bottom of the baffle which in turn caused resuspension of settled particles at the bottom of the tank, while a decreasing submergence depth reduced kinetic energy dissipation resulting in more turbulent flow. An optimum value for maximum removal efficiency could be found for different operating conditions and water qualities. They concluded a relative submergence depth $H_b/H$ between 0.2-0.5 was optimal where $H_b$ is the height of the baffle in the tank. The submergence ratio of the upper baffles in MEL5 is $H_b/H = 0.22$

Shahrokhi et al., 2010 [55] studied the effects of different numbers of baffles in a rectangular primary ST and a thorough literature review of baffle effects in ST's is included. They found that optimal positioning could improve the hydraulic efficiency of sedimentation, create a uniform flow field, and minimise the recirculation region volume. The latter criterion is used for measuring efficiency. They cautioned that improper use of baffles can worsen ST performance compared to tanks without baffles.

They found that a baffle positioned on the tank floor at $x/L$=0.125 where $x$ is measured from the inlet was the optimum position for hydraulic efficiency. A later study [55] confirmed this distance and specified a submergence depth of $H_b/H = 0.176$, slightly lower than the range recommended above by Liu et al. Indeed they found that any values of $H_b/H$>0.22 resulted in a less efficient tank compared to a tank without any baffles. It

should be noted that the inlet was located on the bottom of the tanks in the Shahrokhi and Liu studies. Imam, 1983 [27] provides further guidelines for relative baffle submergence.

Razmi et al., 2009 [50], also found that the best location of a single floor baffle is at the 12.5% of the tank length from the inlet slot (the bottom of the velocity reduction chamber in this study) which would be 0.125*5.90m = 0.74m, very close to the actualy position of the Stage 1 wall. Tamayol et al. 2010 [60] suggested placing baffles on the floor of SST's to disrupt density currents and decrease short-circuiting in flows where buoyancy forces are of importance. Zhou & McCorquodale, 1992 [69] discussed the importance of reaction baffles in settling tanks to restrict entrainment of ambient fluid into the density waterfall near the inlet zone and Baffle 1 in MEL5 is helpful in this regard. Hadi & Kris, 2009 [23] added internal baffles and modified the outlet launders to reduce effluent SS in an operational ST in Slovakia by disrupting entrainment of clear water into the density waterfall.

WEF, 2006 [67] distinguish two types of floor baffles as low and high. Both can be used to disrupt the density current but can be disadvantageous under certain conditions. For example a high baffle can cause a jetting effect over its top under high loading and therefore short-circuiting to the surface. It effectively divides the tank into two tanks in series and the stage 1 wall in MEL5 acts as this type of barrier. A low baffle could increase effluent SS under dynamic loading due to plumes being entrained from the built up sludge bed upstream of the baffle. In most ST's the presence of either type would greatly complicate sludge withdrawal though in MEL5 the usual practice is to desludge the tank by emptying it of water then sucking the sludge out through a hose vacuum hose and into a tanker truck. This process would be largely unaffected by additional floor baffles. Longitudinally orientated floor baffles can be used to decrease the Reynolds number and increase the densimetric Froude number of the flow to avoid backmixing and excessive horizontal jetting [13].

## 2.4 Sedimentation theory

Sedimentation is the oldest and still the most widely used form of water treatment. The process relies on gravity to settle suspended particles out of a mixture in a container over a sufficient period of time. This conceptually simple mechanism has been advanced over centuries as engineers strive to optimise the process and modern treatment plants may incorporate not only sedimentation but biological and chemical processes as well.

The efficiency of a sedimentation tank, or settlement tank (ST, used interchangeably in this study) depends on its design, elaborated upon in Section 2.3. The optimal design of a ST depends on the sedimentation processes being considered. There are four distinct suspension types based on the particles' concentration and tendency to flocculate. These will be discussed in the following subsections and a visual summary can be seen in Figure 2.10.

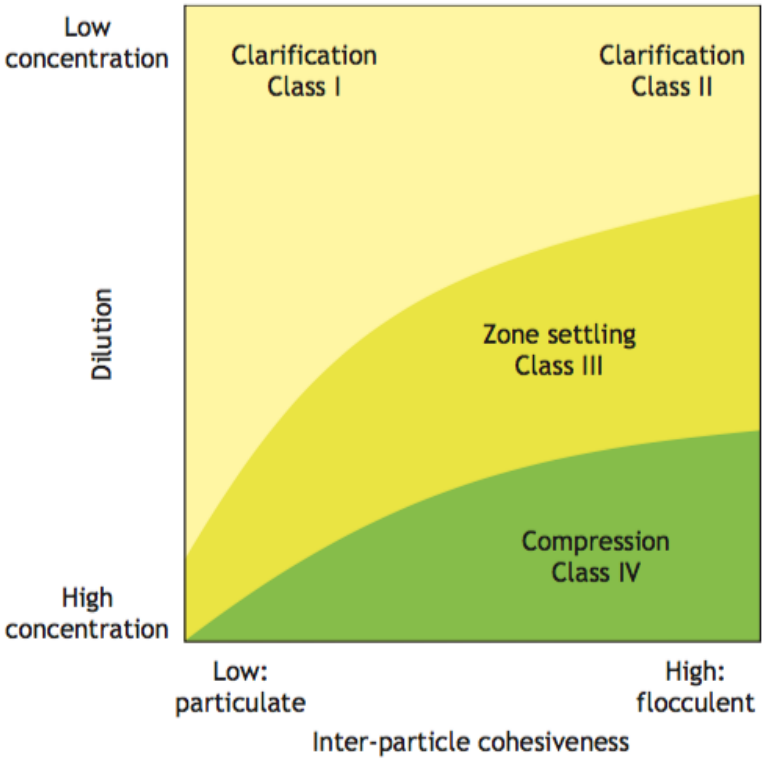


Figure 2.10: Sedimentation processes (from [63])

### 2.4.1 Type I: Discrete settling

This type of settling considers discrete, well-spaced (low concentration), non-interacting suspended particles. It is the dominant type of settling in PSTs. For this type of settling to be effective the gravitational acceleration must exceed the random Brownian motion the particles experience and thus very small discrete particles may settle poorly or not at all. Such particles are known as colloids and they remain in suspension due to their small size and negative charge [13]. Their diameters range from $10^{-9}$ to $10^{-5}$m and clay particles are a typical example [26].

Discrete settling is governed by Stokes' law which balances gravitational, drag and buoyancy forces acting on the particle. The Stokes settling velocity is given as the terminal velocity a particle reaches when these forces balance each other exactly, i.e.

$$F_g + F_d + F_b = 0 \tag{2.13}$$

Here $F_g$ is the gravitational force, $mg$, acting in the downward direction on a particle of mass $m$, diameter $d_p$, volume $V_p$ (assumed to be spherical) and density $\rho_p$. The buoyant force is given by $F_B = \rho_c V_p g$ where $\rho_c$ is the density of the continuous phase (i.e. the carrier fluid, water).

$F_D$ represents the drag force which has the form $F_D = \frac{1}{2}\rho_c C_D A_p v_s^2$. $A_p$ is the projected area of the spherical particle normal to the direction of settling (i.e. $\pi d_p^2/4$), $v_s$ is the discrete settling velocity and $C_D$ is the drag coefficient. Equation 2.13 can then be rewritten as

$$v_s = \sqrt{\frac{4gd_p(\rho_p - \rho_c)}{3\rho_c C_D}} \tag{2.14}$$

The drag coefficient has been shown experimentally to depend on the particle Reynolds number, and is given by:

$$Re_p = \frac{\rho_p |u_p - u| d_p}{\mu} \tag{2.15}$$

for a relative velocity between phases $|u_p - u|$ and nominal length scale equal to the particle diameter $d_p$ and dynamic viscosity $\mu$. In the laminar flow regime $C_D$ can be approximated by $24/Re_p$ and combining this approximation with equations 2.14 and 2.15 yields Stokes' Law for discrete settling velocity $v_s$:

$$v_s = \frac{(\rho_p - \rho_c) g d_p}{18\mu} \tag{2.16}$$

We note that $v_S$ is a function of temperature since the viscosity of water decreases with increasing temperature. Temperature also affects the fluid density as does salinity. The assumption that all suspended particles have a spherical shape is inadequate when considering the geological makeup of the particles treated by MEL5, discussed later in Section 2.5. The laminar flow condition necessary for this form of Stokes' equation is often violated in ST's. It should be borne in mind that Stokes settling is appropriate only for low Reynolds numbers and small particles as it can largely overestimate the settling velocity of larger ones [7].

### 2.4.2 Type II: Flocculated settling

Discrete particles that collide under favourable conditions (involving the particles' velocities, surface electric charges and densities) may aggregate and form 'flocs'. These flocs can gradually grow in size and settle faster as a result of thier increased mass. Chemical coagulants can be introduced into the mixture to promote flocculation.

Favourable conditions in the inlet zone occur because of turbulent mixing in the high-velocity flow field, and occur in the stilling zone because of differential settling whereby particles aligned in the vertical direction with different settling velocities overtake one another and agglomerate [3].

Flocculation processes are difficult to describe accurately with mathematical models due to the many factors that dictate it. The kinetics of various flocculation models are outlined in [9] each of which are differentiated by the cause of collisions (random motion, mixing due to velocity gradients, differential settling). Lyn et al, 1992 [37] was the first to attempt flocculation modelling in a full scale CFD study of a ST and used a population balance model. More modern approaches are outlined in [44]

Flocculation can be promoted in ST's with the addition of coagulants. Such chemicals, most often polyaluminium chloride, are sometimes employed in MEL5 when particularly high concentrations of solids are encountered, adding them to the inlet region where they mix and react. Coagulants are also necessary for very small particles that cannot settle out individually by gravity alone.

### 2.4.3 Type III: Hindered or zone settling

This type of settling takes place when, as solids concentrations increase towards the bottom of the tank, the fluid displaced upwards by settling particles is impeded by the presence of neighbouring particles. The result is an effective increase in drag and a slowing of settling. A blanket of particles forms and settles as a whole, trapping other particles underneath and a clear water zone, known as the supernatant, is formed above the blanket. The concentration at which the transition to type III settling takes place depends on the flocculation state of the suspension (see Figure 2.10 and can range from 0.5g/l to 5g/l depending on the sediment.

An early model for hindered settling was the Vesilind model [7] which describes $v_s$ as an exponentially decaying function of concentration: $v_s = Ae^{-kC}$. This largely over-predicts the settling velocity at lower concentrations. The improved double exponential model of Takács et. al, 1991 [59] is often used to describe hindered, flocculated and early compression settling using the following equation:

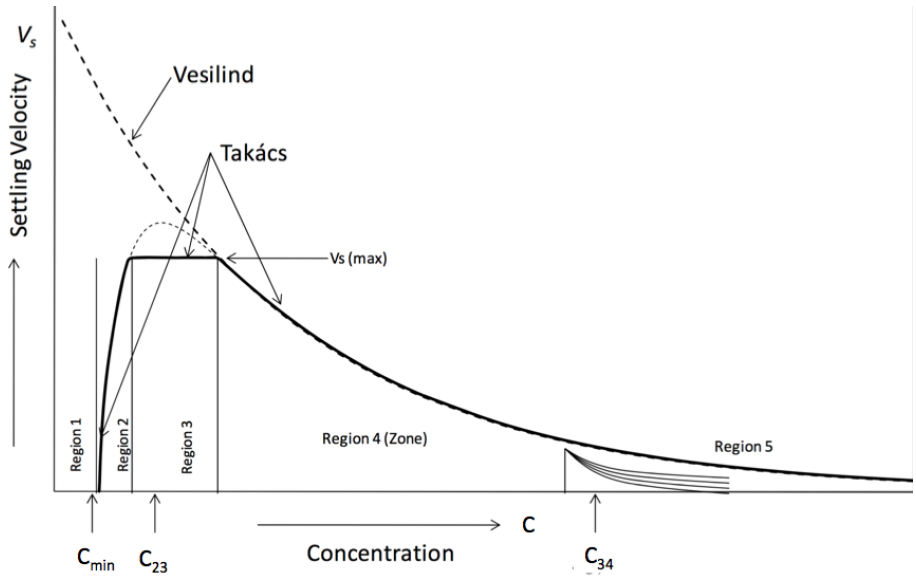


Figure 2.11: Settling velocity as a function of concentration in the Vesilind and Takács schemes (adapted from [9])

$$v_s = v_0[e^{-r_1(C-C_{min})} - e^{-r_2(C-C_{min})}] \tag{2.17}$$

were $C_{min}$ is the concentration of non-settleable particles, $v_0$ is the settling velocity of a single particle in an infinite quiescent medium (Brennan,2001), i.e. an ideal basin. $r_1$ and $r_2$ are the parameters for hindered and poorly settling particles, respectively. Typical values for secondary clarifiers are $r_1$=0.0005 l/mg and $r_2$=0.015 l/mg [7, 34]. A typical Takács curve of settling velocity as a function of concentration is shown in Figure 2.11.

The Figure depicts five regions within the Takács settling model. In region 1, concentrations are lower than $C_{min}$ no settling takes place. Type I and II settling occur in region 2 for concentrations lower than the critical concentration for type III settling $C_{23}$ at which the settling velocity reaches its maximum. At concentrations higher than $C_{23}$ after a transition period , region 3, the settling velocity decays exponentially through region 4 and this is the hindered settling zone. In region 5 type IV compression settling is initiated after a concentration $C_{34}$ (see next section).

In addition, Takács et al gave the following guidelines: (1)The concentration of unsettleable solids $C_{min}$ will be a few milligrams per litre, e.g. <5 mg/L. Burt, 2010 [9]

suggests 0.2% while WEF [67] suggest 0.1-0.3% of the initial concentration to estimate $C_{min}$. It can be seen from Equation 2.17 that when $C = C_{min}$ the settling velocity reduces to zero.
(2) Slowly settleable solids, consisting of floc that have been separated from the large floc but can be reflocculated: $C_{min} < C <$100 mg/L. These are accounted for in the second exponential term in Equation 2.17 with the parameter $-r_2$. (3) Highly settleable solids, consisting of large flocs: $C >$100 mg/L. These are accounted for in the first exponential term in Equation 2.17 with the parameter $-r_1$.

The Takács has some shortcomings outlined in [8]. Its double exponential is nonetheless superior to the single exponential Vesilind model which is known to give unrealistically high settling rates at low concentrations. An improvement to the Takács model that includes compression settling is the 'HTC model' of Ramin et al, 2014 [49].

Zhou et al, 1992 [69] showed that a 2D model using the double exponential better described the solids concentrations in secondary rectangular treatment tanks when compared to a single exponential model. Hindered settling tests were conducted as part of this study to quantify the hindered settling characteristics and are described in Section 4.2.

### 2.4.4 Type IV: Compression settling

At the bottom of the tank high concentrations of settled particles gradually accumulate on top of each other and begin to consolidate under their own weight, ejecting interstitial fluid in the process resulting in compaction over time. The concentration at which compression settling begins is $C_{gel}$, the concentration at which particles are touching each other.

This process is rarely included explicitly in CFD models presumably because of the large time-scales involved compared to type I-III settling. In addition many ST's and ST models include a constant sludge removal from the bottom of the tank before compaction can take effect.

## 2.5 Sediment characteristics

### 2.5.1 Geology

The Dublin area where MEL5 is usually employed is mostly underlain by Dublin Boulder Clay (DBC) produced during the penultimate Ice Age. The bedrock is a dark, argillaceous, finegrained Carboniferous limestone known as 'calp' limestone [35]. The DBC can be classified into four distinct formations. The typical specific gravity of these formations is 2.70 and varies little. The mineralogy is >76% clay minerals comprising a small fraction of kaolinite (i.e. 4% to 14%), with the balance being split between the illite (28% - 43%) and interstratified illite / smectite (48% - 57%). The shape of settling particles is often assumed to be spherical for simplicity. The unchanging projected area normal to the flow of a sphere simplifies the drag calculation, no torque is exerted on the spheres, etc. DBC particles, however, can be both platy and rotund while concrete dust particles at a microscale are angular [25]. For reference a microscopic view of upper black DBC is shown in Figure 2.12.

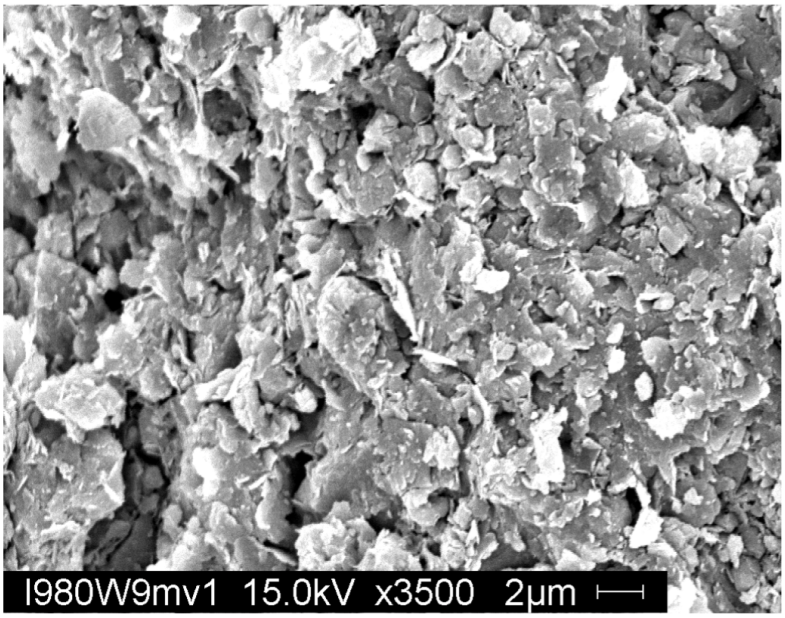


Figure 2.12: Typical view of the fabric of the upper black boulder clay (from [35])

A geotechnical report prepared for the site investigation of the location where MEL5

was recently deployed describes typical characteristics of the sediment encountered there. A sample of the same sediments were taken by the author for the batch settling tests described in chapter 5. The sediment sampled was from the soft cohesive layer of marine & esturine alluvium overlaying the DBC and it is described in the report as being *'soft grey (slightly) sandy SILT, silty CLAY or clayey SILT'.*

### 2.5.2 Cohesiveness

Sediments can be modelled as either cohesive or non-cohesive. Non-cohesive sediments comprise coarser grained particles and this type has been studied most extensively in the literature. However the smaller clay and silt particles in ST's are in reality cohesive and some assumptions made in the modelling of non-cohesive sediments are incompatible with the true cohesive nature of the sludge in ST's [7].

Cohesive sediments experience physio-chemical forces and their diameters are typically $< 60\mu m$ [65] i.e. clays and silts. In the sludge bed region cohesive characteristics are an important consideration in the context of settlement and resuspension. Cohesive sediment is considered to exist in four states: a mobile suspended sediment, a high concentration near bed layer, a newly deposited weakly consolidated bed, and a settled, firmly consolidated bed [12, 64].

Directly above the weakly consolidated sludge bed is the high-concentration near-bed region and it is from here that particles settle into the sludge bed (deposition) or are resuspended (erosion). The physical processes describing erosion and deposition differ depending on whether the sediment is cohesive or non-cohesive. Authors such as [69, 37] assume simpler, non-cohesive sediments where deposition and erosion are in equilibrium for a given bed shear stress and occur at a specified rate. Stamou, 1997 [57] cites the use of a resuspension parameter model the equilibrium exchange of particles between the bed and the density current.

Much of the literature concerning cohesive sediment bed erosion and deposition exists in

the field of sediment transport related to coastal, river and estuary engineering but the results can equally be applied to this study. In terms of applicability to ST's Dahl, 1993 [14] uses a cohesive sediment model where only flocs strong enough to settle through the high shear near-bed region will settle and resuspension only occurs when a critical shear stress is reached and described experimental methods to determine this shear stress.

Re-suspension of non-cohesive sediments assumes that each sediment particle behaves individually and is modelled with an effective diffusivity dependant on turbulent fluctuations [7]. The forces keeping the non-cohesive particles in the bed are purely gravitational and frictional. Particle movement will occur when the instantaneous fluid force on a particle is just larger than the instantaneous resisting force related to the submerged particle weight and the friction coefficient [64].

With cohesive sediments on the other hand particles are bonded to the bed and together form an aggregate structural network because the particles are small but have a large enough specific surface area to yield strong enough interparticle physical-chemical forces to be comparable with their inertia [65, 7]). They will not move until their yield stress (see Section 3.4) has been exceeded and so are not as dependent on turbulent shear stresses as non-cohesive sediments.

In terms of cohesive sludge beds, Bartzke et al., 2013 [5] found that silts have a stabilising effect on sand beds by increasing the erosion threshold and decreasing erosion rates, essentially by filling up the interstitial spaces between the sand grains. Pantet et al, 2010 [46] found that the yield stress of the bed increased with the fine fraction of solids, something elaborated upon by [65]. Berlamont et al. 1993 [6] discuss the relative complexities of characterising cohesive sediments and outline laboratory techniques to determine their physical and rheological properties. As mentioned in the previous section, the silts and clays taken from the site and modelled in this study are cohesive.

### 2.5.3 Scouring

Scouring of the sludge blanket is the process of resuspension of settled particles due to a sufficiently high horizontal shear velocity in the blanket interface region. The horizontal velocity in the tank for a flow $Q$, width $W$ and height $H$ is given by $v_H = \frac{Q}{WH}$. However as discussed in Section 2.3 this expression is only accurate for an ideal basin. One of the advantages of using CFD models in MEL5 is the ability to estimate the velocity above the sludge bed with much greater accuracy.

The scour velocity needed to resuspend a settled particle of a particular type is given by an empirical relationship known as the Shields equation 2.18, where the particle's specific gravity $SG$ and diameter $d$ affect the critical horizontal scour velocity $v_c$ at which particles can be resuspended. The parameter $\beta$ can be taken as a constant depending on the type of bed and $f$ is the Darcy-Weisbach friction factor, also taken as constant with a value between 0.01 and 0.03 depending on the bed surface roughness and the Reynolds number [26, 42, 64].

$$v_c = \left[\frac{8\beta}{f} g(SG-1)d\right]^{0.5} \tag{2.18}$$

In some wastewater treatment units such as grit chambers the scour velocity is intentionally high enough to resuspend organic particles and leave only heavier particles behind. In this study resuspension of settled clay and silt particles from the sludge bed is undesirable and the critical velocity for resuspension $v_c$ is calculated to determine whether it occurs.

Clay particles with 2$\mu$m diameter and a specific gravity of 2.65, a friction factor of 0.03 and $\beta$=0.04 will have a critical scour velocity $v_c$=0.0186m/s. 2$\mu$m is typically the smallest diameter clay particle in Dublin boulder clay [35] and thus represents a lower limit of $v_c$ with the above parameter values. Fine and medium silt particles with diameters of 25$\mu$m and 50$\mu$m would have critical scour velocities of $v_c \approx$0.06m/s to 0.1m/s respectively.

Fine-grained cohesive sediments have a greater propensity to accumulate certain contam-

inants due to their electrochemical activity. This means that a settled bed of cohesive sediment subject to resuspension can become a significant source of pollutants especially heavy metals and organic chemicals. [65].

Berlamont et al. 1993 [6] discuss the relative complexities of characterising cohesive sediments and outline laboratory techniques to determine their physical and rheological properties.

## 2.6 CFD: OpenFOAM

OpenFOAM® is a free, open source CFD software package distributed by OpenCFD Ltd and the OpenFOAM Foundation under GPL license [45]. It provides the user with a customisable C++ toolbox for numerical solver development, mesh generation and pre- and post-processing utilities for a wide range of continuum mechanics problems.

The main advantage of OpenFOAM over commercial packages like ANSYS or Flow3D is that its source code is highly modular allowing user requirements to be tailored and its inner workings easily studied. For support there is a user guide, a programmers manual, active online user forums and a user-managed wiki. It is also compatible with a wide range of pre- and post-processing packages many of which are open source also.

This study uses OpenFoam 4.1, released in June 2016, on Ubuntu 16.04.1, a Linux-based operating system for all simulations. Details of the solvers used, their mathematical formulation and solution algorithms are discussed in Section 3, the OpenFOAM case setup is detailed in Section 4 and the simulation results are discussed in Section 5.

# Chapter 3

# Mathematical formulation

## 3.1 Single-phase flows

The first part of this study involved determining the hydrodynamics inside the ST i.e. the behaviour of the single-phase flow field and how it is influenced by the internal design of the ST.

The governing equations for fluid flow are the Navier-Stokes equations for continuity (Equation 3.1) and momentum (Equation 3.2) presented below in vector form with velocity $U$, pressure $p$, viscous stress $\tau$ and $f_b$ are the body forces acting on the fluid. The terms on the left side of the momentum equation are due to unsteady flow acceleration and advective acceleration. The right side accounts for pressure gradients, viscous stresses and other body forces respectively.

$$\frac{\partial \rho}{\partial t} + \nabla \rho \cdot \mathbf{U} = 0 \tag{3.1}$$

$$\frac{\partial \rho \mathbf{U}}{\partial t} + \nabla \cdot (\rho \mathbf{U}\mathbf{U}) = -\nabla p + \nabla \cdot \tau + \mathbf{f_b} \tag{3.2}$$

For an incompressible fluid the continuity equation can be simplified to $\nabla \cdot \mathbf{U} = 0$ and

for a Newtonian fluid the viscous stress $\tau$ is interpreted as the diffusion of momentum and takes the form $\mu\nabla \cdot \left((\nabla \mathbf{U}) + (\nabla \mathbf{U})^T\right)$ where $\mu$ is the fluid viscosity, acting as a proportionality constant between the viscous stresses and shear strain rate. The body forces due to gravity are the most common and are represented by $-\rho g$ where $g$ is the acceleration due to gravity.

The Navier-Stokes are a non-linear set of partial differential equations that provide a complete mathematical model of fluid flow. There is no analytical solution for the four independent variables in the equations (except in special cases), a result of the non-linear convection term on the left hand side of the momentum equation as written above. With CFD however it became possible to generate numerical solutions that would have been too complex to calculate previously [26]. The Navier-Stokes equations by themselves do not describe particle-laden flow and must be modified to study settlement of solids, discussed below in 3.2. The very wide spectrum of important length and time scales in particle laden flows prevents detailed solution of the Navier-Stokes equations [17].

### 3.1.1 Turbulence modelling

In practice the flow quantities in the above equations exhibit turbulent oscillations in space and time, and would be difficult to resolve exactly at the smallest turbulent length and time scales. Therefore a common approach is to solve the equations in terms of the mean values of the variables of interest then introduce a turbulence closure model to approximate the smaller-scale quantities. These mean, time-averaged values are obtained by Reynolds decomposition to obtain a similar set of equations known as the RANS (Reynolds-averaged Navier-Stokes) equations.

Consider the turbulent evolution of some quantity $\phi$ at a fixed point $x_0$ given by

$$\phi(x_0, t) = \bar{\phi}(x_0) + \phi'_(x_0, t) \tag{3.3}$$

where $\bar{\phi}$ is the time-averaged value at the fixed point and $\phi'$ are the chaotic oscillations

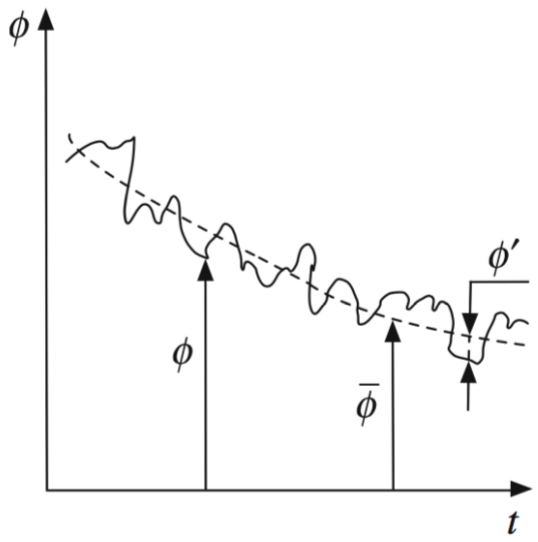


Figure 3.1: Chaotic oscillations of some quantity $\phi$ (taken from [43])

over time at the fixed point (see Figure 3.1). By substituting equation 3.3 into equations 3.1 and 3.2 for each of the quantities $\mathbf{U}$ and $p$ and using statistical averaging laws we arrive at the RANS equations as follows:

$$\nabla \cdot \bar{\mathbf{U}} = 0 \tag{3.4}$$

$$\frac{\partial \rho \bar{\mathbf{U}}}{\partial t} + \nabla \cdot (\rho \bar{\mathbf{U}} \mathbf{U}) = -\nabla \bar{p} + \nabla \cdot \mathbf{T} + \rho \mathbf{f_b} - \rho \overline{u_i u_j} \tag{3.5}$$

The additional term $-\rho\overline{u_i u_j}$, which does not appear in Equation 3.2, is known as the Reynolds stress tensor $\tau_{ij^t}$ and it represents the mean rate of transport of momentum due to turbulent velocity fluctuations. As we have introduced more unknowns into the Navier-Stokes equations without adding more equations we are faced with a closure problem which is overcome by relating $\tau_{ij}^t$ to mean flow quantities [7].

This is usually achieved using Boussinesq's 'eddy viscosity' approximation which assumes that the components of the Reynolds stress tensor vary linearly with the mean rate of strain tensor as follows: $-\overline{u_i u_j} = \nu_t({}^{dU_i}/_{dx_j} + dU_j/dx_i) - 2/3k\delta_{ij}$ where $\nu_t$ is the turbulent eddy viscosity, similar to the viscous sress - strain rate relations of a Newtonian fluid.

The underlying assumption that the transport of momentum by turbulent fluctuations is similar to random molecular motion in laminar flows and is purely phenomenological; it is not a physical viscosity. Models which are based on a turbulent (eddy) viscosity are called eddy viscosity models.

Now in addition to the Reynolds averaged continuity and momentum equations some additional equations are needed to model the turbulence closure. The $k-\epsilon$ model is one of the most commonly used in industry and academia due to its robustness, relatively low computational requirements and satisfactory accuracy [15, 28]. It is, however, known to perform poorly in regions of strong recirculation. It is also only technically valid in fully turbulent flows and not in near wall regions, thus requiring wall function implementation [7], whereby its values near solid boundaries are interpolated to the mean flow region, something OpenFOAM is capable of.

The quantities $k$ and $\epsilon$ represent the turbulent kinetic energy and its rate of dissipation, respectively. Their initial values are approximated by:

$$k = \frac{1}{2}\sqrt{\bar{u'} + \bar{v'} + \bar{w'}} \tag{3.6}$$

where $u', v'$ and $w'$ are the turbulent velocity fluctuations of the $x, y, z$ components of the velocity $\mathbf{U}$ respectively.

$$\epsilon = C_d \frac{k^{3/2}}{l} \tag{3.7}$$

where $C_d$ is an empirical coefficient and the turbulent viscosity is defined in terms of $k$ and $\epsilon$ by:

$$\nu_t = C_\mu \frac{k^2}{\epsilon} \tag{3.8}$$

where $C_\mu = 0.09$ is a commonly used empirical coefficient.

Two transport equations for $k$ and $\epsilon$ are then introduced as follows:

$$\frac{\partial k}{\partial t} + U_j \frac{\partial k}{\partial x_j} = \frac{\mu_t}{\rho} S^2 - \epsilon + \frac{\partial}{\partial x_j}\left[\frac{1}{\rho}(\mu + \frac{\mu_t}{\sigma_k})\frac{\partial k}{\partial x_j}\right] \tag{3.9}$$

$$\frac{\partial \epsilon}{\partial t} + U_j \frac{\partial \epsilon}{\partial x_j} = \frac{\epsilon}{k}\left(C_{1\epsilon}\frac{\mu_t}{\rho} S^2 - C_{2\epsilon}\right) + \frac{\partial}{\partial x_j}\left[\frac{1}{\rho}(\mu + \frac{\mu_t}{\sigma_\epsilon})\frac{\partial \epsilon}{\partial x_j}\right] \tag{3.10}$$

These equations include 5 free constants $\sigma_k, \sigma_\epsilon, C_{1\epsilon}, C_{2\epsilon}, C_\mu$ for which the $k$-$\epsilon$ model has standard values. The standard k-$\epsilon$ model outlined above is one of many turbulence models. Theoretically, the traditional high-Reynolds k-$\epsilon$ model is restricted to locally isotropic and highly turbulent flows [15]. Karpsinka & Bridgeman, 2016 [28] provide an overview of some of the most commonly applied turbulence models and their respective advantages and disadvantages. An appropriate turbulence model is necessary and considered good modelling practice in ST studies [68].

Turbulence modelling in two-phase models needs to take account of the effect of the dispersed phase on the turbulence quantities. Brennan, 2001[7] highlights the need for a buoyancy production term in the $k$ equation and found turbulent production was damped in the density current by the density stratification, reducing turbulent viscosity and the transfer of momentum out of the density current by mixing. The need for including a buoyancy term depends on the degree to which buoyancy effects dominate the flow, indicated by the densimetric Froude and Reynolds numbers (see Section 2.3.3 Lyn & Rodi, 1992 [37] showed that in density stratified flows the eddy viscosity depends on stratification and that the inclusion of stable stratific ation effects in the $k$-equation resulted in a marked general decrease in the ratio of turbulent viscosity to fluid viscosity $\nu_t : \nu$. The degree of coupling (see Section3.2.1) between phases influences the turbulence, enhancing production when the particle relaxation times are long and enhancing dissipation when short [17].

Later it will be shown that turbulence is damped to such a degree by the presence of

particles in the sludge bed region, where concentrations are highest, to the point where the eddy viscosity is smaller than the mixture viscosity of the slurry, which is how the model simulates the sludge bed evolution (Section3.4).

## 3.2 Multiphase flows

Multiphase flows are of interest in fields such as chemical, automotive, environmental, industrial process and bio engineering. They are used to describe mixtures of any combination of gas, liquid and solid phases. This is a study of two-phase flows, one phase being a continuous fluid phase and the other being a dispersed solid phase. We define three principal frameworks used to model two-phase flows: Euler-Euler, Euler-Lagrange, and mixture approaches. A summary of these approaches and their usefulness can be found in Karpinska et al, 2016 [28].

We first describe Eulerian and Lagrangian formulations in fluid mechanics. The Eulerian formulation can be thought of as a 'field' approach in which the equations of motion are solved to produce a field in time and space in which any physical quantities associated with the flow (such as pressure, velocity, density) are defined at every point.

On the other hand the Lagrangian formulation can be thought of as a 'particle' approach where individual particles or fluid parcels are tracked through the fluid. The resulting trajectories are used to infer flow field properties as the momentum of each particle is influenced by the sum of forces acting on it (such as drag, lift, viscous stresses etc.)

While hydrodynamical modelling has advanced significantly over the past 30 years with CFD the same cannot be said for the modelling of settleability of solids, the weakest part of modelling ST's [8]. There are many factors to consider when modelling settlement of a dispersed solid phase within a fluid phase such as the degree of coupling between the phases, the importance of different forces acting on the particles, how accurately the particles' physical properties are represented in the model, the effect of particles on turbulence and which mathematical model is best suited to the case at hand.

### 3.2.1 Euler-Lagrange modelling

In the Lagrangian formulation each individual dispersed phase particle is tracked by computing its trajectory within the continuous phase (which is treated in an Eulerian manner). The particle's local acceleration is expressed as the sum of forces acting upon it at each point along its trajectory.

The equation of particle motion in its simplest form is written as:

$$\rho_d \frac{du_d}{dt} = \sum_i F_i \tag{3.11}$$

where subscript $d$ denotes the dispersed phase and $F_i$ are the individual forces acting on it. A more complete description of each term in $F_i$ can be found in [17] and [21] they are omitted here for brevity.

The Lagrangian particles can be coupled to the flow field to reproduce momentum and energy transfer between the solid and liquid phases which can significantly affect the flow field, increasingly so for higher volume fractions and larger particle diameters [61].

There are three possibilities - one-way coupling, two-way and four-way coupling. In one-way coupling only the effect of the continuous phase on the dispersed phase is taken into account and particles simply follow the flow lines of the carrier fluid passively. In two-way coupling the continuous and dispersed phase affect each other and inter-phase momentum exchange must be taken into account. Four-way coupling (also known as granular flow) adds particle collision modelling to two-way coupling with, i.e. the particles affect each other as well as affecting, and being affected by the carrier fluid. The degree of coupling is based on the volume fraction. In the literature the consensus is that one-way coupling is acceptable for suspended solids concentrations of <150-200mg/l [33, 34, 58]. Elghobashi [17] recommended one-way coupling for dispersed phase volume fraction $\alpha_d < 10^{-6}$, two-way coupling for $10^{-6} < \alpha_d < 10^{-3}$ and four-way coupling for granular flows with $\alpha_d > 10^{-3}$.

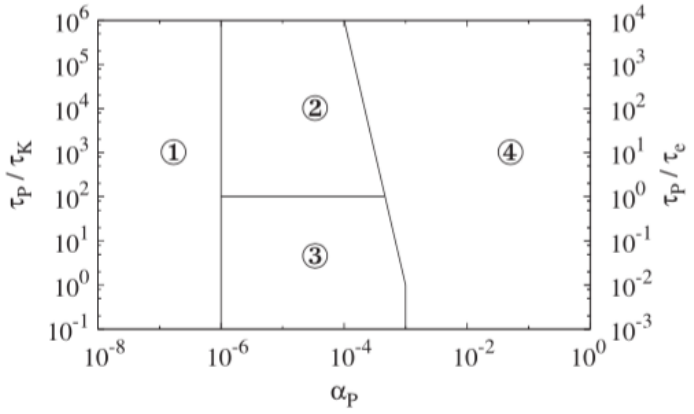


Figure 3.2: Classification of coupling with (1) one-way coupling, (2) two-way coupling where particles enhance turbulence production, (3) two-way coupling where particles enhance turbulence dissipation, and (4) four-way coupling.(from [21])

Figure 3.2 depicts Elghobashi's coupling classifications as a function of volume fraction. A distinction is made in the two-way classification regarding its effect on turbulence depending on the ratio of the particle's relaxation time $\tau_p = {\rho_p d_p}/{18\mu}$ and the Kolmogorov time scale $\tau_K = \left({\nu}/{\epsilon^2}\right)$. $\tau_p$ is a measure of how long a particle takes to return to equilibrium after being perturbed by an applied stress and $\tau_K$ is the turnover time for the smallest scale turbulent flow eddies. The nature of the particles being treated by MEL5 and their concentrations would suggest classification (3) in which two-way coupling enhances turbulence dissipation due to an increased dispersed phase surface area. Greifzu et al, 2016[21], investigated dispersion models and found that particle motion in dilute suspensions ($\alpha_d < 10^-6$) is influenced mainly by the hydrodynamic forces acting on the particles and that in these cases one-way coupling is considered sufficient, which in MEL5 would correspond to concentrations of <10mg/l. In other words two-way coupling is almost always needed.

Burt, 2002 [10] demonstrated that Lagrangian particle tracking models are unsuitable for modelling sedimentation in combined sewer overflow side weir units as the hold up is not accurately accounted for, with particles numerically disappearing from the simulations in order to achieve steady state solutions. They found the multiphase Eulerian CFD model to be a better predictor of experimental results.

One advantage of this formulation is that it tracks individual particles or packets of

particles and therefore it is possible to define detailed particle characteristics such as shape, size and density. It has been used in scenarios with low volume fractions (such as potable water treatment tanks) and negligible bed effects [20, 62, 23].

In ST's the number of particles is so large that the Lagrangian approach is considered too computationally expensive to solve the equations of motion for each one [7, 28] and the upper limit of computational capability is considered to be 10-12% volume fraction of solids [15, 20]. For this reason it is often rejected and was therefore not chosen for this study.

### 3.2.2 Euler-Euler modelling

In the Euler-Euler approach both phases are treated in the Eulerian formulation. Both phases are treated as inter-penetrating continua and the 'two-fluids model' is derived by statistical averaging techniques [7, 38]. There are four equations to be solved in the two-fluids model - one continuity and one momentum equation for each phase. Each phase $i$ is treated as a volume fraction $\alpha_i$ in each computational cell which sum to 100% of the cell's volume. The volume fraction can be related to the concentration of the dispersed phase via the particle density: $C = \rho\alpha$.

The phases are coupled via inter-phase exchange terms defined as sources or sinks in the conservation equations. Momentum exchange in a treatment tank can tank the form of lift, drag, buoyancy or other subgrid scale forces. These are modelled with constitutive relations based on the physical processes or experimental correlations, many of which are case-specific [28] and necessary to close the equation set.

Thus the modified Navier-Stokes equations for multiphase flow in the Eulerian formulation are presented in equations 3.12 and 3.13 where summation over $i$ phases is implied and $\tau_i^t$ is due to the Reynolds stress tensor of the phase $i$, discussed in the previous section. The additional $\mathbf{M}$ term represents the interfacial momentum transfer between each phase

[38].

$$\frac{\partial \alpha_i \rho_i}{\partial t} + \nabla \cdot \alpha_i \rho_i \mathbf{U}_i = 0 \tag{3.12}$$

$$\frac{\partial \alpha_i \rho_i \mathbf{U}_i}{\partial t} + \nabla \cdot (\alpha_i \rho_i \mathbf{U}_i \mathbf{U}_i) = -\alpha_i \nabla p + \nabla \cdot \left[\alpha_i (\tau_i + \tau_i^t)\right] + \alpha_i \rho_i \mathbf{g} + \mathbf{M}_i \tag{3.13}$$

It is assumed the same pressure acts on both phases. The momentum transfer term is inherently problematic and its calculation causes instability in numerical models [7, 15] Whether or not it is necessary to include this term depends on the degree of coupling between the phases. In the case of ST's this is influenced by the concentration of suspended solids and their densities [17]. Degrees of coupling are discussed in greater detail in the above Section 3.2.1. If one way coupling can be assumed then $M_i$ can be approximated as zero.

Another limitation of the Euler-Euler model is that the properties of each sludge particle (such as density, shape, settling velocity) may in reality be distributed over many value and though it is possible to capture each of these explicitly in the model by solving for a large number of phases $i$, this would require large computational effort.

According to Tarpagkou & Pantokratoras 2013 & 2014 [61, 62] the Euler-Euler approach is used for almost all diffusion-dominated problems in the literature. Brennan, 2001 [7] notes that the approach may be over-elaborate for modelling ST's. A simplified Eulerian approach known as the 'drift flux' formulation was chosen for this study and is described in the next section.

### 3.2.3 Mixture modelling of two-phase flows

The drift flux model (also known as the algebraic slip model or the homogeneous mixture model) [9, 28, 34]is derived from the Euler-Euler two-fluid model. Whereas the two-fluid model solves the continuity and momentum equations for each individual phase and couples them via interfacial momentum transfer terms ($M_i$ in equation 3.13), the drift flux model solves a single continuity and momentum equation for the mixture as a

whole. In other words, the two phases are treated together as a single fluid mixture whose properties such as velocity, pressure and density are properties of the mixture and not of the individual phases.

The phases are related as follows for a two phase mixture:

$$\alpha_c + \alpha_d = 1 \tag{3.14}$$

$$\rho_m = \rho_c \alpha_c + \rho_d \alpha_d \tag{3.15}$$

$$\mathbf{U}_m = \frac{\alpha_c \rho_c \mathbf{U}_c + \alpha_d \rho_d \mathbf{U}_d}{\rho_m} \tag{3.16}$$

The subscripts $c, d, m$ refer to the continuous phase, the dispersed phase and the mixture centre of mass, respectively. In addition to the continuity and momentum equations a diffusion equation is specified for the dispersed phase transport using a constitutive relationship for the movement of the dispersed phase relative to the mixture centre of mass. The detailed mathematical description of the coupling between the phases is replaced by a constitutive relationship in which the relative motion of the dispersed phase is assumed to be constant.

Thus a total of three equations are required to represent the drift flux model and it is therefore advantageous compared to the two-fluid Eulerian model which requires four equations, two of which include the troublesome interfacial momentum transfer terms. However some information about the detailed movement of the phases is lost when we approximate it by kinematic constitutive equations [7] and it is only valid under certain conditions.

A fundamental assumption of the drift flux model is that the primary source of slip between the phases is gravitational settling of the dispersed phase. This is valid only if the

dispersed phase particles have a short relaxation time for interphase momentum exchange through drag. If this is the case then the particles will approximate perfect advection through the continuous phase in the streamwise direction while possessing a fixed settling velocity relative to this motion in the vertical direction i.e. local equilibrium is reached over a short spatial length scale. This close coupling between the phases is essential for the drift flux approximation to be valid. It is not valid for large particles such as coarse sand or particles that undergo a phase change. An approximate relaxation time for a single clay particle is $0.5\mu s$ and for a single fine silt particle $90\mu s$.

The full derivation of the drift flux equations is not presented here (the reader is referred to Manninen, 1996 [38]). Essentially the Navier stokes equations are written in terms of the mixture quantities $(\alpha_m, \rho_m, \mathbf{U}_m)$. A 'diffusion velocity' is defined relating the velocities of each phase to the mixture centre of mass velocity $\mathbf{U}_m$. The diffusion velocity then is related algebraically to the drift velocity of the dispersed phase (i.e. the settling velocity in this case) which can be used as an input for the model after being obtained experimentally in settling tests. This model is the one most frequently used in clarifier modelling [9, 67].

The equations, presented below are the mixture continuity equation (Equation 3.17), the diffusion/dispersed phase continuity equation (Equation 3.19, used to calculate the distribution of the dispersed phase within the solution), and the mixture momentum equation (Equation 3.18).

$$\frac{\partial \rho_m}{\partial t} + \nabla\cdot(\rho_m \mathbf{U}_m) = 0 \tag{3.17}$$

$$\frac{\partial \rho_m \mathbf{U}_m}{\partial t} + \nabla\cdot(\rho_m U_m U_m) = -\nabla p_m + \nabla\cdot(\tau + \tau^T) - \nabla\cdot\Big(\frac{\alpha_d}{1-\alpha_d}\frac{\rho_c \rho_d}{\rho_m} U_{dj} U_{dj}\Big) + \rho_m g + M_m \tag{3.18}$$

$$\frac{\partial \alpha_d}{\partial t} + \nabla\cdot(\alpha_d \mathbf{U}_m) = -\nabla\cdot\Big(\frac{\alpha_d \rho_c}{\rho_m}\mathbf{U}_{dj}\Big) + \nabla\cdot\Gamma\nabla\alpha_d \tag{3.19}$$

Here $\tau^T$ is the turbulent stress term and $u_{dj}$ is the drift velocity of the second phase whose

value is determined by experiment. $p_m$ is the mixture pressure which is averaged between the phases although each phase in practice is assumed to be subject to the same pressure [38]. The most noticeable difference between this momentum equation is and Equation 3.13 is the additional term

$$\nabla\cdot\Big(\frac{\alpha_d}{1-\alpha_d}\frac{\rho_c\rho_d}{\rho_m}U_{dj}U_{dj}\Big) \tag{3.20}$$

which can be thought of as an extra stress term representing additional diffusion of momentum due to the relative motion between the phases. The third equation in the model, 3.19, is needed to predict the motion of the dispersed phase in the form of a standard convection-diffusion equation in terms of the relative settling velocity and the mixture terms.

There exist other formulations of this model that incorporate multiple diffusion equations for the dispersed phase, each corresponding to a different drift velocity (i.e. multiple populations of dispersed particles with a different settling velocities) thus allowing modelling of a range of particle diameters and densities (making the necessary extensions to equations 3.14 - 3.16). See for instance [9, 34]. The solver that uses the drift flux approach in OpenFOAM allows for modelling only of one dispersed phase. It calculates the settling velocity $\mathbf{U}_{dj}$, hereafter refered to as $v_s$, from the hindered settling model of Takács (Section 2.4.3) whose parameters $v_0, r_1, r_2, C_{min}$ are model inputs.

The viscous stress terms $\tau$ in this set of equations require non-Newtonian treatment in two-phase models because the apparent viscosity of the suspension is affected by the addition of the dispersed phase, an effect most pronounced in and directly above the settled sludge bed as it is a function of the solids concentration. The bed can become liquidised or fluidised under certain shearing conditions. See Section 3.4 for further details.

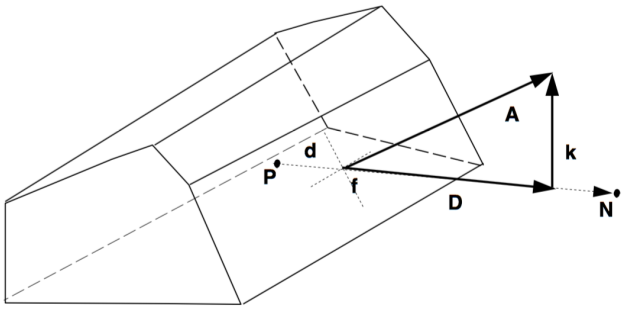


Figure 3.3: Arbitrary discretised polyhedral cell (from [7])

## 3.3 CFD discretisation

OpenFOAM uses the finite volume method (FVM) numerical technique in all of its solvers. It is the most widely used technique in modern CFD and is popular due to its flexibility with regard to domain discretisation and boundary condition application. [43, 67].

The solution domain is divided into a number of polyhedral cells known as finite volumes which form a grid. The system of partial differential equations describing the fluid flow are then converted to a set of linear algebraic equations on this grid and can be solved numerically.

The cells are contiguous (i.e. they are non-overlapping and completely fill the domain) and can have any number of faces but generally are either prisms or hexahedra. The faces are flat and are shared with only one neighbouring cell face. The dependant variables are stored at the cell centres ('co-located') and then interpolated to the faces via a user-defined interpolation scheme.

Figure 3.3 shows a typical control volume with the computational point $P$ at its centre. $P$ is connected with the neighbouring cell's centre point $N$ via the vector $\mathbf{d}$. Each face has an associated normal vector pointing out of the control volume with a magnitude equal to the area of the face, $\mathbf{A}$.

Discretisation of the equations is achieved using the divergence theorem for the flux of a

quantity $\phi$ through a closed surface:

$$\int_f \nabla \cdot \phi dV = \int_S \phi \cdot dS \tag{3.21}$$

Thus we see how differential functions of variables of interest in the Navier-Stokes equations such as $U$ are written numerically by being integrated over control volumes $V$ to produce surface integrals over the control volume's bounding faces $S$ which can be summed. Each type of term (convection, diffusion, source etc.) requires its own type of treatment

For example the continuity Equation 3.1 can be discretised as follows:

$$\int_V \nabla \cdot U dV = \int_S U \cdot dS \approx \sum_f d\mathbf{A} \cdot U_f \tag{3.22}$$

where $U_f$ is the interpolated value of $U$ at the face, calculated from its value in the owner and neighbouring cell centres $P$ and $N$. The result is a sum of fluxes through the faces. The discretisation of the momentum equation is less straight forward. The convection term $(\nabla \cdot UU)$ is linearised to take the form $a_P U_P + \sum_N a_N U_N$ and thus the semi-discretised momentum equation is written as:

$$a_P U_P + \sum_N a_N U_N = r - \nabla p \tag{3.23}$$

where $a_P$ and $a_N$ represent all coefficients associated with the velocities at the centre of the cell $(U_P)$ and the sum of its neighbouring points $(U_N)$ respectively, $r$ are the unsteady source terms and the pressure gradient is kept in its original form. By introducing the operator $H(U) = r - \sum_N a_N U_N$ the equation is algebraically solved for $U$ in each cell as follows:

$$U_p = a_P^{-1}\big(H(U) - \nabla p\big) \tag{3.24}$$

Using equation 3.22 with equation (3.24) above allows us to write the pressure equation:

$$\nabla \cdot (a_P^{-1} H(U)) = \nabla \cdot \left(a_P^{-1} \nabla p\right) = \sum_f \left(a_P^{-1} H(U)\right)_f \tag{3.25}$$

(3.25) and (3.24) effectively define the discretised form of the Navier-Stokes equations necessary for their solution on the FVM grid. A more detailed explanation of the derivations of the final system of equations can be found in [7, 43] as well as the FVM methodology for discretising boundary conditions. Solving these systems of equations numerically requires the use of iterative pressure-velocity coupling algorithms such as the SIMPLE and PISO algorithms which are used by the solvers in this study and discussed further in Section 4.

Both algorithms involve calculating an estimated velocity field from Equation (3.23) using a guessed pressure (usually the pressure from the previous time step). The estimated velocity is used to solve an estimated pressure from (3.25) but it will not yet satisfy continuity and so further corrections are made to it, and the momentum equation can then be rewritten in terms of those corrected velocities and pressures and iterated until convergence. PISO, in contrast to SIMPLE, uses explicit calculations (i.e. based on the previous time step) to solve the momentum equation and it is time-dependent meaning the unsteady terms must be dealt with. A detailed mathematical description of both algorithms can be found in [43, 47].

## 3.4 Sludge rheology

Rheology is the study of flow and deformation of fluids under applied forces. In the context of ST modelling it can have significant effects on the transport and overall removal of solids as well as on bed flow and turbulence. Gathering data for rheological properties should be considered a priority to produce an accurate model [15, 34, 49].

The rheology of the flow of a single continuous phase inside the tank can be described as Newtonian, meaning there is a linear relationship between the applied shear stress and

rate of deformation of an infinitesimal fluid parcel. This is expressed as:

$$\tau = \mu\dot{\gamma} \tag{3.26}$$

where $\tau$ is the applied shear stress, $\dot{\gamma}$ is the strain rate and $\mu$ is the dynamic viscosity.

The presence of a dispersed solid phase introduces non-Newtonian behaviour into the system, i.e. the strain rate no longer varies linearly with the shear stress. This is due to the complex micro-structure of the solid particles and their influence on the continuous phase. Non-Newtonian behaviour is negligible for low concentrations (concentrations <4% by weight according to Brennan, 2001 [7]. The critical concentration to transform a Newtonian to a non-Newtonian fluid is highly dependent on the concentration of fines according to Wang, 2013 [65].

Non-Newtonian fluids can display shear-thinning (plastic or pseudo-plastic) or shear-thickening (dilatant) behaviour. The viscosity of a shear-thinning fluid reduces with increasing shear rate while the viscosity of a shear thickening fluid increases with increasing shear. The relationships between Newtonian and different kinds of non-Newtonian fluids are summarised in figure 3.4.

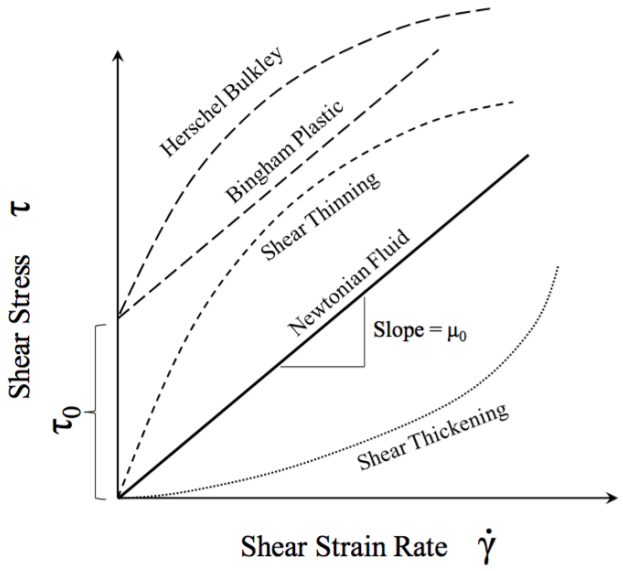


Figure 3.4: Rheogram depicting various rheological regimes (adapted from [9])

Sludges in ST's exhibits shear-thinning behaviour. They may or may not possess a yield

stress $\tau_0$, a threshold value below which there will be no plastic deformation (refer to figure 3.4). When $\tau_0$ of a settled bed is exceeded it will begin to flow due to the breakup of the interparticle structural network [65]. The yield stress depends on the inter-particle forces and concentration of particles. In addition ST sludge may be thixotropic, meaning its apparent viscosity is time-dependent as well as shear-thinning due to changes in its internal structure as it deforms [15].

Non-Newtonian fluids have an apparent viscosity (or plastic viscosity for a shear-thinning fluid) which changes with concentration and applied stress. It is found at any point on the rheogram by the gradient of the curve $\tau(\gamma)$. A general representation for shear thinning fluids in tensorial form is:

$$\tau_{ij} = \tau_0 + K(\dot{\gamma_{ij}})^n \tag{3.27}$$

where $\tau_{ij}$ is the three dimensional stress tensor, $\tau_0$ is the yield stress, $K$ is the consistency coefficient (measured in $kgm^{-1}s^{-1}$) and $\gamma_{ij}$ is the strain rate tensor. Two common models are derived from equation 3.27. The Bingham plastic model is one of the most commonly applied to wastewater CFD models. It is the limiting case of equation 3.27 where n=1 and $K$ is the plastic viscosity. In this model the rate of strain and shear stress have a linear relationship, similar to a Newtonian fluid, but only after the yield stress has been exceeded. This model was used in the studies of Brennan [7], Dahl [14] and Liu & García [34] to name a few.

The Herschel-Bulkley model takes the form of equation 3.27 with $0 < n < \infty$. Several authors have argued that the Herschel-Bulkley model is more suitable than Bingham's for low strain rates ($<20s^{-}1$) over muds. It provides a more realistic power law increase in effective viscosity after the yield stress $\tau_0$ has been exceeded whereas the Bingham model exhibits a linear increase [9, 65]. It has been used in the studies of Burt [9] and de Clercq [15]. The Bingham and Hercschel-Bulkley models are the two most commonly implemented models in the literature [54] and the Bingham model was chosen for this

study.

The yield stress $\tau_0$ and plastic viscosity $\mu_0$ need to be modelled with constitutive relationships which take the form

$$\Phi = aC^{b\alpha} \tag{3.28}$$

where $\Phi$ is the physical quantity (i.e. $\tau_0$ and $\mu_0$), $a$ and $c$ are constants fitted to experimental data, $C$ is the exponent set (often $e$ or 10) and $\alpha$ is the volume fraction of the solids.

Turbulence modelling is also affected by non-Newtonian behaviour due to damping of the turbulent and viscosity field. In regions of high particle concentration, in particular the sludge blanket region, the non-Newtonian molecular viscosity becomes the dominant term in the flow [34] and can reduce the mixture momentum to the extent that thickening is reproduced [9]. Therefore by including an accurate rheological model the sludge bed height and behaviour can be reproduced by the CFD model.

While it is important to include rheological effects to produce an accurate model, gathering the necessary data to do so accurately can be difficult [49]). Ideally the yield stresses and plastic viscosity of the sludge should be known a priori to implement the rheological model.

# Chapter 4

# Model setup and calibration

## 4.1 CFD setup

The following sections deal with the setup of and configuration settings of OpenFOAM that were used in the simulations. Details of mesh generation, solvers used and boundary conditions (BC's) are presented for reproducibility. The calibration of the settling model which incorporated settling tests, is discussed in detaul.

### 4.1.1 The Mesh

The mesh was created with the program Gmsh, an open source 3D finite element mesh generator [19]. Gmsh generates unstructured grids, meaning no predefined order relation exists between any two elements. Gmsh was chosen over OpenFOAM's native `blockMesh` utility as it provides fast and light mesh generation through which changes to the tank's internal configuration could be made more freely.

Some simplifications were made to the geometry of Stage 1 (refer to Figure 2.1. The velocity reduction chamber was made to extend across the width of the tank when in reality it is boxed off and occupies about 1/3 of the width in the centre of the tank. A shelf that sits below the velocity reduction chamber and slopes downwards to either side

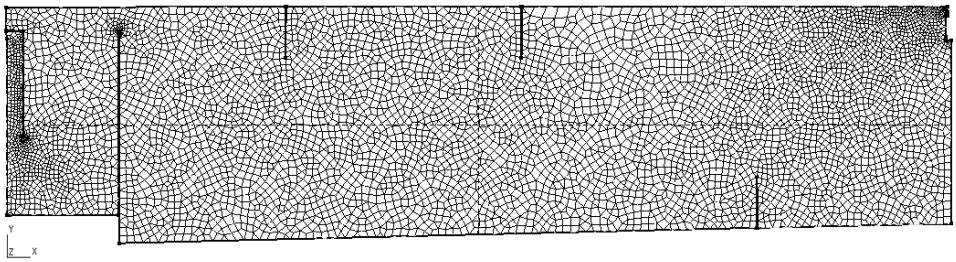

Figure 4.1: 2D computational mesh

was not included, however its effect of distributing the flow to the left and right of the chamber may be reproduced by the wider chamber in the mesh. Below the The Stage 1 floor also has two levels of of which only the upper one is meshed across the tank width. The lower area serves as a desludging chamber for Stage 1 and often quickly fills with sediment. The outlet chamber was omitted and the outlet was defined at the Stage 3 weir, the component that dictates the outlet hydraulics.

The mesh was refined where sharp gradients occur such as the inlet and outlet regions. A mesh independence test was carried out by comparing results from coarse, medium, and fine grids which had 40593, 283290 and 956508 cells respectively. According to Wicklein et al, 2016[68], these tests are recommended for good modelling practice and examples can be found in [62, 9].

The results are shown in Figure 4.2 for steady state single-phase velocity magnitudes in the 2.5l/s flow scenario. A 2-D slice is taken through the midway points of the $x, y$ and $z$ planes (i.e. at $L/2, H/2$ and $W/2$ respectively where $L, H$ and $W$ are the length, height and width of the tank). The line over which the velocity is plotted extends across opposite corners of the 2-D slices from bottom to top. Each grid resolves the salient features of the flow pattern to a good degree. The coarse performs consistently worse than the medium and fine grids and fails to match the same magnitudes at the peaks. The medium and fine grids show better agreement with each other. The medium grid was considered sufficiently accurate and was found to result in much faster simulations than the fine grid and therefore was used throughout the rest of the study. The medium mesh is shown in Figure 4.1.

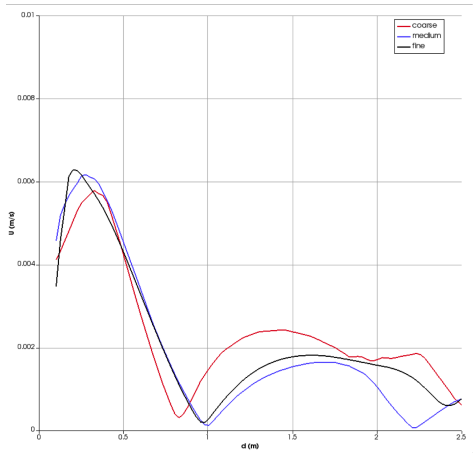


(a)

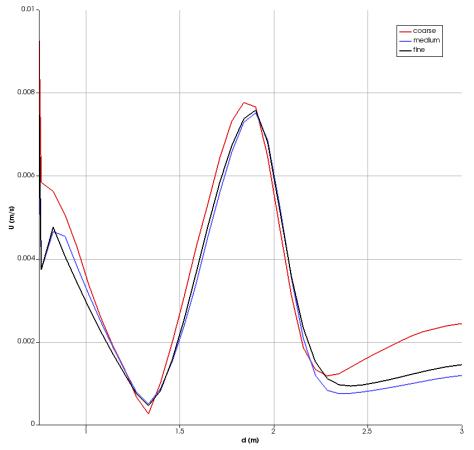


(b)

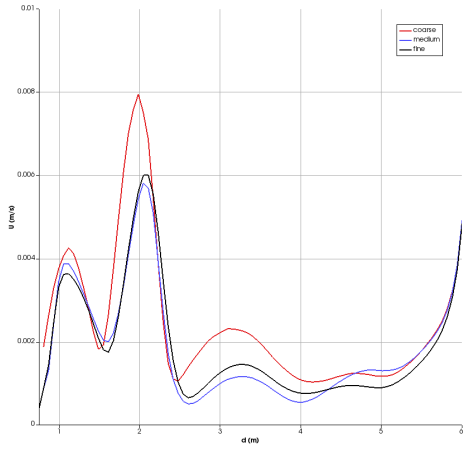


(c)

Figure 4.2: Mesh independence study showing velocity magnitude for coarse, medium and fine 3D grids taken along (a) the $x$-plane at $L/2$, (b) the $y$-plane at $H/2$ and (c) the $z$-plane at $W/2$

| Folder | File | Description |
|---|---|---|
| 0/ | | Boundary and initial conditions |
| | U | Velocity |
| | p_rgh | Pressure |
| | k | Turbulent kinetic energy term |
| | epsilon | Turbulent energy dissipation term |
| | nut | Turbulent viscosity term |
| | alpha.sludge | Dispersed phase volume fraction |
| constant/ | | Model parameters and mesh files |
| | polyMesh/ | Folder containing all mesh files |
| | g | Gravitational acceleration |
| | transportProperties | Input parameters for settling velocity models, non-Newtonian models, model selection and fluid properties |
| | turbulenceProperties | Selection of turbulence model and parameters |
| system/ | | Model parameters and mesh |
| | controlDict | Simulation controls such as time step, write interval, run time, post processing functions |
| | fvSchemes | Finite volume discretisation schemes |
| | fvSolution | Finite volume algorithm controls |

Table 4.1: Generic case directory structure for OpenFOAM simulations

Mesh statistics and quality checks can be obtained by using OpenFOAM's `checkMesh` function. The mesh maximum skewness for the medium mesh was 0.894. This is a measure of how much cell faces deviate from an equilateral shape (calculated as a function of each corner's angles) and should be below 0.9 [68]. The maximum aspect ratio was 65.64 which is OK according to OpenFOAM. `checkMesh` does not provide average values for these quantities but in general they should be minimised. Efforts were made to minimise these metrics by forcing gmsh to generate quadrangular cells instead of triangles where possible.

### 4.1.2 OpenFOAM setup

The case directories for each OpenFOAM simulation all follows the same hierarchy and it is illustrated in Table 4.1 below for a simulation using the `driftFluxFoam` solver with a k-$\epsilon$ turbulence model.

Other files may appear in certain directories, for example script files to allow the user to easily clean a case and run a new simulation. Another example is run time post processing file in the `system` folder called `probes` used to record data from points of interest inside the tank during simulations, such as the value of `alpha.sludge` at the outlet. The gmsh meshing files are contained in a separate directory and are compiled into an OpenFOAM format with the `>gmshToFoam` command and it is these files which are outputted to the `constant/polyMesh` folder.

### 4.1.3 OpenFOAM Solvers

OpenFOAM has dozens of in-built solvers, and many more open source user-built solvers, for a wide range of settings but just two of these were needed for this study and are described below.

#### `simpleFoam`

The `simpleFoam` solver was used to investigate the single-phase tank hydrodynamics. It uses the SIMPLE (semi-implicit pressure-linked equations) algorithm to solve the steady state Navier-Stokes equations (see section 3.3).

In OpenFOAM this solver converges when the residuals between time steps reach a user-defined tolerance which is prescribed in the `fvSolution`. The under-relaxation factor must also be specified here, a value between 0 and 1 that the SIMPLE algorithm needs to converge, and different values were tested to achieve a good balance between convergence and numerical stability.

The other input parameters are the initial and boundary conditions present in the '0' folder, discussed below. A standard k-$\epsilon$ turbulence model was chosen, consistent with the literature [28]. The results of these simulations are presented in section 5.1.

### `driftFluxFoam`

The `driftFluxFoam` solver was used for the two-phase simulations to investigate settling behaviour. It is a transient solver for two incompressible fluids treated as a mixture as outlined in Section 3.2.3 It uses the PIMPLE algorithm which unlike the SIMPLE algorithm can handle larger time steps and does not rely on under-relaxation, as well as being time-dependent.

This solver requires additional input parameters from the user in the `transportProperties` file for the Takacs equation for hindered settling velocity, which were estimated by experiment (and are summarised in Table 4.4). This file also contains input for viscosity model for the non-Newtonian behaviour of the mixture, which was estimated from the literature. As discussed in Section 3.4 the non-Newtonian parameters are often estimated by constitutive models of the form $\Phi = aC^{b\alpha}$ with $\Phi$ for some quantity $\Phi$.

The `driftFluxFoam` solver calculates the plastic viscosity and yield stress based on models such as this and requires inputs for $a$ and $b$. For plastic viscosity the Bingham baseline model was selected based on its prevalence in the literature. The value $a = 2.431\text{e-}4$ kg/ms and $b = 179.26$ were chosen for the constitutive equation, values based on the works of Brennan, 2001[7] and Dahl, 1993 [14]. OpenFOAM is programmed to use the exponent set $C$=10. The yield stress values entered were $a$=1.1e-4 kg/m$s^2$ and $b$=0.98, also used in the works of de Clercq, 2003[15] and Liu & García, 2011[34]. More accurate estimation of these parameters for specific cases can be performed with lock-exchange experiments (see [67]). The density of the particles is specified as 2650kg/$m^3$ [35, 56] in the same file. OpenFOAM uses a slightly different version of the above relation to calculate the apparent mixture viscosity:

$$\mu = max\big(\mu_c + a(10^{b\alpha} - 1), muMax\big) \tag{4.1}$$

where $\mu_c$ is the viscosity of the continuous phase and `muMax` is supplied by the user and was chosen to be 10 kg/ms.

The standard $k - \epsilon$ model was also chosen for the `driftFluxFoam` simulations.

### 4.1.4 Boundary Conditions

The boundary conditions for each of the variables are defined in their respective files in the '0' folder. Surfaces in the computational mesh are given physical names which are inlet, outlet, atmosphere (the top of the tank) and fixed walls. A BC must be defined for each variable on each of these surfaces. 2D simulations are realised by defining an additional 'front and back' surface which is given the BC 'empty' for all variables meaning the governing equations are not solved in the direction normal to the 'empty' plane. The initial value of the internal field can also be prescribed in each variable's file.

The below table summarises the boundary conditions used on each plane for the two solvers discussed in the previous section. The variables are the velocity $U$, the total pressure $p$, the total pressure minus the hydrostatic pressure (i.e. the dynamic pressure) $p\_rgh$, the solid phase fraction alpha.sludge, and the turbulence variables of kinetic energy $k$, dissipation rate $\epsilon$ and turbulent viscosity nut.

The fixedValue condition prescribes a fixed numerical value to the boundary in question. The pressureInletOutletVelocity condition calculates the velocity based on the pressure field and allows for backflow during the solution process which can occur at the outlet and atmosphere. Similarly the inletOutlet condition allows for backflow at an outlet. The no slip condition is imposed on the walls and is defined by noSlip and a slip condition is prescribed to the velocity at the surface of the tank. OpenFOAM contains built-in wall functions to calculate the turbulence varaibles as they approach solid surfaces and calculated calculates a variable's value based on the field variables surrounding it.

| Solver | Parameter | Inlet | Outlet | Walls | Atmosphere |
|---|---|---|---|---|---|
| `simpleFoam` | U | fixedValue | pressureInletOutletVelocity | noSlip | slip |
| | p | fixedFluxPressure | fixedValue | fixedFluxPressure | fixedFluxPressure |
| | k | fixedValue | inletOutlet | epsilonWallFunction | inletOutlet |
| | epsilon | fixedValue | inletOutlet | kqRWallFunction | inletOutlet |
| | nut | calculated | calculated | calculated | nutkWallFuntion |
| `driftFluxFoam` | U | fixedValue | pressureInletOutletVelocity | noSlip | slip |
| | alpha.sludge | fixedValue | inletOutlet | zeroGradient | slip |
| | p_rgh | fixedFluxPressure | fixedValue | fixedFluxPressure | fixedFluxPressure |
| | k | fixedValue | inletOutlet | epsilonWallFunction | inletOutlet |
| | epsilon | fixedValue | inletOutlet | kqRWallFunction | inletOutlet |
| | nut | calculated | calculated | calculated | nutkWallFuntion |

Table 4.2: Boundary conditions for each boundary and solver

A turbulence intensity of 2% was assumed at the inlet. Despite all the possible variations of outlet boundary conditions, Lyn et al. (1992) noted that they do not have a large impact on the mean flow field; they only have a local effect i.e. near the outlet itself.

## 4.2 Model calibration

Several tests exist for determining the settling characteristics of sludge such as its settling velocity and settleability, both of which are functions of concentration and flocculation tendency (see Figure 2.10). Batch settling tests are useful in that they eliminate hydrodynamic effects allowing one to focus on the settling characteristics alone [63]. Settling tests were performed in this study with a sample of sediments obtained from a site where MEL5 was used in order to calibrate the settling velocity in the CFD model.

The hindered settling velocity can be obtained by recording the height of the sludge-water interface in a settling column (for suitably concentrated mixtures), $h(t)$, and calculating the maximum slope of the resulting curve. Furthermore, a relationship between the hindered settling velocity and the concentration can be derived by successively diluting an initial concentration and obtaining the settling curve for each dilution [13]. Taking the slopes of each curve results in a velocity profile as a function of concentration to which a function can later be fitted. The procedure adopted is outlined below.

### 4.2.1 Measuring suspended solids

Solids in water and wastewater consist of a suspended and a dissolved portion. In a laboratory they are measured by drying a sample of water containing solids in an oven at a specified temperature (usually 103-105°C), then weighing the resulting residue. Dissolved solids are those which can pass through a filter of specified pore size (usually $0.45\mu m$, [51]) while suspended solids will be retained by such a filter [2]. Turbid Water samples sent to the laboratory were subject to this type of analysis.

The total suspended solids (TSS) is the quantity of interest in the present study as it is the quantity limited by the discharge licence (Table 2.2). It is measured in situ using submersible turbidity probes. The relationship between turbidity and TSS is then determined comparing measured turbidity values with lab TSS analysis of those samples. A linear relationship between turbidity and TSS is generally assumed and this is calibrated with lab results of site-specific sediment-water mixtures. The company has various turbidity probes at its disposal with varying ranges and some have additional capabilities such as temperature, pH and electrical conductivity monitoring.

According to the standard method 2540D [2] the water sample to be analysed should not be stored for more than 24 hours after being taken and should be preserved at 4°C to minimise microbial decomposition of solids, which may have affected the sediments sampled on this site as they were described as occasionally organic in the site investigation report. Also they were not analysed by the laboratory for 3 weeks after collection.

### 4.2.2 Measuring flow velocity

CFD studies of flow in ST's are often verified by comparing predicated flow velocities with measured values [30, 31, 33]. The velocity is usually measured via Doppler velocimetry. This equipment was not available for the present work and even had it been, access to the tank is limited through the top due to a fixed walkway that covers the majority of the tank. Though the velocity field in the tank was not measured experimentally, the simulation results agree qualitatively with typical ST flow fields found in other studies.

### 4.2.3 Zone settling experiments

The stages of settling in the settling column test are shown in Figure 4.3 based on the evolution of four zones. At $t_0$ the mixture is poured into the column and after a lag time $t_1$ the four distinct zones materialise. Zone A is the supernatant, the clarified water above the interface. Zone B is the uniform settling zone whose concentration remains

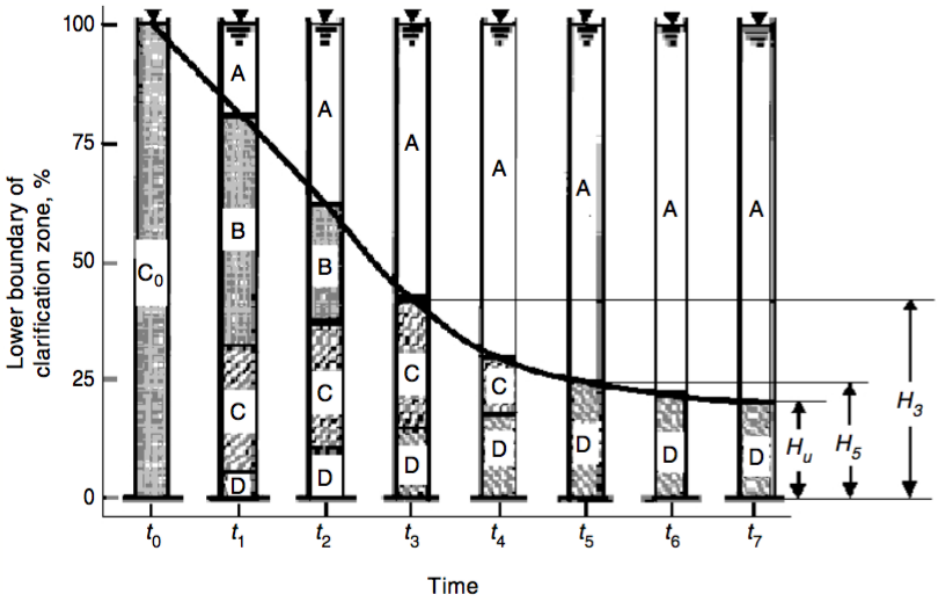


Figure 4.3: Evolution of sludge zones in settling column tests (from [56])

equal to $C_0$. Zone C is the thickening zone with a concentration gradient between the concentrations in B and D. At a time $t_3$ zone B disappears and at $t_5$ zone C disappears, at which time only compression is taking place. This continues until $t_7$, when the sludge interface height no longer changes in time.

Because the concentration in B is constant and equal to $C_0$ and its interface AB settles at a constant velocity until $t_3$, the hindered settling velocities as functions of concentration, $v_s(C)$, can be computed for each batch using the gradient of the interface's height in time.

The purpose of the experiment was to ascertain whether or not zonal settling (type III settling, see Section 2.4.3) was taking place in the tank with this type of sediment in high concentration regions near the sludge blanket and to use the results to calibrate the OpenFOAM settling model. The interface AB is expected to develop and slowly move downwards as settlement proceeds while compression takes place at the bottom of the column.

A perspex column 1m in height and 100mm in diameter was used to conduct the settling tests. A ruler accurate to 1mm was attached to the side of the column and it was fixed in an upright position as shown in Figure 4.4. The column was secured firmly in position and made exactly level using a spirit level. Samples of site sediment were mixed gently

into a large basin of clear water and this was used as the baseline mixture, concentration $C_0$ to be diluted in each experiment. An initial mixture of approximately 1kg of wet sediments in the 40L basin of water was insufficient to produce interface and the mixture was therefore concentrated (by adding a further 3kg) and an interface was formed as shown in figure 4.5. A sample of this mixture was taken and sent to a laboratory to obtain the TSS value for $C_0$, which was 26,200 mg/l i.e. volume fraction $\alpha \approx 0.01$.

Figure 4.4: Experimental setup for zone settling tests

When the sludge blanket - supernatant interface (A-B zone interface from Figure 4.3) was seen to form its height was recorded every minute and a $h(t)$ plot was generated as seen in Figure 4.6 where $h$ is the height of the interface in mm measured from the bottom of the column and $t$ is the time in minutes. The three distinct zones of hindered, transition and compression settling can clearly be seen and the plot is typical of those found in the literature (for example [49, 9] and Figure 4.3 above). The turbidity probe was used to

Figure 4.5: Interface in zone settling test

measure the turbidity value at the top of the column intermittently and these values were observed to descend uniformly with time.

When the settling was deemed to be in the compression phase ($t > t_5$) the column was emptied and the test was performed again with a more diluted initial concentration. In this way several concentration-specific $h(t)$ curves were obtained and the range in which zonal settling takes place was discovered. A sample of the lowest concentration to produce hindered settling was sent to the laboratory and had a concentration of 10,700mg/l. Therefore it was confirmed that hindered settling is likely to occur inside the tank at concentrations in close to this value and over when these sediments are introduced.

The left part of the $h(t)$ plot in Figure 4.6 is the hindered settling region which should approximate a straight line, the velocity being constant. The curved part in the middle is the transition zone which begins when the plotted points deviate from the fitted line. The compression zone where the curve levels out is on the right. The slopes of straight line in the hindered settling regions for all initial concentrations give the hindered settling velocities, $v_s$ and these slopes were found by fitting linear functions of the form $h =$

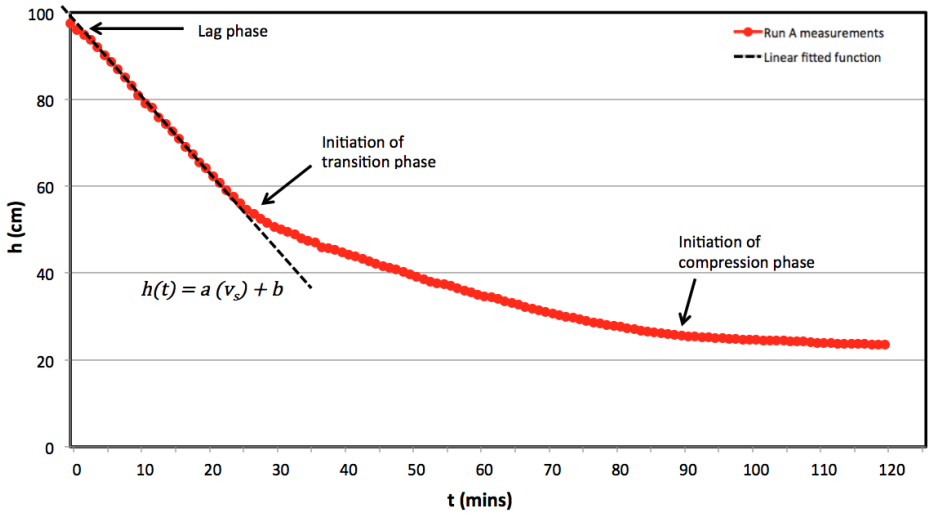


Figure 4.6: Graph of interface height in time for Run A with a linear function fitted to obtain the hindered settling velocity

| Run | Concentration (mg/l) | $v_s$ (mm/s) |
|---|---|---|
| A | 26200[a] | 0.286 |
| B | 22500[a] | 0.352 |
| C | 23580 | 0.305 |
| D | 19125 | 0.395 |
| E | 20960 | 0.322 |
| F | 15820 | 0.306 |
| G | 13500 | 0.384 |
| H | 10700[a] | 0.504 |

Table 4.3: Fitted values of experimental hindered settling velocity

$av_s + b$ where $a$ and $b$ are constants. The resulting velocities and their corresponding concentrations are summarised in Table 4.3.

The 'Run' column labels each run in terms of its dilution percentage (percentage of the initial concentration $C_0$). The superscript $^a$ refers to laboratory results, from which the other concentrations are extrapolated. The fitted slope $v_s$ was fitted to a $R^2$ value of 0.99 in every case.

The interface became less well defined with successive dilutions. This is because the concentrations are lower in the upper regions and discrete/flocculated settling is more visible than in the less diluted suspensions. This is also obvious from the increasing turbidity values at early stages of each dilution where the interface is less sharply defined.

The collected $v_s$ data was then used to calibrate the Takács model for hindered settling, recalling its form $v_s = v_0\left(e^{-r_1(C-C_{min})} - e^{-r2(C-C_{min})}\right)$. The minimum concentration of colloidal particles that do not settle out of suspension by gravity alone, $C_{min}$, was determined to be 15.7mg/l by the laboratory which analysed a sample taken of the supernatant of Run E following overnight settling. $C_{min}$ is often reported as a percentage of the initial concentration and would be 0.075% in this case. The parameters $v_0$ (the maximum settling velocity), $r_1$ (the parameter for hindered settling particles) and $r_2$ (the parameter for poorly settling particles) were found by using the Solver function in Microsoft Excel to minimise the RSS (residual sum of squares) error between the experimental and predicted hindered settling velocities for each concentration (i.e. $\sum_i \left[v_s(C_i)_{experimental} - v_s(C_i)_{predicted}\right]^2$ where the subscript $i$ refers to the concentrations of each Run). All values of concentration $C$ in mg/l were converted to the dimensionless volume fraction $\alpha$ using the formula $C = 1000\rho\alpha$ as this is the value used by OpenFoam. A density of $\rho$ =2650$kg/m^3$ was assumed. The values of $r_1$ and $r_2$ were also non-dimensionalised in this way.

The Solver returned values for all the parameters with an RSS error of the order $6 \times 10^{-9}$. This result necessitated removing the Run F result from the calculation as it was a significant outlier. It was found that the model was very sensitive to $v_0$ and $r_1$ but not $r_2$ or $C_{min}$. Bibliographical values for this parameter, to the author's knowledge, are unavailable for this type of sediment. Flamant et al., 2004[18] report a value of 41l/g in a potable water treatment plant which may approximate the characteristics of the solids in this study but they give no details of the sediments in their case. Most other bibliographical values relate to activated sludge and range from 3-15l/g ([7, 9, 59] with WEF, 2006 [67] in particular citing a value of 4l/g for poorly-settling particles). The value of $r_2$ which minimised the RSS error was 1.28g/l which indicates poorly settling particles. As manually varying $r_2$ did not appreciably affect the RSS error a value of 0.38l/g was chosen to move the peak of the Takács curve to the region where hindered settling was observed to cease in the experiments ($\alpha \approx$ 3.8x10$^{-6}$. The final parameters chosen for the Takács model after the above procedures are shown in Table 4.4 and the resulting curve is shown in Figure 4.7, including the experimental data points. The curve resembles those

| Parameter | Value |
|---|---|
| $v_0$ (mm/s) | 0.6679 |
| $r_1$ | 84.377 |
| $r_2$ | 1000 |
| $\alpha_{min}$ | $5.92\text{x}10^{-6}$ |

Table 4.4: Final values of the calibrated Takács model

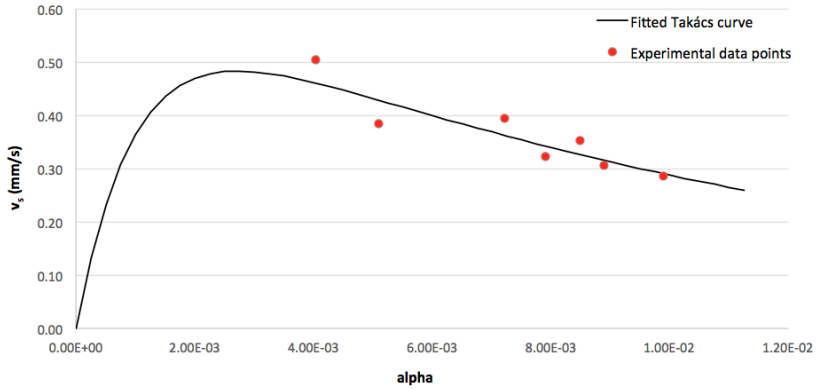


Figure 4.7: Experimental data fitted with Takács curve for hindered settling velocities as a function of concentration using the parameter array in Table 4.4

typically found in the literature and in Figure 2.11.

The validity of the calibrated parameters were tested in OpenFOAM by performing a simulation designed to mimic the laboratory settling column experiment in a 3D column of the same dimensions and with the same initial concentration of solids, shown in Figure 4.8. The goal was to see how the behaviour of the interface compared in the experimental and simulated environments. In Figure 4.8, showing the column at some time $t_1 < t < t_3$ for Run A in the experiment, the zones A, B and D are clearly visible and the interface height is tracked using the graph on the right. The values of $h(t)$ from the simulation were compared with the experimental $h(t)$ values and there was good agreement in the hindered zone (Figure 4.9) though the simulation did not simulate a noticeable transition zone and compression began later than in the experiments. This is because the settling velocity is computed with the Takács equation alone which is not valid in the compression region. This could mean an over-prediction of settling velocity in the sludge zone in the simulations.

Turbulence was not modelled in the settling test simulations as it caused instabilities in

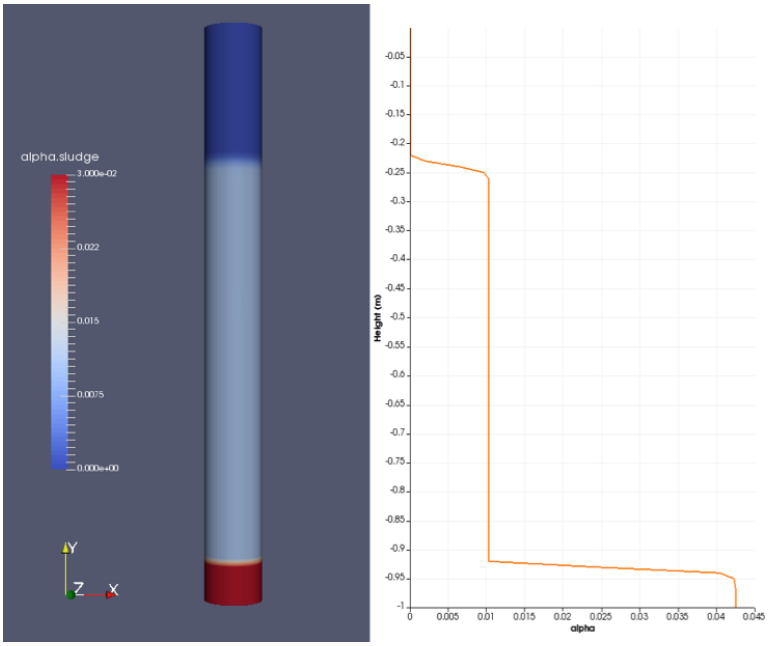


Figure 4.8: Screen shot from the settling column test simulation

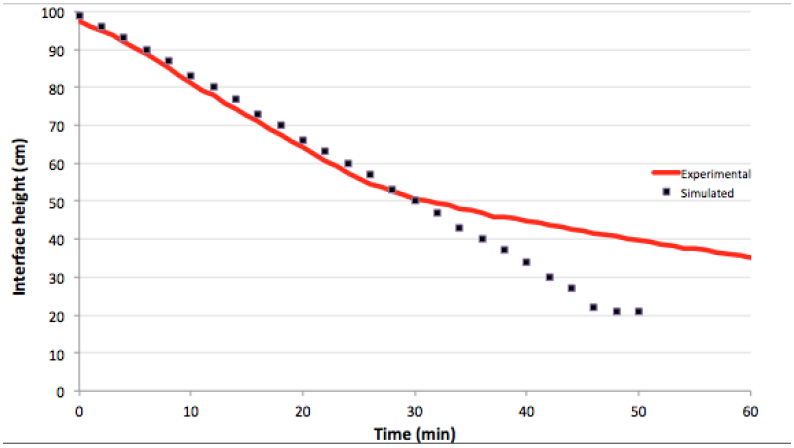


Figure 4.9: Height of interface in simulated settling test vs. experimental settling test

the high-concentration regions and was found not to differ from the laminar simulations in the hindered portion of the simulation.

Ramin et al, 2014 [49] elaborate on the Takács model by formulating a settling model to include hindered, transient and compression settling, thereby obtaining better fits to experimental data similar to that shown in this section. They mention that while it is relatively straightforward to obtain a good fit to the settling velocity curve, a more complex model is required to reproduce the concentration at the bottom of the settling column and therefore only calibrating the settling velocity model to sludge blanket height measurements does not correctly predict all the settling regimes.

Although the site water that fills the tank is often brackish with an electrical conductivity of 35mS/cm the water used in the settling tests was tap water with an electrical conductivity of $<35\mu$S/cm. Because brackish water is more dense it could be expected that the sediments settle more slowly in the site setting. This may also have an effect on flocculation tendency under operating conditions.

### 4.2.4 Flocculation tendency experiments

The goal of these experiments was to determine if flocculation was an important feature of the settlement of these particular solids. A simple experiment was set up whereby two identical containers were filled with turbid water. One was allowed to settle for 30 minutes while the other was gently stirred (at a rate of approximately 0.5 rps) for 5 minutes then allowed to settle for 25 minutes.

The hand-held TSS meter was then used to measure the TSS value in the top of two containers to see if the stirred sample, where there would in theory be a greater opportunity for the sediments to agglomerate and therefore settle faster, had a lower value than the unstirred sample. The experiment was carried out for container sizes of 250ml and 1000ml and the results are summarised in Table 4.5 below.

This experiment would ideally be performed in a larger container such as the settling

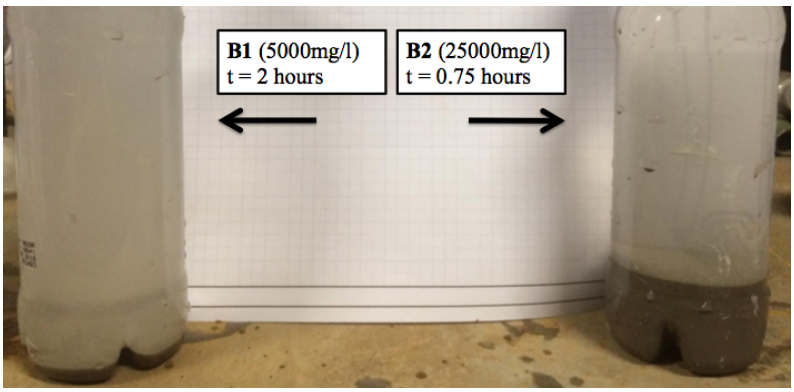


Figure 4.10: Flocculation tendency seen in two bottles

column and for a variety of concentrations. Nonetheless it gives an indication that the sediment particles tend to flocculate at this concentration and tank performance may be increased by promoting such behaviour.

Table 4.5: Flocculation tendency test

| **Container size** *ml* | **Stirred sample TSS** *mg/l* | **Unstirred sample TSS** *mg/l* | **Difference in TSS with gentle stirring** |
|---|---|---|---|
| 250 | 161 | 344 | -53% |
| 1000 | 258 | 456 | -43% |

It was also noticed when two clear plastic bottles were left to stand with initial concentrations of approximately 5000mg/l (bottle B1) and 25000mg/l (bottle B2), the sediment in B2 settled out of suspension much more quickly and left very clear water above the sediments gathered at the bottom. Bottle 1, even after a sediment blanket had accumulated, had somewhat turbid water remaining in it upper part and took much longer to settle (see Figure 4.10). This was theorised to be due to a higher flocculation tendency in B2, where a higher initial concentration of particles increases their chances of collision.

An even more advanced test to characterise discrete and flocculated settling behaviour involves extracting samples from different depths of a settling column over time and measuring their TSS. This allows one to determine the percentage removed at different depths and can be used as a design consideration in relation to hydraulic detention time (see detailed descriptions in [2, 26]). These tests however use specialised equipment that was not available for this work. A test procedure for flocculation tendency in full-scale clarifiers

is given in [63]. Tendency to flocculate would be expected in light of the discussion on the cohesiveness of silt and clay sediments in Section 2.5 and the simple experiments and observations discussed above add credence to this assumption.

# Chapter 5

# Results and discussion

## 5.1 Single-phase simulations

The steady state results of the 3D simulation follow are discussed first. The velocity field at 1l/s, 2l/s and 10l/s are shown in Figures 5.1-5.3. Each of these graphics show (a) a side view along the centre line z-plane ($z = W/2$ where $W$ is the tank width), (b) a side view of the velocity vector field along the centre line z-plane and (c) a plan view of the y-plane close to the top of the tank ($y = 0.95H$ where $H$ is the tank height). All figures are coloured to the velocity magnitude, Note that the velocity scales change according to the flow. The scales range from 0 to $U_0/2$ where $U_0$ is the inlet flow velocity and its colour spectrum is biased towards the lower velocities to highlight all flow features.

These figures illustrate the key flow features of the tank, among which are:

- The effectiveness of the inlet zone in reducing the velocity of the incoming flow, clearly visible in (a) and (c)
- The distribution of the flow field after stage 1 is not even across the tank, visible in (c)
- The effect of the Baffle 1 in deflecting the flow downwards, highlighted in (a) and

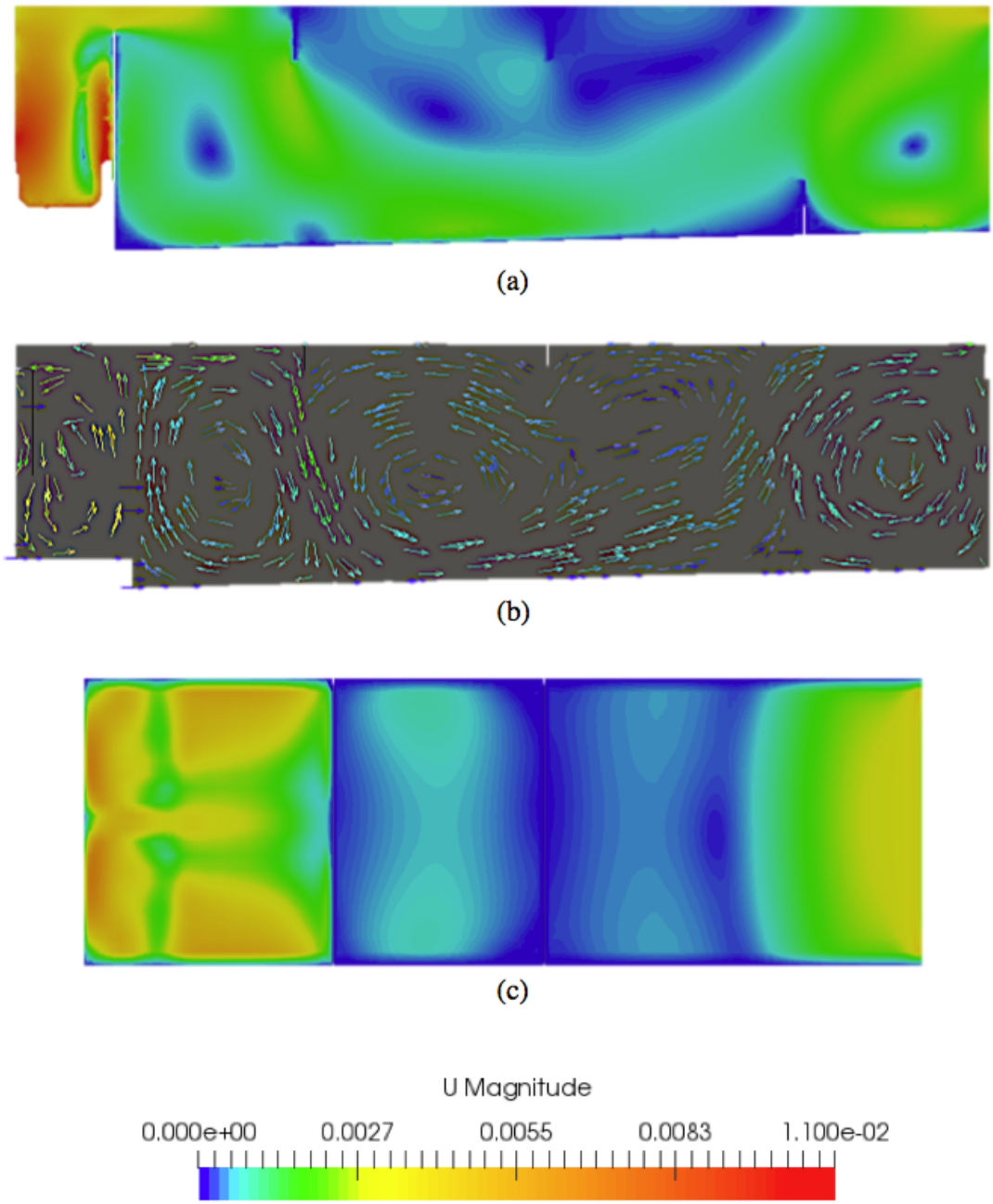


Figure 5.1: 1l/s velocity field (a) side view along the $z = W/2$ centre plane, (b) side view vector plot along the $z = W/2$ centre plane and (c) top view along the $y = 0.95H$ plane

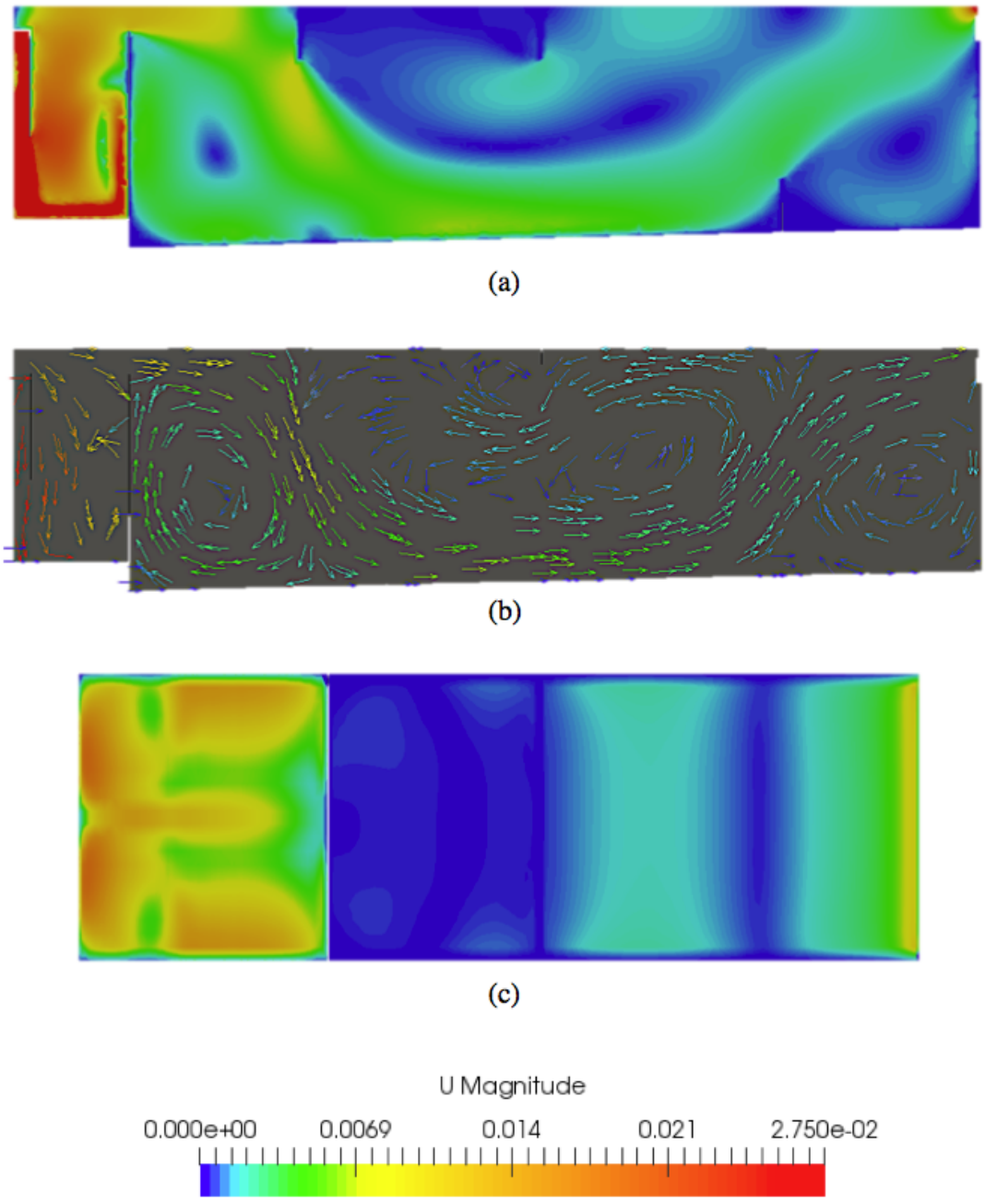


Figure 5.2: 2.5l/s velocity field (a) side view along the $z = W/2$ centre plane, (b) side view vector plot along the $z = W/2$ centre plane and (c) top view along the $y = 0.95H$ plane

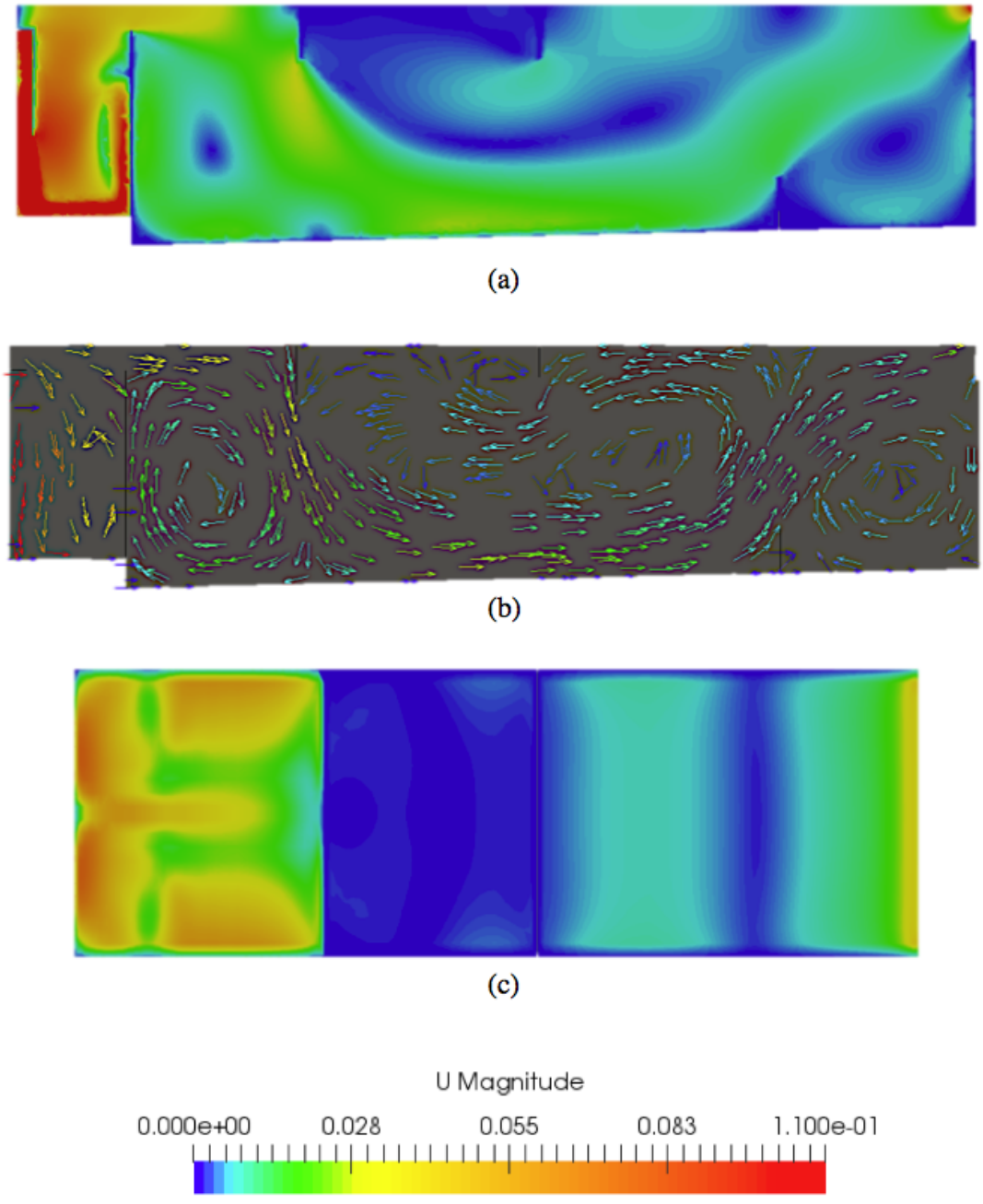


Figure 5.3: 10l/s velocity field (a) side view along the $z = W/2$ centre plane, (b) side view vector plot along the $z = W/2$ centre plane and (c) top view along the $y = 0.95H$ plane

(b) and consistent with the findings of [69]

- The recirculation zone which forms after the Stage 1 wall due to Baffle 1 (a common 'backward-facing step' phenomenon [21])
- The recirculation zone in the upper middle part of Stage 2 due to flow along the bottom of the tank, most evident in (b) and (c)
- The recirculation zone at the end of the tank due to Baffle 3
- Short-circuiting occurs through the bottom of Stage 2

A streamline plot for the 2.5ls simulation can be found Figure 5.6a in the next chapter. Figure 5.4 shows a scaled 'mountain' plot for the 3D velocity field in the direction of the flow at the midpoint of the tank $x/L = 0.5$ for a flow of 2.5l/s. The flow is seen to be relatively uniform and the upper recirculation zone is evident.

Brennan, 2001 [7] questions the usefulness of single phase models in the study of STs, the answer of course depending on the degree to which the dispersed phase affects the flow field. This in turn will depend on the solids concentrations and densities and their degree of coupling, which for small-diameter particles such as clays, silts and concrete dust at concentrations of less than 150-200mg/l, is potentially negligible. Effects associated with high solids concentrations such as density currents and turbulence damping will not be captured by single-phase models.

Single phase flow models are nonetheless useful for estimating the effect of the internal configuration of baffles on the recirculation zones, the effectiveness of the velocity reduction chamber and as a comparative tool to study the influence of the dispersed phase on the continuous phase when the two-phase simulations are performed. It was used to analyse the effects of non-levelling in the tank when the outlet is effectively to one side, producing large recirculation regions and short-circuiting. It is a good approximation for low influent concentrations of solids and can give an idea of shear stresses along the bottom of the tank in conditions where there are no influent solids but a sludge bed is

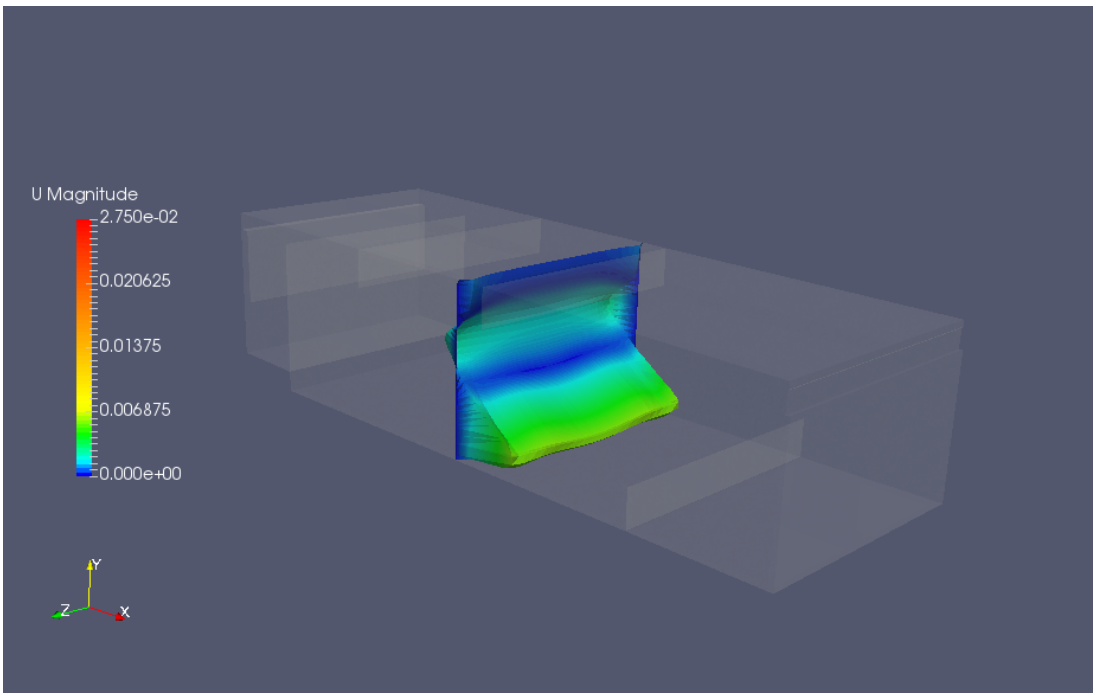


Figure 5.4: 3D mountain plot of velocity field at the midway point ($x = L/2$) of the tank for a flow of 2.5l/s

present which is important when studying scouring. Other researchers have used single-phase models combined with a passive scalar transport model for the dispersed phase [12] and such models are particularly useful for investigating mixing and chemical treatment [28].

In the next section we will examine the effect solids loading on the flow field and the settling dynamics inside the tank.

## 5.2 Two-phase simulations

To include the dispersed-phase in the simulations the `driftFluxFoam` was used, which required additional inputs such as models for non-Newtonian viscosity and settling velocity. It is assumed that the drift flux formulation assumptions are valid in that there is little or no interphase momentum exchange in the horizontal direction i.e. the particles have a low relaxation time, allowing the relative motion in the gravitational direction to be described algebraically as a constant drift (discussed in chapter 3).

### 5.2.1 3D simulations

Base case 3D simulations were performed with a flow of 2.5l/s and with inlet concentrations $C_0$ of 200mg/l. The licence parameters in Table 2.2 often include effluent TSS concentrations as low as 100mg/l with a maximum 200mg/l and the tank should be able to treat at least this influent concentration. The outlet TSS was measured and used as an indication of tank performance. At the beginning of the simulation the tank contained only fluid at rest.

Figure 5.5 shows the simulation result after 8400 seconds, equivalent to $1.1\theta_r$ where $\theta_r$ is the retention time for the tank with a flow of 2.5l/s. It was considered desirable to run the simulation for at least this duration.

By comparing Figures 5.5 and 5.2 we can see the flow field inside the tank has clearly been influenced by the presence of the dispersed phase. The flow exiting Stage 1 is no longer diverted to the bottom of the tank by the first baffle, but instead is carried directly to the bottom of the tank by the density waterfall (Section 2.3.4). The density current develops an appreciable momentum but is disrupted by Baffle 3 on the floor of the tank. This baffle retains much of the settled solids and a sludge bed is seen to build up behind it (Figure 5.8). There is some spill over the baffle and some solids are scoured over it and transported towards the outlet.

The recirculation zones after the Stage 1 wall and after Baffle 3 in the single-phase simulations are no longer present; the density current is the dominant feature along the bottom of the tank. A large recirculation zone in the upper part of the tank is visible in the two-phase simulation, caused by the density current and consistent with typical models in the literature. The differences in the flow fields between the two simulations is most readily seen in the streamline plots in Figures 5.6. Buoyancy effects are evident in the two-phase simulation.

A contour plot of the concentration profile in the tank is shown in Figure 5.8. The tank is clearly stratified in Stage 2 with high concentrations in the bed and near bed ($10C_0$)

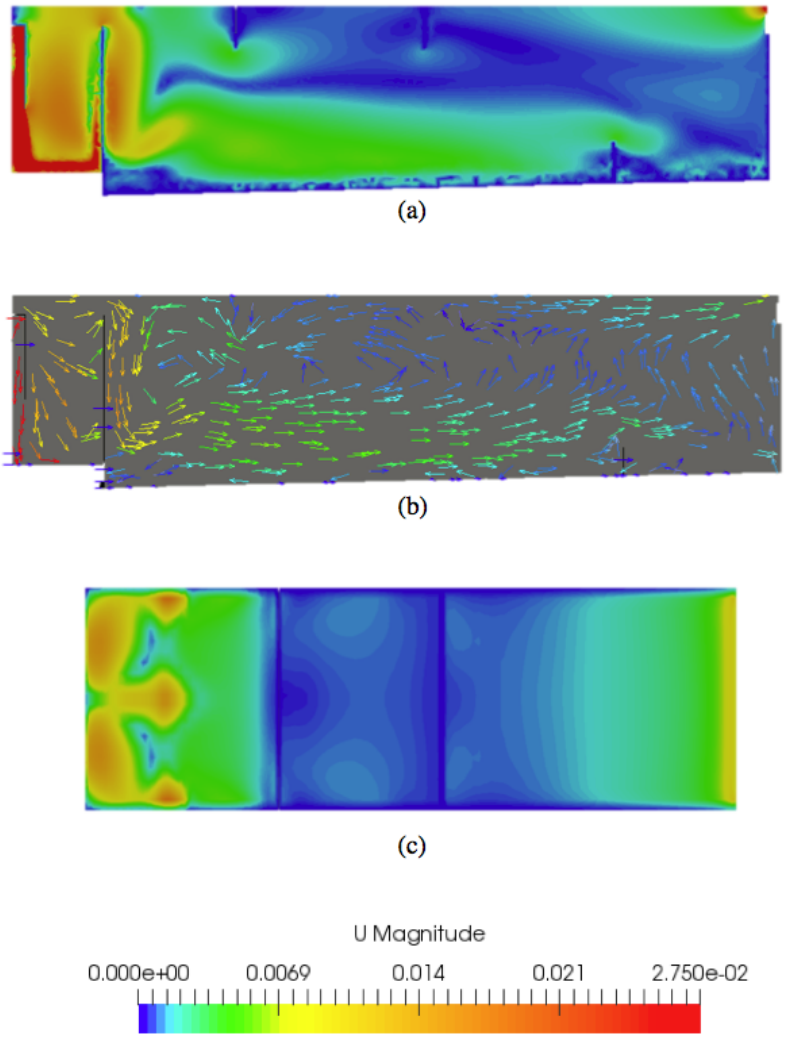


Figure 5.5: Simulation results for 2.5l/s flow with inlet concentration 200mg/l (a) velocity field side view along the $z = W/2$ centre plane, (b) side view vector plot along the $z = W/2$ centre plane and (c) velocity field top view along the $y = 0.95H$ plane

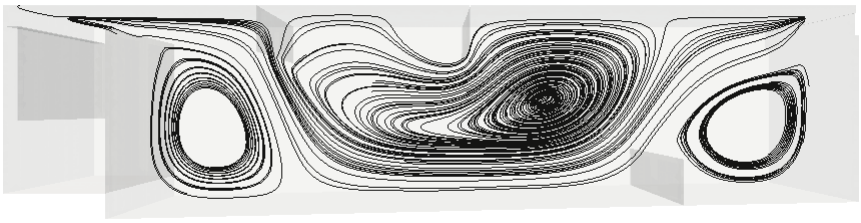

(a) Single phase streamlines

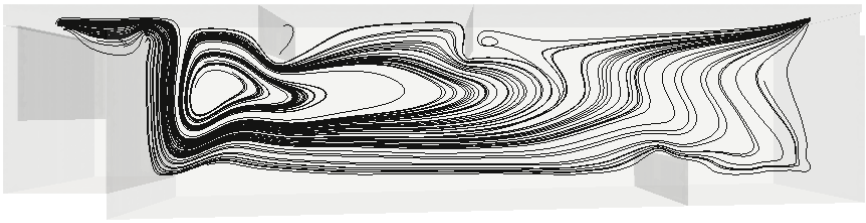

(b) Two-phase streamlines with inlet concentration 200mg/l

Figure 5.6: Comparing single-phase and two-phase streamlines for a flow of 2.5l/s in 3D simulation after 8350s

and low values in the upper half of the tank (0-0.25$C_0$). Stage 1 retains fewer solids than expected as all the solids appear to be washed out from it. In practice it as been noted that Stage 1 contains more sand and gravel sediments (which are inevitably pumped into the tank as well as the predominant silt/clay particles) than Stage 2, their high density and diameter trapping them in this compartment.

The most concentrated region occurs in the accumulated deposits between Baffle 3 and the end wall. The effluent suspended solids (ESS) are of the order 10mg/l after 8400 seconds. The sloped floor of the tank promotes accumulation of sludge at the early part of Stage 2 near the desludging valve, at the bottom of the Stage 1 wall. A similar pattern was observed in different $xy$-plane depths suggesting a uniform concentration field across the width of the tank in the $z$ direction. This is visualised more clearly in Figure 5.9 where the concentration contours are drawn on $yz$ planes at various lengths $x$ along the tank.

The evolution of the solids concentration profile over time is shown for the 200mg/l case in Figure 5.7 with the `alpha.sludge` scale set to 200mg/l as its maximum. At 400s

the dispersed phase has started to pass over the Stage 1 wall and the density current has formed after 1600s. It is stopped by Baffle 3 on the tank floor and solids begin to accumulate in front of the baffle. There is a reverse shock wave from this sudden collision of the density current with the wall and this travels backwards until it reaches the density waterfall again, seen as the bulge in concentration directly after the stage one wall after 3600s. This pattern stabilises for the remainder of the simulation and the bottom layers gradually become more concentrated. For higher initial concentrations the density waterfall is seen to form faster and have a higher velocity due to the added potential energy into the system ([67]. However it stabilises in a similar manner to the lower concentrations and evolves steadily upwards in, only the initial behaviour differs.

The 2.5l/s 1000mg/l simulation was, after 8400 seconds, run until 54000 seconds (15 hours) to see if any important flow features or effects were missed. In practice the tank is never subject to this sort of prolonged loading, as site work which is the cause of the turbid water, rarely continues into the night and 10 hours is the typical working day. This time, along with the 8400 seconds mark are indicated on the graph of TSS at the outlet and time in Figure 5.10.

There is a second steep rise in effluent TSS after approximately 6.5 hours. The evolution of the bed continues in the same manner as in the previous simulations, with stratified concentration zones gradually rising and causing the outlet TSS to rise accordingly (figures not shown). It does not appear to accelerate at any point. There is no particular moment where scouring becomes noticeable, this is discussed more in Section 5.3.

### 5.2.2 2D approximation

Before proceeding with other computationally expensive 3D simulations a check was done to determine if a 2D simplification could be made for the remaining simulations. This was done by comparing the results of the above 3D simulation with a 2D simulation for the same flow rate and inlet concentrations. Figure 5.11 shows the velocity and concentration profiles along the $xy$-plane at $z{=}W/2$ and good agreement can be seen between the 2D and

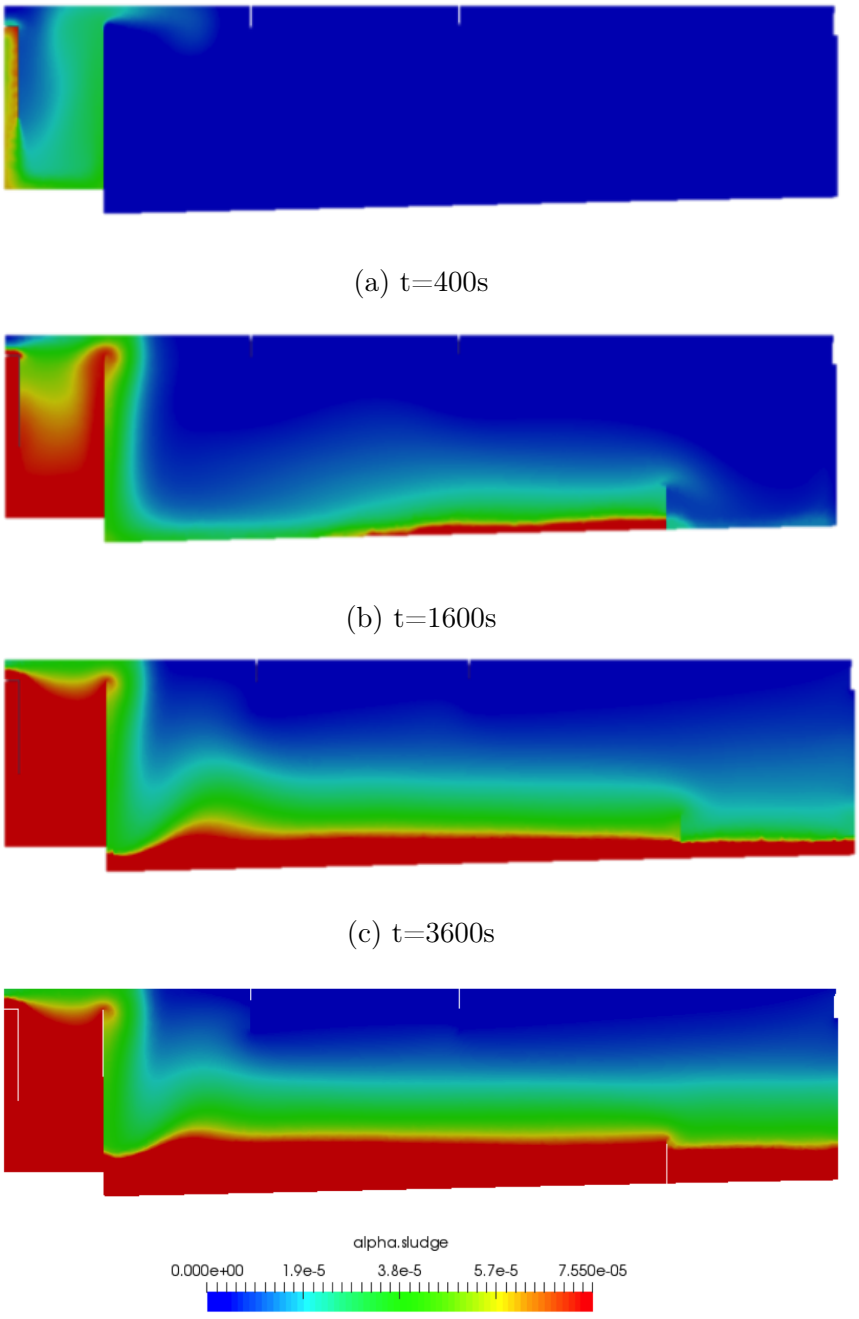


(a) t=400s

(b) t=1600s

(c) t=3600s

(d) t=8400s

Figure 5.7: Time evolutions of the `alpha.sludge` field 2.5l/s and 200mg/l 3D simulation on the $z$=W/2 plane

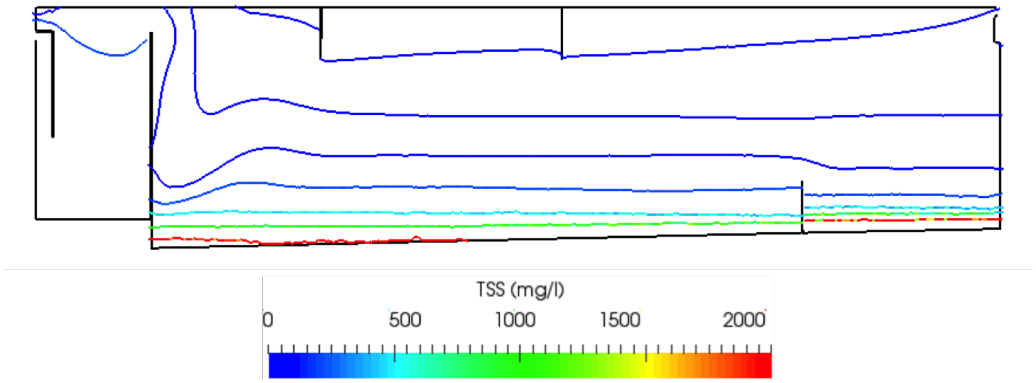


Figure 5.8: Contour plot of the TSS concentration profile for the 3D simulation of 2.5l/s with inlet concentration 200mg/l

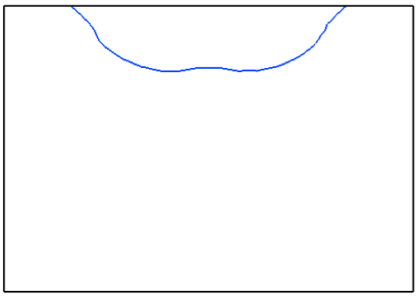

(a) x=0.45m, Stage 1

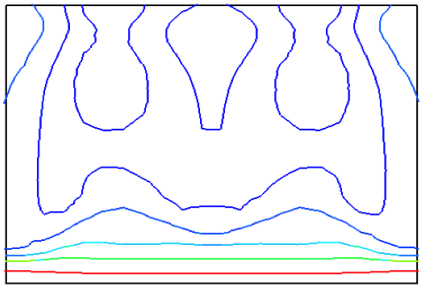

(b) $x$=0.8m, after Stage 1 wall

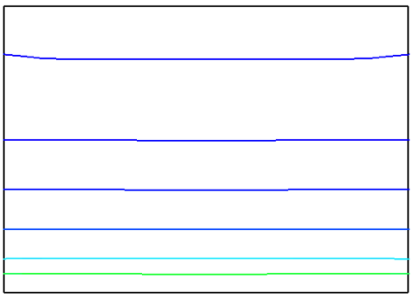

(c) $x$=3m, mid point of tank

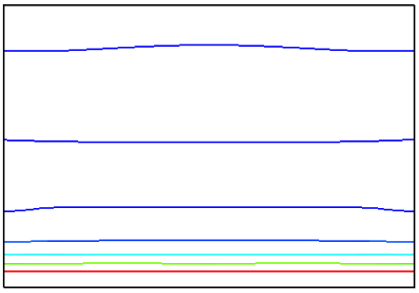

(d) $x$=5m, near outlet

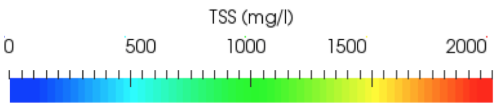


Figure 5.9: TSS concentration contours at various points along the $x$ axis for a flow of 2.5l/s with 200mg/l inlet concentration

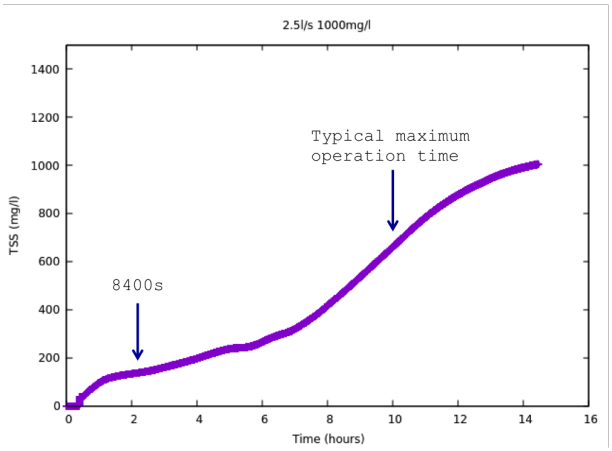


Figure 5.10: Outlet TSS in extended simulation of 2.5l/s with 1000mg/l to 50000 seconds

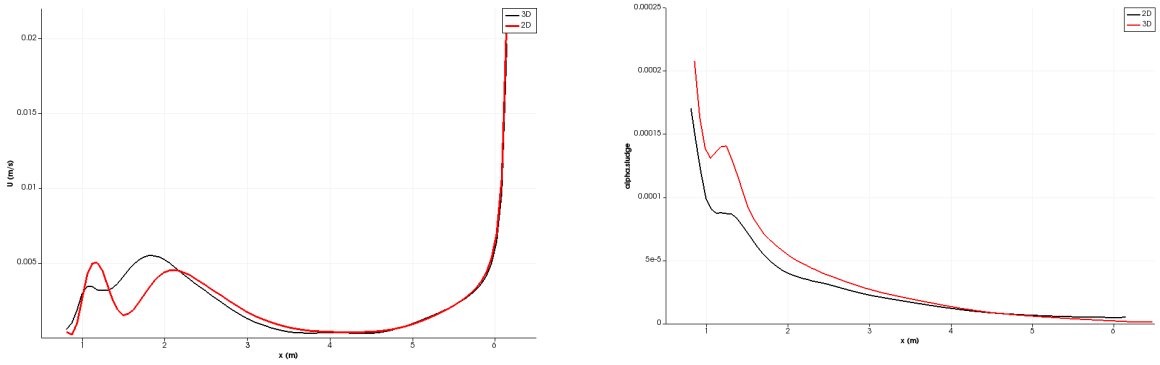


(a) Velocity magnitude

(b) `alpha.sludge`

Figure 5.11: Comparison of 3D and 2D mesh results for 2.5l/s and 200mg/l

3D results for the two variables, particularly for the outlet TSS which is the performance criteria used.

Having determined that the 2D and 3D simulations results were suitably similar, the remaining two-phase simulations were done in 2D. The region where 3D effects were most noticeable was in the inlet region and this was not the primary area of interest nor was it thought to affect the overall Stage 2 flow field.

### 5.2.3 2D simulations

A series of simulations were performed to investigate the tank's treatment capacity under different loading conditions, summarised in Table 5.1 where $Q_{in}$ and $C_{in}$ are the flow rates

| $Q_{in}$ (l/s) | $C_{in}$ (mg/l) | $C_{out}$ (mg/l) | $\eta$ % |
|---|---|---|---|
| 2.5 | 200 | 17 | 92 |
| 2.5 | 1000 | 141 | 86 |
| 2.5 | 5000 | 1754 | 65 |
| 10 | 200 | 198 | 1 |
| 10 | 1000 | 1007 | 0 |

Table 5.1: Tank efficiencies across flow and solids loading rates

and concentrations entering the tank, $C_{out}$ is the outlet concentration after 8400 seconds and $\eta$ is the removal efficiency, defined as $^{(C_{in}-C_{out})}/_{C_{in}}$. The results show the tank is ineffective at high flow rates of 10l/s. Referring back to Table 2.4 we see this flow rate is outside recommended design parameters for SOR and $\theta_r$. For 1000mg/l at 10l/s the TSS is higher at the outlet than the inlet because during the early stages of the simulation the tank accumulates sediments to a certain degree but these are later washed out as the tank is overloaded. Tank efficiency is good at lower flow and solids concentrations. Its 65% removal rate for 5000mg/l at 2.5l/s is an encouraging figure, though this value would exceed most discharge licence limits.

The outlet concentration throughout each of the simulations was recorded and is plotted in Figure 5.12. While flows and inlet concentrations vary a similar pattern is visible throughout whereby a steep initial rise in effluent concentration later levels out.

## 5.3 Scouring

The issue of scouring refers to the resuspension of settled solids from the sludge blanket due to high shear velocities above the bed layer (see Section 2.5.3). Scouring can increase effluent concentrations of suspended solids or certain pollutants such as heavy metals that adhere to the particles (see Section 2.5). The critical scour velocity for the settled bed was previously given by the Shields equation (Equation 2.18) and a lower limit for the tank was determined as 0.0186m/s based on the Shields value for a clay particle of diameter

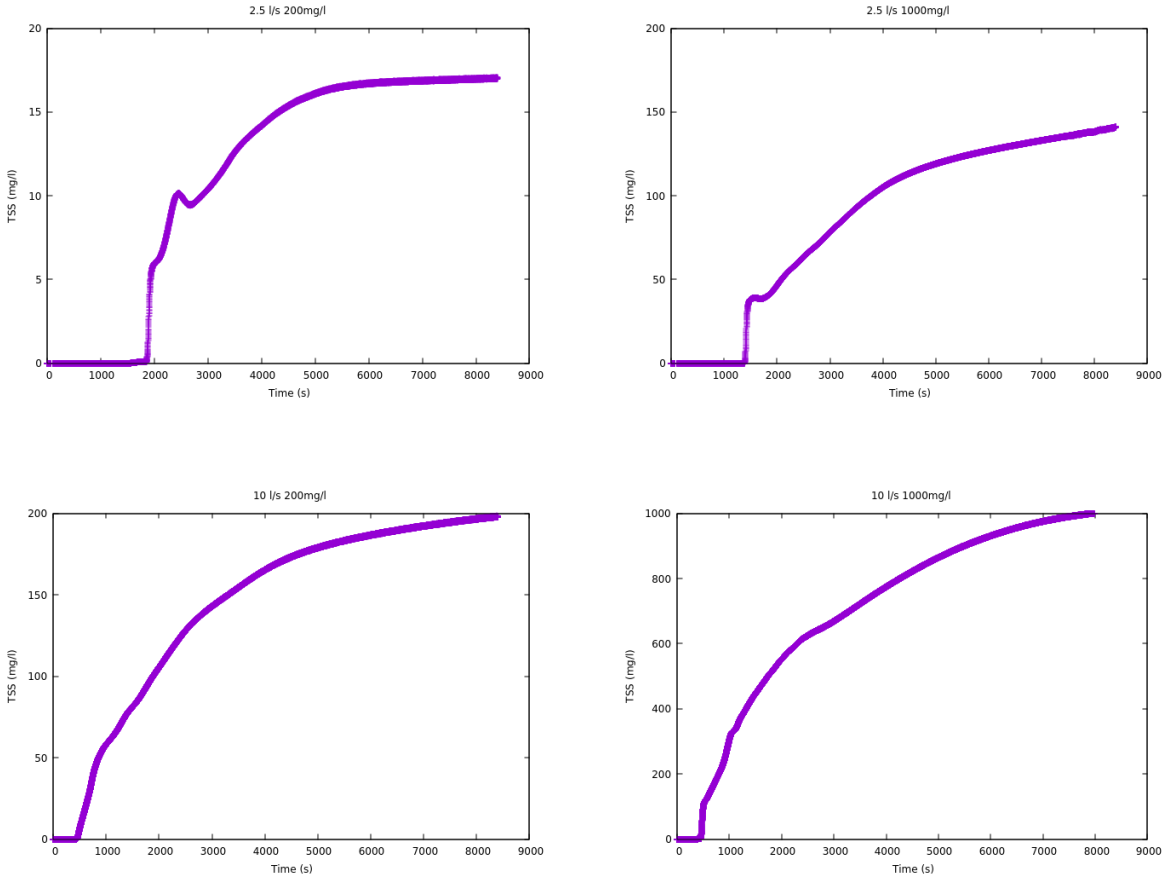


Figure 5.12: Effluent TSS concentration as a function of time for various flow rates and inlet concentrations

$2\mu$m and density 2650kg/m$^3$. For silt and other particles it is expected to be higher as it scales with particle diameter.

The velocity on the bottom of the tank over the sludge bed depends on the tank's cross sectional area and when the tank fills with sediment over a period of time the cross sectional area is naturally reduced, which increases the horizontal flow through velocity and therefore the likelihood of scouring. One of the objectives in this study was investigate what flow rates produce scouring and at what effect does bed height have on it.

Different bed heights $H_b$ were simulated by shrinking the tank floor in the mesh by a distance $H_b$ and the resulting shear velocity over these was measured and compared to the critical Shields value. The aim was to determine if there existed a 'critical' bed depth beyond which scouring was more likely to occur for certain flows. This would give a guideline as to when the tank would be in need of desludging. The assumption of a horizontal bed was made.

The velocity profiles along the top of the sludge bed are shown in Figure 5.13 for inlet concentrations of 0mg/l, 200mg/l and 1000mg/l and a flow rate of 2.5 l/s[1]. It is clear that even the lowest values of the Shields critical velocity are not reached at this flow rate.

Since the velocities at 0mg/l and 1000mg/l were similar in magnitude the 0mg/l case was used as an indicator in further comparisons. These comparisons are shown in Figure 5.14 for flows between 1-10l/s in the region of interest $x$=1.5-4m and only at 10l/s does the shear velocity exceed 0.0186m/s, the critical Shields velocity for a clay particle. This may mean that silt particles even at these flow rates are unlikely to be scoured.

The shear velocity across the bed increases with the reduced cross-sectional area due to bed buildup. For low flow operating conditions less than 10l/s, which are common, scouring should not be a major concern. Some resuspension may occur at the bottom of the density waterfall as it impinges vertically on the sludge bed (see Figure 5.7) but this is not described in the Shields formulation, which only refers to tangential shear stresses.

[1]The velocity profile for 0mg/l is taken along the tank floor as there is no sludge bed at this concentration

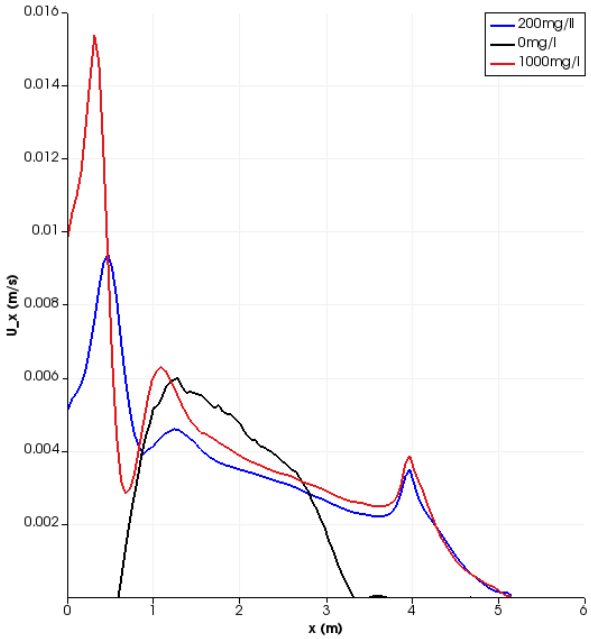


Figure 5.13: Shear velocity at tank bottom for 2.5l/s with various initial solids concentrations

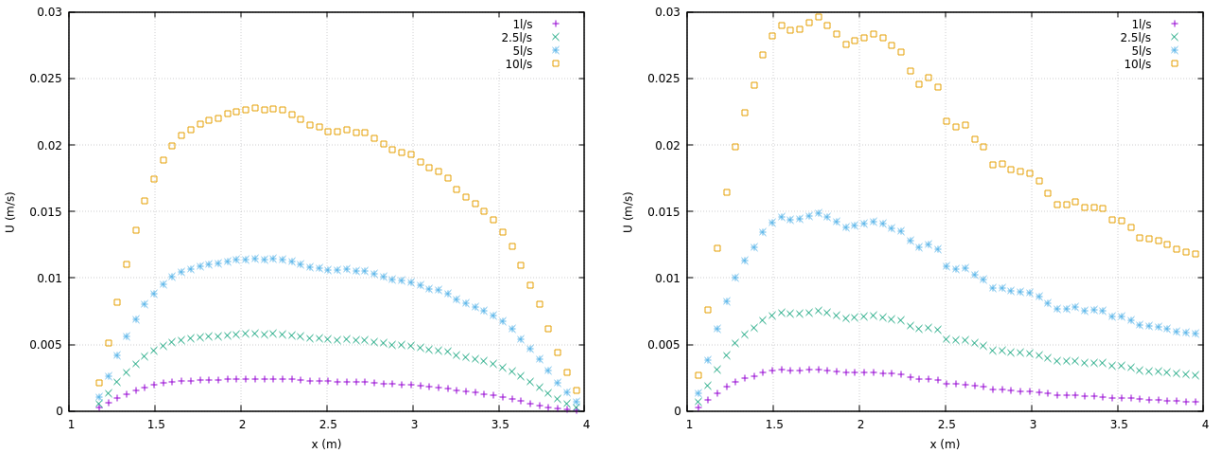


(a) (b)

Figure 5.14: Shear velocity at tank bottom for (a) the tank with no sludge bed and (b) the tank with a sludge bed of height 0.5m

Simulating scour using OpenFOAM does not model exactly the resuspension of solids from a consolidated solids bed, bearing in mind that the Takács model only describes hindered settling velocities. The drift flux model includes a mixture viscosity which in highly concentrated regions displays non-Newtonian behaviour and limits the viscosity to the point where thickening should be simulated.

A simulation with an initial condition of a concentrated bed region with 265000mg/l and a 0.25m height at the bottom of Stage 2 was tested to investigate whether scouring was captured. This resulted in erosion of the bed until it was dispersed throughout the tnak and this is not considered accurate as in reality flows have been observed to pass over the settled sludge beds without this level of erosion. Therefore a weakness in the model is its inability to reproduce a compacted sludge bed of cohesive sediments. However a first approximation to bed buildup can be garnered from contour plots such as Figure 5.8 and likelihood of scouring by using the critical Shields value at simulated velocities at the bottom of the tank.

## 5.4 Proposed modifications

One of the stated aims of this study was to recommend changes to the tank's internal design in order to improve efficiency. Suggested modifications are quantitatively compared to the existing tank in terms of the effluent TSS plotted over time under the same operating conditions (flow rate and inlet TSS concentration).

The modifications are suggested within the practical possibilities of the current tank. For example, suggestions would not be made to move one of the baffles 0.5m towards the front or the end of the tank, as the baffles sit inside grooves that are welded onto the tank that allow them to slide up and down with ease but not to be easily relocated. Modifications involving lowering, raising, shortening, extending or removing internal walls or baffles were explored.

More drastic changes could be made by retrofitting internal structures such a lamellar

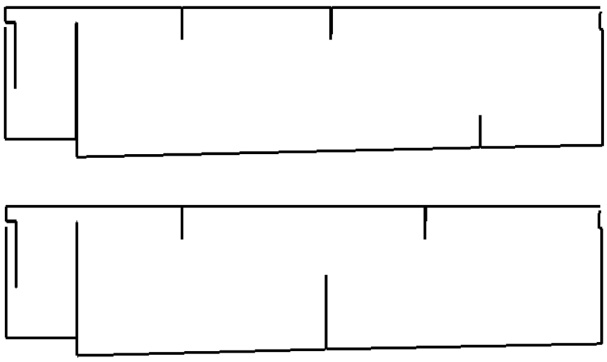

Figure 5.15: Current tank configuration (top) compared with modification M1 (bottom)

plates or tubes (see section 2.3.2), baffles, the construction of new inner walls and/or surface launders or new outlet channels. An entirely new design was not considered as both it and the above approach would have to be subject to a cost-benefit and requirements analysis to determine the design parameters, which was not a part of this study.

One of the first modification to show improved results was the lowering of Baffle 2 and doubling its height to $H/2$ where $H$ is the tank height. This was called modification 'M1' and its design can be seen in Figure 5.15 alongside the base configuration. The effluent concentrations were improved by 25% and 15% compared to the unmodified case for concentrations of 200mg/l and 1000mg/l respectively for a flow of 2.5l/s. A direct comparison of effluent concentrations between the unmodified and modified case M1 can be seen in Figure 5.16. These modifications, however, did not show significant improvement for the 10l/s case which, as before, exhibits velocities that are too large to allow for particles to settle and they are simply washed through the tank.

The success of this modification can be understood by analysing the TSS concentration contour plots in Figure 5.17 below for a flow of 2.5l/s and inlet concentration of 200mg/l at $t$=4000s and 8400s. Whereas in the unmodified case the density current reaches the end wall relatively quickly, the M1 case retains the density current earlier, and it is not allowed to spill over the wall until it has built up to a certain height. Meanwhile the unmodified case is already building up high concentrations on the bottom of the tank after 4000 seconds. The unmodified case builds up uniformly and as such its higher

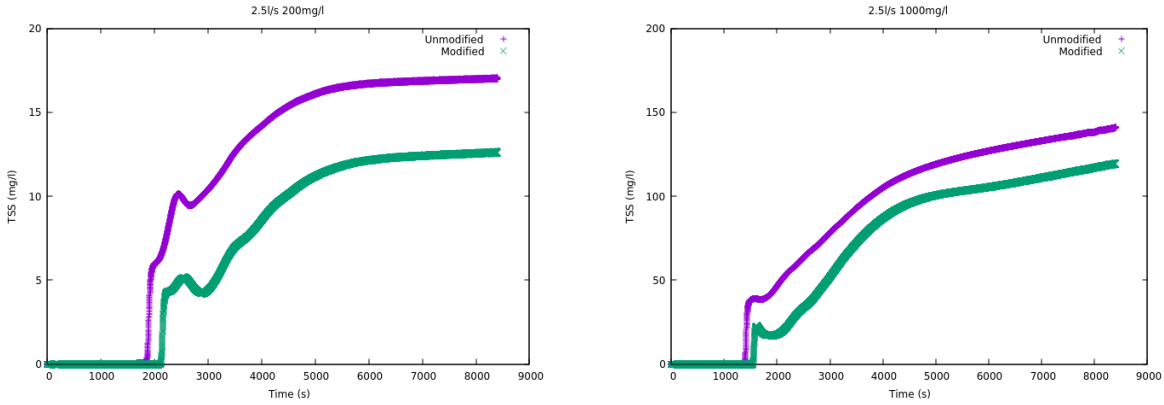


Figure 5.16: Effluent TSS concentration as a function of time with modification M1

concentration contours reach teh outlet before those of the M1 case, which build up more slowly in the second half of the tank because if the solids being retained behind the wall. The final baffle in the M1 case also protects from particles being scoured over the wall from short-circuiting towards the outlet.

An earlier version of this modification with a lower middle wall did not work as well because of the earlier spill over that occurred which lead to the density current reaching the end wall at a similar time to the unmodified version and showing little improvement in outlet TSS. Therefore the higher wall is seen as an important feature of this modification. It should be noted that this modification may require more frequent desludging as it will fill up faster than the unmodified case. However the sludge will conveniently build up directly above the desludging valve allowing for easy removal. The high wall also has the advantage of reducing the dead zone volume in the upper part of the tank caused by the density current.

No modifications were found that could improve the 10l/s flow rate and this is considered too high fot the tank to function adequately. The tank's performance at lower, 2.5l/s flows is good for all solids concentrations tested and it can be improved with the proposed modification M1.

Table 5.2 below gives the improvement in tank performance compared to the unmodified

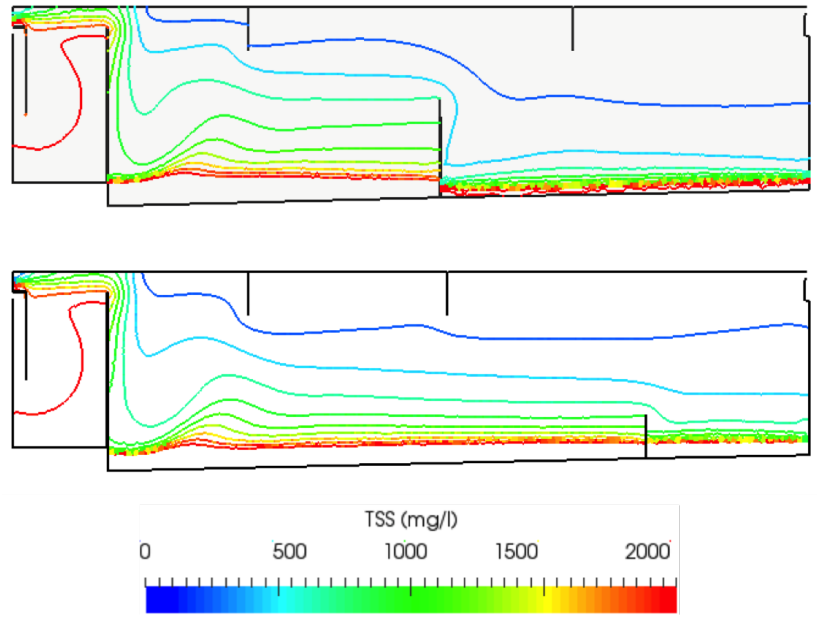


(a)

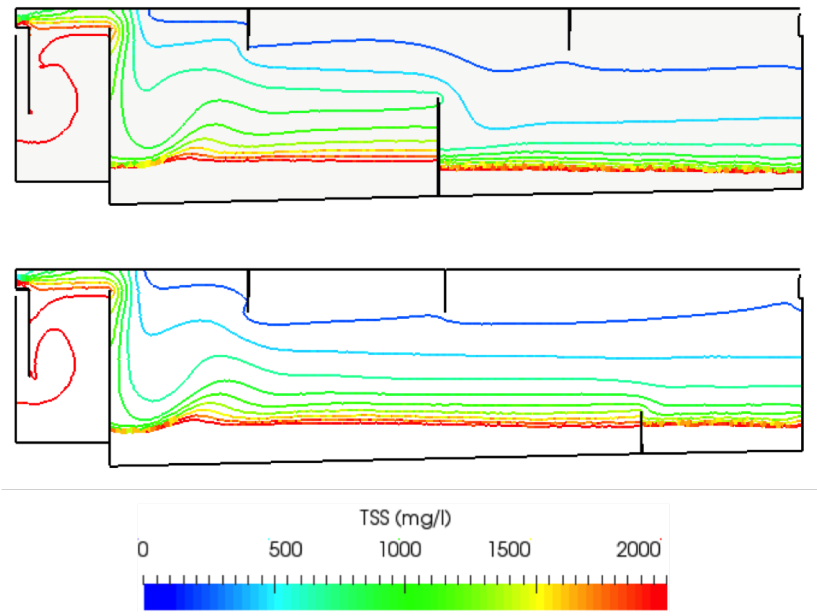


(b)

Figure 5.17: Contour plots of TSS concentration after (a) 4000s and (b) 8400s for the unmodified and modified M1 cases

| Setting | | Without modification | | With modification M1 | |
|---|---|---|---|---|---|
| Flow | $C_0$ | $\eta$ | TSS (mg/l) | $\eta$ | TSS (mg/l) |
| 2.5l/s | 200mg/l | 92% | 17 | 94% | 13 |
| 2.5l/s | 1000mg/l | 86% | 141 | 86% | 119 |
| 2.5l/s | 5000mg/l | 65% | 1754 | 65% | 1314 |
| 10l/s | 200mg/l | 1% | 198 | 0% | 201 |
| 10l/s | 1000mg/l | 0% | 1007 | 1% | 991 |

Table 5.2: Table of removal efficiencies and outlet concentrations with and without proposed modification

tank in terms of the removal efficiency, $\eta$, and outlet TSS.

It is worth mentioning some of the modifications that produced no or worse improvement.

- Widening the velocity reduction chamber in an attempt to reduce the jetting effect. This reduced the functionality of the velocity reduction chamber and settling in Stage 2 was affected.
- Lowering the Stage 1 wall to reduce the density current fall. This had the effect of sediments being dispersed from Stage 1 throughout the tank at a much higher rate.
- Removing Baffles 1,2 and 3. This was to determine their importance and indeed the flow field was found to be less stable and greater upwelling from the end wall to the outlet reduced tank efficiency.

More sophisticated modifications to consider would be two or three longitudinal launders from the end of the tank to approximately one third of its length back from the end to collect the upper fluid at a reduced velocity, the installation of lamellar plates, the effect of porous baffle, placement of longitudinal floor baffle to steady the flow. These would require more advanced CFD models and a more in depth analysis of the sediments, settling tests, tank flows and site conditions would need to be conducted prior to investing in such modifications.

# Chapter 6

# Conclusion

## 6.1 Summary of achievements

This work set out to investigate the operation of an industrial ST used by a company on construction dewatering sites in the Dublin area. The inner workings of the tank and its operating capacity were not well-understood and there was a desire to study these aspects of the tank and determine whether viable improvements to it could be made.

A CFD model was created to simulate the flow and settling dynamics within the tank and delivers a useful tool for understanding the workings of the tank. There were several stages to this process. A literature review of the state of the art of CFD ST modelling was conducted, followed by a study of the theoretical background of ST design. An appropriate mathematical formulation for the settling model was chosen based on the sediment characteristics and expected sedimentation processes and the model was partially calibrated by experiment. A computational mesh was created for the company's ST 'MEL5' and CFD simulations were performed using OpenFOAM software to analyse some of the basic mechanisms underlying its functionality.

The results highlighted previously unknown flow field patterns, provided useful visualisations of settlement processes, identify the working range of the tank in terms of flow rates

and suspended solids concentrations, and finally were used to propose modifications that improved the efficiency of the ST in removing particles from suspension. General guidelines for optimum operating conditions are given in relation to tank removal efficiency, scouring and resuspension, and flow rates.

## 6.2 Applications

The dewatering process is a necessary part of almost all construction sites in Dublin where the company is based and indeed any construction setting in countries with wet weather conditions and areas with high water tables such as estuarine or fluvial environments. Such sites need to be dewatered in order for them to be safe and workable and the resulting waste water must be adequately treated. Often space is limited on such sites and maximising the space occupied by the tank is important, therefore it should be designed as efficiently as possible. Treating suspended natural sediments is not limited to construction dewatering but may also have applications in water purification.

The model presented here is intended to be flexible. It can used with site or situation-specific inputs for the rheology and hindered settling parameters as well as flow rates and inlet concentrations. If any modifications to the tank are to be considered, the model provides a useful tool to study the effects on hydrodynamics and settling dynamics. Possible improvements and extensions to the model could include:

- Obtaining a detailed CAD model of the tank and using more advanced meshing tools such as OpenFOAM's `snappyHexMesh` utility to make the mesh more similar to the physical tank
- Introducing a compression term to the settling velocity model, similar to the work of Ramin eet al, 2014 [49]
- Modelling mixing of chemical agents such as hydrochloric acid and coagulants which are sometimes used to treat high-pH and extremely turbid water, respectively.

- Extending the drift flux model to incorporate a distribution of settling velocities, done in the study of Burt, 2010 [9]
- Obtaining instrumentation to measure the flow field velocities within the tank to improve model calibration (see Section 4.2.2)
- Performing lab experiments to more accurately determine type II settling parameters (see Section 4.2.4 to improve calibration of the $r_2$ parameter in the Takács model
- Performing lab experiments to determine the rheological properties of the sludge, lock exchange experiments etc.
- Using alternative mathematical formulations to study other aspects of sedimentation such as a Lagrangian model to model flocculation or settling between lamellar plates
- Because OpenFOAM is open source its code can be modified and specific modifications relevant to the study of STs could be written for it such as a new rheological model

The model as presented here can be used by the company to predict the performance of the tank under specific operating conditions and inform it about the tank's weaknesses and shortcomings. It can be used to produce operation guidelines and make modifications to the tank in certain settings. The methodology followed could be used to recreate models for similar tanks or designing new tanks should the need arise.

## 6.3 Future Work

CFD can be a very useful tool for designing and analysing the performance of water treatment tanks. It allows for a more thorough understanding of the hydrodynamics and settling behaviour of suspended solids compared to older, empirical approaches. The majority of early CFD studies for wastewater treatment focussed on primary tanks but today secondary settlement tanks dominate the literature. No works were found for

industrial treatment tanks for construction dewatering applications even though such studies would be beneficial to the industry.

# Bibliography


[1] E. Adams and W. Rodi, *Modeling Flow and Mixing in Sedimentation Tanks*, Journal of Hydraulic Engineering, 116 (1990).

[2] American Public Health Association, American Water Works Association, and Water Environment Federation, *Standard Methods For The Examination Of Water And Wastewater*, 22 ed., 2012.

[3] American Water Works Association, *Water Quality And Treatment - A Handbook of Community Water Supplies*, McGraw-Hill, Inc., 5 ed., 1999.

[4] AWWA and ASCE, *Water Treatment Plant Design*, McGraw-Hill, 4 ed., 2005.

[5] G. Bartzke, K. Bryan, A. Pilditch, and K. Huhn, *On the Stabilizing Influence of Silt On Sand Beds*, SEPM Society for Sedimentary Geology, 83 (2013), pp. 691–703.

[6] J. Berlamont, M. Ockenden, E. Toorman, and J. Winterwerp, *The characterisation of cohesive sediment properties*, Coastal Engineering, 21 (1993), pp. 105–128.

[7] D. Brennan, *The numerical simulation of two phase flows in settling tanks*, PhD thesis, Imperial College London, 2001.

[8] R. Bürger, S. Diehl, and I. Nopens, *A consistent modelling methodology for secondary settling tanks in wastewater treatment*, Water Research, 45 (2011), pp. 2247–2260.

[9] D. Burt, *Improved Design of Settling Tanks Using an Extended Drift Flux Model*, PhD thesis, MMI Engineering, 2010.

[10] D. Burt, M. Corton, D. Hetherington, and D. Balmforth, *Multiphase Modeling and the Prediction of Retention Efficiency in a Side Weir CSO*, in ASCE 9th International Conference on Urban Drainage, Oregon, USA, 2002, ASCE.

[11] T. R. Camp, *Sedimentation and the design of settling tanks*, Trans. ASCE, 111 (1946), pp. 895–936.

[12] I. Celik and W. Rodi, *Modeling Suspended Sediment Transport In Nonequilibrium Situations*, Journal of Hydraulic Engineering, 114 (1988), p. 1157.

[13] J. C. Crittenden, R. Rhodes Trussel, D. W. Hand, K. J. Howe, and G. Tchobanoglous, *MWH's Water Treatment: Principles and Design*, John Wiley & Sons, Inc., 3 ed., 2012.

[14] C. Dahl, *Numerical modelling of flow and settling in secondary settling tanks.*, PhD thesis, Dept of Civil Engineering, Aalborg Univeristy, Denmark, 1993.

[15] B. de Clercq, *Computational fluid dynamics of settling tanks: development of experiments and rheological, settling, and scraper submodels.*, PhD thesis, Department of Applied Mathematics, Biometrics and Process Control (BIOMATH) of Ghent University, 2003.

[16] R. Dick, *Sedimentation since Camp*, J Society of Civil Engnrs, (1982), pp. 199–235.

[17] S. Elghobashi, *On predicting particle-laden turbulent flows*, Applied Scientific Research, 52 (1994), pp. 309–329.

[18] O. Flamant, A. Cockx, V. Guimet, and Z. Doquang, *Experimental Analysis and Simulation of Settling Process*, Process Safety and Environmental Protection, 82 (2004), pp. 312–318.

[19] C. Geuzaine and J.-F. Remacle, *Gmsh: a three-dimensional finite element mesh generator with built-in pre-and post-processing facilities*, International Journal For Numerical Methods In Engineering, 0 (2009), pp. 1–24.

[20] A. M. Goula, M. Kostoglou, T. D. Karapantsios, and A. I. Zouboulis, *The effect of influent temperature variations in a sedimentation tank for potable water treatment - A computational fluid dynamics study*, Water Research, (2008).

[21] F. Greifzu, C. Kratzsch, T. Forgber, F. Lindner, and R. Schwarze, *Assessment of particle-tracking models for dispersed particle-laden flows implemented in OpenFOAM and ANSYS FLUENT*, Engineering Applications of Computational Fluid Mechanics, 10 (2016), pp. 30–43.

[22] A. Griborio, J. A. Mccorquodale, and J. A. Rodriguez, *CFD Modeling of Primary Clarifiers: The State-of-the-Art*, in WEFTEC Proceedings, vol. 510-518, WEF, 2014, pp. 1926–1949.

[23] G. A. Hadi and J. Kriš, *A CFD methodology for the design of rectangular sedimentation tanks in potable water treatment plants*, Journal of Water Supply: Research and Technology - AQUA, (2009).

[24] A. Hazen, *On sedimentation*, Trans. ASCE, 53 (1904), pp. 45–88.

[25] H. He, P. Stroeven, E. Pirard, and L. Courard, *On the Shape Simulation of Aggregate and Cement Particles in a DEM System*, Advances in Materials Science and Engineering, 2015 (2015).

[26] D. W. Hendricks, *Water Treatment Unit Processes : Physical and Chemical*, CRC Press, 2006.

[27] E. Imam, J. A. Mccorquodale, and J. K. Bewtra, *Numerical Modelling of Sedimentation Tanks*, Journal of Hydraulic Engineering, 109 (1983).

[28] A. M. Karpinska and J. Bridgeman, *CFD-aided modelling of activated sludge systems – A critical review*, Water Research, 88 (2016), pp. 861–879.

[29] W. P. Kowalski, *The method of calculations of the sedimentation efficiency in tanks with lamella packets*, Archives of Hydroengineering and Environmental Mechanics, 51 (2004), pp. 371–385.

[30] P. Krebs, M. Armbruster, and W. Rodi, *Laboratory experiments of buoyancy-influenced flow in clarifiers*, Journal of Hydraulic Research, 36 (1998), pp. 831–851.

[31] P. Larsen, *On the hydraulics of rectangular settling basins - Experimental and theoretical studies*, Rep. No. 1001, Dept. of Water Resources Engineering, Lund, Sweden., (1977).

[32] J. Laurent, R. W. Samstag, J. M. Ducoste, A. Griborio, I. Nopens, D. J. Batstone, J. D. Wicks, S. Saunders, and O. Potier, *A protocol for the use of computational fluid dynamics as a supportive tool for wastewater treatment plant modelling*, Water Science and Technology, (2014).

[33] B. Liu, J. Ma, L. Luo, Y. Bai, S. Wang, and J. Zhang, *Two-Dimensional LDV Measurement, Modeling, and Optimal Design of Rectangular Primary Settling Tanks*, J. Hydraul. Eng., 137 (2011), pp. 343–355.

[34] X. Liu and M. H. García, *Computational Fluid Dynamics Modeling for the Design of Large Primary Settling Tanks*, Journal of Hydraulic Engineering, 137 (2011), pp. 343–355.

[35] M. Long and C. O. Menkiti, *Geotechnical Properties Of Dublin Boulder Clay*, tech. rep., UCD, Dublin, 2007.

[36] D. A. Lyn and W. Rodi, *Turbulence Measurements In Model Settling Tank*, Journal of Hydraulic Engineering, 116 (1990).

[37] D. A. Lyn, A. I. Stamou, and W. Rodi, *Denisty currents and shear-induced flocculation in sedimentation tanks*, J. Hydraul. Eng., 118 (1992), pp. 849–867.

[38] M. Manninen, V. Taivassalo, S. Kallio, and A. Akademi, *On the mixture model for multiphase flow*, VTT Publications, (1996), p. 67.

[39] T. Matko, N. Fawcett, A. Sharp, and T. Stephenson², *Recent Progress In The Numerical Modelling Of Wastewater Sedimentation Tanks*, Trans IChemE, 74 (1996).

[40] G. MAZZOLANI, F. PIROZZI, and G. DANTONOI, *A generalized settling approach in the numerical modeling of sedimentation tanks*, Water Science and Technology, 38 (1998), pp. 95–102.

[41] J. A. Mccorquodale and S. Zhou, *Effects of hydraulic and solids loading on clarifier performance Effects of hydraulic and solids loading on clarifier performance Influence du debit et de la charge en matières solides sur Ie fonctionnement des décanteurs*, Journal of Hydraulic Research, 314 (1993), pp. 461–478.

[42] Metcalf & Eddy, *Wastewater Engineering : Treatment and Reuse*, McGraw-Hill Education, London, 4 ed., 2003.

[43] F. Moukalled, L. Mangani, and M. Darwish, *The Finite Volume Method in Computational Fluid Dynamics*, Springer International Publishing, 1 ed., 2015.

[44] I. Nopens, E. Torfs, J. Ducoste, P. Vanrolleghem, and K. Gernaey, *Population Balance Models: A useful complementary modelling framework for future WWTP modelling*, (2014), pp. 129–138.

[45] OpenFOAM, *The OpenFOAM Foundation User Guide version 4.0*, 2016.

[46] A. Pantet, S. Robert, S. Jarny, and S. Kervella, *Effect of Coarse Particle Volume Fraction on the Yield Stress of Muddy Sediments from Marennes Oléron Bay*, Advances in Materials Science and Engineering, 2010 (2010).

[47] S. Patankar, *Numerical Heat Transfer and Fluid Flow*, CRC Press, 1980.

[48] P. J. Powers, A. B. Corwin, P. C. Schmall, and W. E. Kaeck, *Construction Dewatering and Groundwater Control: New Methods and Applications*, John Wiley & Sons, Inc., third ed., 2007.

[49] E. Ramin, D. S. Wágner, L. Yde, P. J. Binning, M. R. Rasmussen, P. S. Mikkelsen, and B. G. Plósz, *A new settling velocity model to describe secondary sedimentation*, Water Research, (2014).

[50] A. M. Razmi, B. Firoozabadi, and A. Goodarz, *Experimental and Numerical Approach to Enlargement of Performance of Primary Settling Tanks*, Journal of Applied Fluid Mechanics, 2 (2009).

[51] P. Roberts Alley, *Water Quality Control Handbook*, McGraw-Hill, 2 ed., 2007.

[52] J. A. Romero Rojas, *Potabilización del Agua*, Alfaomega, México DF, 3 ed., 1999.

[53] F. Rostami, M. Shahrokhi, M. A. Md Said, R. Abdullah, and Syafalni, *Numerical modeling on inlet aperture effects on flow pattern in primary settling tanks*, Applied Mathematical Modelling, 35 (2011), pp. 3012–3020.

[54] R. Samstag, I. Nopens, D. Batstone, J. Wicks, S. Saunders, E. Wicklein, G. Kenny, and J. Laurent, *Water science and technology : a journal of the International Association on Water Pollution Research.*, Water Science & Technology, 74 (2016), pp. 549–563.

[55] M. Shahrokhi, F. Rostami, M. A. Md Said, S. R. Sabbagh Yazdi, and Syafalni, *The effect of number of baffles on the improvement efficiency of primary sedimentation tanks*, Applied Mathematical Modelling, (2012).

[56] A. P. Sincero and G. Sincero, *Physical–Chemical Treatment Of Water And Wastewater*, CRC Press, London, 2003.

[57] A. I. Stamou, *Optimising the design of secondary clarifiers using mathematical models*, Transactions on Ecology and the Environment, 14 (1997).

[58] A. I. Stamou, E. W. Adams, and W. Rodi, *Numerical modeling of flow and settling in primary rectangular clarifiers*, Journal of Hydraulic Research, 27 (1989), pp. 665–682.

[59] I. Takács, G. Patry, and D. Nolasco, *A dynamic model of the clarification-thickening process*, Water Research, 25 (1991), pp. 1263–1271.

[60] A. Tamayol, . B. Firoozabadi, and M. A. Ashjari, *Hydrodynamics of Secondary Settling Tanks and Increasing Their Performance Using Baffles*, Journal of Environmental Engineering, 136 (2010).

[61] R. Tarpagkou and A. Pantokratoras, *CFD methodology for sedimentation tanks: The effect of secondary phase on fluid phase using DPM coupled calculations*, Applied Mathematical Modelling, 37 (2013), pp. 3478–3494.

[62] ——, *The influence of lamellar settler in sedimentation tanks for potable water treatment — A computational fluid dynamic study*, Powder Technology, 268 (2014), pp. 139–149.

[63] M. van Loosdrecht, P. Nielsen, C. Lopez-Vazquez, and D. Brdjanovic, *Experimental Methods in Wastewater Treatment*, IWA Publishing, London, 1 ed., 2016.

[64] L. C. Van Rijn, *A Unified View Of Sediment Transport By Currents And Waves, Part 1: Initiation Of Motion, Bed Roughness And Bed Load Transport*, Journal Of Hydraulic Engineering, 113 (2007).

[65] Y. C. B. Wang, *Effects Of Physical Properties And Rheological Characteristics On Critical Shear Stress Of Fine Sediments*, PhD thesis, Georgia Institute of Technology, 2013.

[66] Water Environment Federation, *Design of Municipal Wastewater Treatment Plants*, McGraw Hill, New York, 4 ed., 2010.

[67] Water Environment Federation. Clarifier Design Task Force., *Clarifier design*, McGraw-Hill Professional, 2006.

[68] E. Wicklein, D. J. Batstone, J. Ducoste, J. Laurent, A. Griborio, J. Wicks, S. Saunders, R. Samstag, O. Potier, and I. Nopens, *Good mod-*

*elling practice in applying computational fluid dynamics for WWTP modelling*, Water Science and Technology, (2016).

[69] S. Zhou and J. A. Mccorquodale, *Modeling Of Rectangular Settling Tanks*, Journal of Hydraulic Engineering, 118 (1992).